POLYSTYRENE-CLAY NANOCOMPOSITE
EXHIBITING SELF-ASSEMBLING PROPERTIES:
MICROVESICLES FOR GUEST-ENCAPSULATION

**THESIS SUBMITTED TO
THE UNIVERSITY OF KERALA
FOR THE DEGREE OF**

**DOCTOR OF PHILOSOPHY
IN CHEMISTRY**

UNDER THE FACULTY OF SCIENCE

By

BINDU P. NAIR

**MATERIALS & MINERALS DIVISION
NATIONAL INSTITUTE FOR INTERDISCIPLINARY SCIENCE
& TECHNOLOGY (CSIR)
THIRUVANANTHAPURAM-695019
KERALA, INDIA**

OCTOBER 2009

Dedicated To My

..........Guide

........Parents &

.......Husband

DECLARATION

I hereby declare that the matter presented in the thesis entitled **"POLYSTYRENE-CLAY NANOCOMPOSITE EXHIBITING SELF-ASSEMBLING PROPERTIES: MICROVESICLES FOR GUEST-ENCAPSULATION"** is the outcome of investigations carried out by me under the supervision of Dr. C. Pavithran, Scientist G, Materials and Minerals Division, National Institute for Interdisciplinary Science and Technology (CSIR), Thiruvananthapuram, India and the results embodied here has not been submitted elsewhere for the award of any other degree.

Bindu P. Nair

Thiruvananthapuram

CERTIFICATE

This is to certify that this thesis entitled "POLYSTYRENE-CLAY NANOCOMPOSITE EXHIBITING SELF-ASSEMBLING PROPERTIES: MICROVESICLES FOR GUEST- ENCAPSULATION" is an authentic record of the investigations carried out by **Ms. Bindu P. Nair** at the Materials and Minerals Division of National Institute for Interdisciplinary Science and Technology (CSIR), Thiruvananthapuram, India, under my supervision and guidance. This thesis or any part thereof has not been submitted elsewhere for the award of any other degree.

Dr. C. Pavithran
(Thesis Supervisor)

Thiruvananthapuram

Acknowledgements

PREFACE

Polymer-clay nanocomposites (PCNs) have attracted great interest during the past two decades because they often exhibit remarkable thermal, mechanical and barrier properties for replacing conventional polymer composites for several applications. These properties have been attributed to dispersion of clay layers having thickness of one nanometer and lateral dimensions of several nanometers in polymer matrix. Generally hydrophilic clays are made organophilic by cation-exchange of interlayer alkali metal ions with long-chain alkylammonium ions. Recently, Polyhedral Oligomeric Silsesquioxane (POSS) have been used as an organomodifier for clay due to its high thermal stability and synergic benefits from dual nano-reinforcements. POSS-modified organoclay with reactive functional groups such as vinyl can be useful for the synthesis of novel PCNs, but are not currently available in the literature. The thesis is focused on the following major aspects: (i) synthesis and properties of organoclays using novel hetero-substituted POSS with vinyl and aminopropyl groups (ii) polystyrene-POSS-clay nanocomposite particles and their solvent-assisted self-assembling to produce microvesicles and microporous film (iii) guest-encapsulated microvesicles and their properties in different solvents. The thesis is divided into six chapters.

The chapter 1 presents a brief introduction to the synthesis, structure and properties of PCNs, limitation of conventional organoclays and recent interest in POSS-modified organoclays. The chapter 2 deals with synthesis of organoclays using hetero-substituted POSS from hydrolytic co-condensation of 3-

v

aminopropyltriethoxysilane (AS) and vinyltriethoxysilane (VS). Effect of AS:VS mole ratio on the structure and properties of POSS-modified organoclays is presented.

The chapter 3 presents a detailed investigation on synthesis of polystyrene-POSS-clay nanocomposite particles and their solvent-assisted self-assembling properties in tetrahydrofuran (THF). Concentration dependent morphological transition of nanocomposite particles ($\sim$ 200 nm) into microvesicles ($\sim$ 2.3-3.5 μm) and microporous film have been observed. Structure of particle and plausible mechanism for the observed morphological transitions are explained.

The chapter 4 presents preparation of guest-encapsulated microvesicles and their properties in water, alcohol and toluene. Vesicles were encapsulated with fluorescent probes- Rhodamine 6G, 8-Anilinonaphthalene sulfonic acid (ANS) and a triglyceride oil in which ANS was dispersed. The vesicles were found stable in aqueous media, exhibited slow release of encapsulated dye molecules in alcohol and spontaneous release in toluene.

The POSS solution from AS:VS mole ratio of 1:3 was found useful for the synthesis of bifunctionalized hybrid silica spheres (HS) having size in the range of 250 nm to 2.5 μm. The chapter 5 presents the mechanism of formation of HS containing POSS-bilayer and siloxane network and its application for synthesizing polystyrene composite with low dielectric constant.

The chapter 6 summarizes the outcome of the research work carried out in the thesis and the scope for future work.

CONTENTS

CHAPTER 1
Introduction to Polymer-Clay Nanocomposites

CHAPTER 2

Polyhedral Oligomeric Silsesquioxane (POSS)-Modified Clays using POSS Solution from Hydrolytic co-condensation of 3-Aminopropyltriethoxysilane and Vinyltriethoxysilane

CHAPTER 3

Polystyrene-Clay Nanocomposite Exhibiting Solvent-assisted Self-assembling Properties

CHAPTER 4

Investigations on Guest-encapsulation and Release Properties of Microvesicles

CHAPTER 5

Bifunctionalized Hybrid Silica Spheres by Hydrolytic Co-condensation of 3-Aminopropyltriethoxysilane and Vinyltriethoxysilane

ix

CHAPTER 6

Chapter 1

Introduction to Polymer-Clay Nanocomposites

Chapter 1 presents introduction to polymer-clay nanocomposites including structure of clays, organoclays, synthesis and characterization techniques, need of novel organoclays, chemically significant morphologies from polymer-clay nanocomposites and scope and objectives of the present research work.

1.1. Introduction

Polymer nanocomposites are a new class of composites that are particle filled systems for which at least one dimension of the dispersed particles is in the nanometer range. They often exhibit physical and chemical properties that are dramatically different from pure polymers and conventional microcomposites and generate interest principally because of their wide potential for applications as high performing structural materials. Nanofillers, because of their smallness, can effectively be agitated by thermal motion that helps to evenly disperse them in polymer matrix. As a result, by embedding just a few volume percent of such nano-fillers, one can significantly modify the mechanical, thermal, transport, electrical, optical, and other properties of matrix polymer.[1,2] Added advantage is that one can still conveniently mold them into complex shapes with pre-existing industrial equipment. There already exist applications of such nanocomposites, as well as many appealing expectations regarding their potential.[3,4] Clays, carbon nanotubes, silica, alumina etc are potential nanofillers that have been in the focus of current research interest.[5-11] Among these nanofillers, clays have been widely used as fillers for thermoplastics like polypropylene, polyethylene, polystyrene and nylon due to its natural abundance, low cost and broadest commercial viability. Although the intercalation chemistry of polymers when mixed with appropriately modified clays has long been known, the field of polymer-clay nanocomposites (PCNs) gained momentum following two major findings. First, the report from Toyota Central Research Laboratory that very moderate clay loading resulted in concomitant enhancement in thermal and mechanical properties of the matrix polymer, Nylon 6.[12] Second, Giannelis et al.[13] found that it was possible to melt-mix polymers with clays without the use of organic solvents. The improved properties of PCNs were attributed

to the dispersion of clay layers having thickness of one nanometer and lateral dimensions of several nanometers in the polymer matrix. Extensive reviews are available in literature on the preparation, structure and properties of PCNs.[14-20]

1.2. Structure of Clays

Clays, alternatively referred as layered silicates are comprised of stacks of hydrated aluminosilicate with thickness of minimum 1 nm and lateral dimension of 50-1000 nm.[2] Framework layers of clays are generated by a combination of tetrahedral and octahedral sheets. Silica is the major component of tetrahedral sheet whereas octahedral sheet comprises diverse elements such as Al, Mg and Fe. Tetrahedral and octahedral sheets stack naturally in specific ratios and modes, leading to the formation of 1:1, 2:1 or 2:1:1 layered silicates or phyllosilicates. Among these, 2:1 phyllosilicates have been used for PCNs due to the ease of separation of individual silicate layers owing to its structural features. The crystal lattice of 2:1 phyllosilicate consists of 1 nm thick aluminosilicate layers, with an octahedral alumina sheet sandwiched between two tetrahedral silica sheets (Figure 1.1). The stacking of the platelets leads to Van der Waals gap or gallery between the platelets. Isomorphic substitution of Al^{3+} in the alumina sheet with cations such as Mg^{2+} or Fe^{2+} produces negative charge to the layers. This negative charge is balanced by alkali cations (Na^+, Li^+ or Ca^{2+}) positioned in the gallery between the aluminosilicate layers which are exchangeable with other inorganic and organic cations and the cation exchange capacity (CEC) is expressed as mequiv/100 g clay. Clays having high CEC are generally used for PCNs. The type of cations positioned in the gallery and its degree of hydration determines the gallery height of pristine clay. 2:1 phyllosilicate include mica, smectite, vermiculite, and chlorite. Smectite group can be further divided into montmorillonite (MMT),

3

nontronite, saponite and hectorite species.[21,22] Typical CEC values of selected 2:1 phyllosilicates are listed in table 1.1.
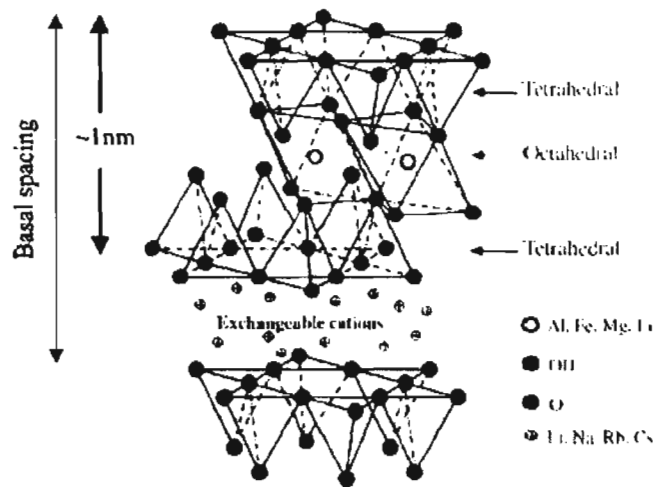
Figure 1.1. *Structure of 2:1 aluminosilicate.*[16]

Table 1.1. *Chemical formula and cation exchange capacity of 2:1 phyllosilicates*[15]

Silicate	Formula	CEC (mequiv/100 g)
Montmorillonite	$M_x(Al_{4-x}Mg_x)Si_8O_{20}(OH)_4$	92.6–120
Hectorite	$M_x(Mg_{6-x} Li_x)Si_8O_{20}(OH)_4$	120
Saponite	$M_xMg_6(Si_{8-x}Al_x)Si_8O_{20}(OH)_4$	86.6
Vermiculite	$(Mg, Fe, Al)_3[(Al, Si)_4O_{10}](OH)_2M_{x \cdot n}H_2O$	150

M represents exchangeable cation and x is the layer charge.

1.3. Organoclays

In its pristine state, clay is hydrophilic and miscible only with hydrophilic polymers whereas most of the polymers are organophilic. Therefore, the clay surface often requires organomodification to make the platelets compatible with organophilic polymer matrix. Clay can be organomodified via cation exchange of Na^+ with

alkylammonium ions including primary, secondary, tertiary and quaternary alkylammonium cations under proper conditions.[23] The space between the silicate layers in the organoclay depends greatly on the length of the alkyl chain of organomodifier and the ratio of cross-sectional area to available area per cation.[24] Organomodification of clays improves the interfacial adhesion properties between the inorganic phase and hydrophobic polymer matrix.

The key issue in the design of PCNs is how to monitor the dispersion of clay platelets at nanometer scale in a polymer matrix. Accordingly, it is necessary to understand the interaction between the clay surfaces and the intercalants. In other words, understanding the structure of organoclays and the interaction of surfactant in clays is of crucial importance in design, fabrication and characterization of PCNs. Proper selection of organoclays depends mainly on the type of polymer matrix used. When the hydrated cations are ion-exchanged with organic cations such as bulky alkyl ammoniums including primary, secondary, tertiary, and quaternary alkylammonium or alkylphosphonium cations, it generally results in larger interlayer spacing. Alkylammonium or alkylphosphonium cations in the organosilicates lower the surface energy of the inorganic host and improve the wetting characteristics of polymer matrix, and result in larger interlayer spacing. Additionally, the alkylammonium or alkylphosphonium cations can provide functional groups that can react with the polymer matrix, or in some cases initiate the polymerization of monomers to improve the strength of the interface between the inorganic and the polymer matrix.[25,26] Traditional structural characterization to determine the orientation and arrangement of the alkyl chain was performed using Wide Angle X-ray diffraction (WAXD). Depending on the packing density, temperature and alkyl chain length, the chains were

5

thought to lay either parallel to the silicate layers forming mono or bilayers, or radiate

away from the silicate layers forming mono or bimolecular arrangements (Figure 1.2).[27]
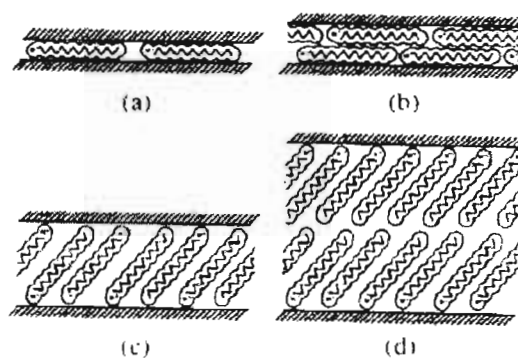
Figure 1.2. *Arrangements of alkylammonium ions in mica-type layered silicates with different layer charges. Hatch areas are silicate layers.*[27]
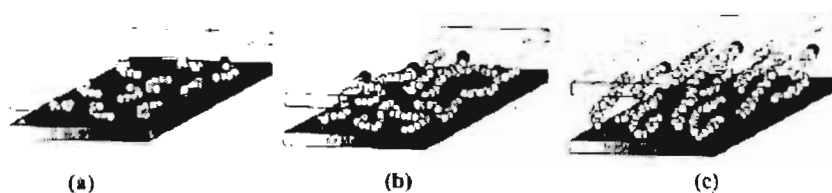
Figure 1.3. *Alkyl chain aggregation models (a) short chain length, the molecules are effectively isolated from each other, (b) medium lengths, quasi-silicate layers form with various degree of in plane disorder and interdigitation between the layers and(c) long lengths, interlayer order increases leading to liquid-crystalline polymer environment. Open circle represent the CH_2 segments while cationic head groups are represented by filled circles.*[28]

However, these idealized structures have been shown to be unrealistic by Vaia et al.[28]

using FTIR experiments. They showed that alkyl chains could vary from liquid-like to

solid-like, with the liquid-like structure dominating as the interlayer density or chain

length decreases, or as the temperature increases. This occurs because of the relatively

small energy differences between the trans and gauche conformers; the idealized

models described earlier assume all trans conformations. In addition, for longer chain

length surfactants, the surfactants in the layered silicate can show thermal transition akin to melting or liquid-crystalline to liquid-like transitions upon heating (Figure 1.3).

1.4. Preparative Methods for PCNs

The preparative methods are divided into three main groups depending on the starting materials and processing techniques:

1.4.1. Intercalation of Polymer or Pre-polymer from Solution

This is based on a solvent system in which the polymer or pre polymer is soluble and the silicate layers are swellable. The layered silicate is first swollen in a solvent, such as water, chloroform, or toluene. When the polymer and the layered silicate solutions are mixed, the polymer chains intercalate and displace the solvent within the interlayer of the silicate. Upon solvent removal, the intercalated structure remains, resulting in nanocomposite.

Water-soluble polymers, such as poly(ethyelene oxide),[29] poly(vinyl alcohol),[30] poly(vinyl pyrolidone),[31] and poly(ethylene vinyl alcohol),[32] have been intercalated into the clay galleries using this method. Examples from non-aqueous solvents are nanocomposites of poly(capro lactone)[33] and polylactide[34] in chloroform as a co-solvent, and high-density polyethylene with xylene and benzonitrile.[35] The thermodynamics involved in this method are when the polymer is exchanged with the previously intercalated solvent in the gallery, a negative variation in the Gibbs free energy is required. The driving force for the polymer intercalation into layered silicate from solution is the entropy gained by desorption of solvent molecules, which compensates for the decreased entropy of the confined, intercalated chains.[36] Using this method, intercalation only occurs for certain polymer/solvent pairs. This method is

7

good for the intercalation of polymers with little or no polarity into layered structures, and facilitates production of thin films with polymer-oriented clay intercalated layers. However, from commercial point of view, this method involves the copious use of organic solvents, which is usually environmentally unfriendly.

1.4.2. In situ Intercalative Polymerization

In this method, the layered silicate is swollen within the liquid monomer or a monomer solution so the polymer formation can occur within the interlamellar region. Polymerization can be initiated either by heat or radiation, by the diffusion of a suitable initiator, or by an organic initiator or catalyst fixed through cation exchange before the swelling step. 1-caprolactam,[12] polyurethane,[37] polystyrene,[38,39] polypropylene,[40] polyethylene,[41] poly(ethylene terephthalate)[42] and epoxy resin[43] are examples of polymers used for in situ intercalation.

1.4.3. Melt Intercalation

This method involves annealing, statistically or under shear, a mixture of the polymer and organoclay above the softening point of the polymer. Nowadays, the melt intercalation technique has become widely accepted method for the preparation of PCNs. This method has great advantages over either in situ intercalative polymerization or polymer solution intercalation. For example, direct melt intercalation is highly specific for the polymer, leading to new hybrids that were previously inaccessible. In addition, the absence of a solvent makes direct melt intercalation an environmentally sound and an economically favorable method for industries. Also it is compatible with current industrial processes, such as extrusion and injection molding.

Vaia and Giannelis have developed mean field, lattice-based thermodynamic model for polymer melt intercalation in organically modified mica type silicates.[37]

They reported that the outcome of polymer intercalation is determined by interplay of entropy and energy change in the system. During polymer melt intercalation, the entropy loss of polymer confinement in the gallery space can be compensated for by the increased conformational freedom of the surfactant chains as the layers separate due to the less confined environment. The entropy change associated with the surfactant increases until the interlayer separation is equal to the fully extended length of the surfactant chains. On the other hand, as the interlayer separation increases, more polymers are confined and the total penalty of polymer confinement per unit area continuously increases. Thus, the penalty for polymer confinement is compensated only up to a critical gallery height. The extent of intermolecular interactions would determine the amount of the intercalated polymer, beyond this critical gallery height. At this stage, the penalty of polymer confinement dominates and strong energetic molecular interactions are needed to overcome the unfavourable entropy changes in the system. When the total entropy change is small, small changes in the free energy of the system determine whether intercalation is thermodynamically stable. For alkylammonium-modified silicates, the free energy change is rendered favourable by maximizing the magnitude and number of favourable polymer-surface interaction while minimizing the magnitude of the number of unfavourable apolar interactions between the polymer and functionalizing alkyl surfactants. For most conventional organosilicates, the tethered surfactant chains are apolar, thus the dispersion forces dominate the polymer-surfactant interactions. In an earlier stage of melt intercalation process, polymer chains from bulk polymer need to be transported from the bulk melt into the expanded clay galleries. This process does not require high shear force. The driving force is the affinity of the polymer chains for the organoclay surfaces. The

9

enthalpy of mixing could be rendered favourable by maximizing the polymer-clay interactions. At later stage, the clay tactoids are exfoliated under shear and stacks of clay platelets tend to slide apart from each other. High shear intensity would assist the formation of PCNs by breaking up the clay platelets and increasing sample uniformity.[15] The process is thus facilitated by both residence time and screw configuration in the extruder.

1.5. Classification of PCNs

Depending on the strength of interfacial interactions between the polymer matrix and layered silicate, three different types of PCNs are thermodynamically achievable (Figure 1.4).

1.5.1. Intercalated Nanocomposites

In intercalated nanocomposites, the insertion of polymer matrix into the layered silicate structure occurs in a crystallographically regular fashion, regardless of the clay to polymer ratio. Properties of the composites typically resemble those of ceramic materials.

1.5.2. Flocculated Nanocomposites

Conceptually this is same as intercalated nanocomposites. However, silicate layers are sometimes flocculated due to hydroxylated edge-edge interaction of the silicate layers.

1.5.3. Exfoliated Nanocomposites

In an exfoliated nanocomposite, the individual clay layers are separated in a continuous polymer matrix by an average distance that depends on clay loading.

10

Usually, the clay content of an exfoliated nanocomposite is much lower than that of an intercalated nanocomposite.
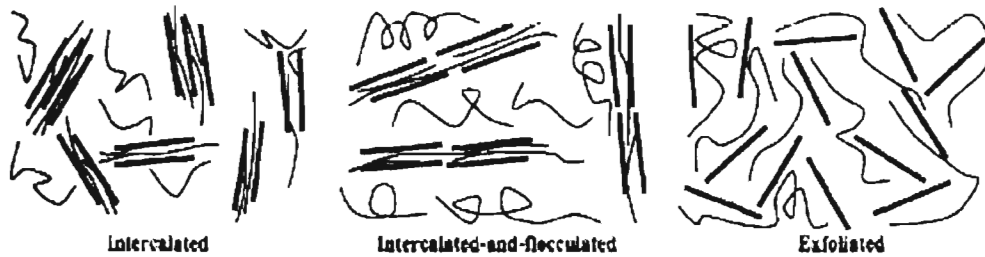
Figure 1.4. *Schematic illustration of three different types of thermodynamically achievable PCNs.*[16]

1.6. Techniques used for the Characterization of PCNs

In addition to the techniques used for the characterization of the respective polymers, the structure of nanocomposites has typically been established using wide Angle X-ray Diffraction (WAXD) analysis and transmission electron micrographic (TEM) observation (Figure 1.5). Due to its easiness and availability, WAXD is most commonly used to probe nanocomposite structure[44] and occasionally to study the kinetics of the polymer melt intercalation.[45,46] By monitoring the position, shape, and intensity of the basal reflections from the distributed silicate layers, the nanocomposite structure (intercalated or exfoliated) may be identified. For example, in an exfoliated nanocomposite, the extensive layer separation associated with the delamination of the original silicate layers in the polymer matrix results in the eventual disappearance of any coherent X-ray diffraction from the distributed silicate layers. On the other hand, for intercalated nanocomposites, the finite layer expansion associated with the polymer intercalation results in the appearance of a new basal reflection corresponding to the larger gallery height.

11
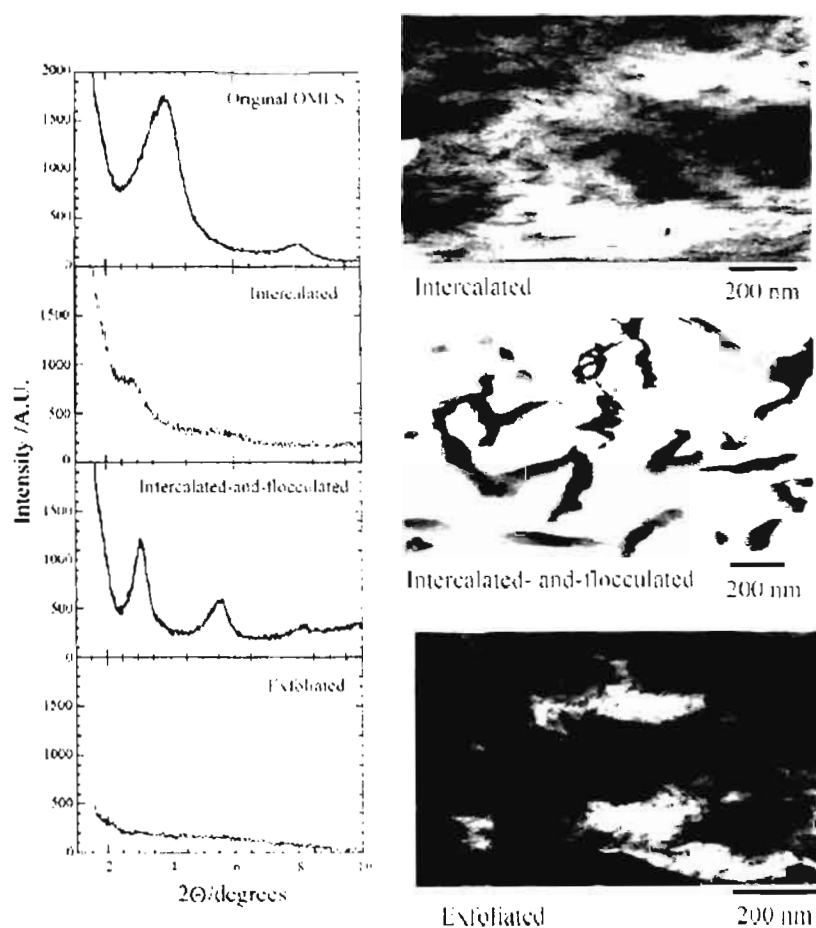
Figure 1.5. *WAXD patterns and TEM images of three different types of nanocomposites.*[16]

Although WAXD offers a convenient method to determine the interlayer spacing of the silicate layers in the original layered silicates and in the intercalated nanocomposites (within 1-4 nm), spatial distribution of the silicate layers or any structural non-homogeneities in nanocomposites cannot be predicted. Also, some layered silicates initially do not exhibit well-defined basal reflections which make systematic analysis of peak broadening and intensity decreases very difficult. Only tentative conclusions concerning the mechanism of nanocomposite formation and their structure can be made based on WAXD patterns alone. TEM allows a qualitative

understanding of the internal structure, spatial distribution of the various phases, and views of the defect structure through direct visualization. However, special care must be made to make a representative cross-section of the sample. TEM is time-intensive, and only gives qualitative information on the sample as a whole, while low-angle peaks in WAXD allow quantification of changes in layer spacing.[14]

1.7. Properties of PCNs

Nanocomposites consisting of a polymer and layered silicate (modified or not) frequently exhibit remarkably improved mechanical and material properties when compared to those of pristine polymers. Improvements include a higher modulus, increased strength and heat resistance, decreased gas permeability and flammability and increased biodegradability of biodegradable polymers. The main reason for these improvements is the stronger interfacial interaction between the matrix and the layered silicate, compared with conventional filler-reinforced systems.

1.7.1. Mechanical Properties

Dynamic mechanical, tensile and flexural properties of polymeric materials showed remarkable improvement when nanocomposites are formed with layered silicates.[47-49]

1.7.2. Thermal Stability

Generally, the incorporation of clay into the polymer matrix was found to enhance the thermal stability by acting as a superior insulator and mass transport barrier to the volatile products produced during decomposition. In some cases, though the clay was found to shift the early stages of thermal decomposition to higher temperature, a reversal in thermal stability due to the heat barrier effect of the stacked silicate layers

13

holding accumulated heat that could be used as a heat source to accelerate the decomposition process in conjunction with the heat flow supplied by the outside heat source, was also observed.[50,51]

1.7.3. Fire Retardant Properties

The nanocomposites' flame retardant mechanism involves a high-performance carbonaceous-silicate char, which builds up on the surface during burning. This insulates the underlying material and slows the mass loss rate of decomposition products.[52]

1.7.4. Heat Distortion Temperature (HDT)

HDT of a polymeric material is an index of heat resistance towards applied load. The increase of HDT due to clay dispersion is a very important property improvement for any polymeric material, not only from application or industrial point of view, but also because it is very difficult to achieve similar HDT enhancements by chemical modification or reinforcement by conventional filler.[53,54]

1.7.5. Gas Barrier Properties

Conventional composite   **Tortuous path in PCNs**
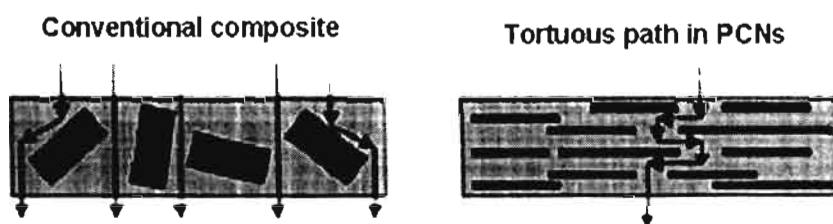
Figure 1.6. *Tortuous path for penetrants in PCNs.*[10]

Clays are believed to increase the barrier properties by creating a maze or 'tortuous path' that retard the progress of gas molecules through the matrix resin. The reduction in permeability arises from the longer diffusive path that the penetrants must

14

travel in the presence of filler, as shown below. A sheet-like morphology is particularly efficient in maximizing the path length due to the large length to width ratio when compared to other filler shapes such as spheres or cubes (Figure 1.6).[55,56]

1.7.6. Optical Properties

Although layered silicates are microns in lateral size, they are just 1 nm thick. Thus, when single layers are dispersed in a polymer matrix, the resulting nanocomposite is optically clear in visible light.[17]

1.7.7. Bio Degradability

Another interesting and exciting aspect of PCNs is the significant improvement of biodegradability after nanocomposite preparation with organoclay. The improved biodegradability of nanocomposites may be due to a catalytic role of the organoclay in the biodegradation mechanism.[57,58]

1.7.8. Other Properties

Polymer-clay nanocomposites also show improvement in most general polymeric properties. For example, in addition to the decreased permeability of liquids and gases, nanocomposites also show significant improvement in solvent uptake. Scratch resistance is another property that is strongly enhanced by the incorporation of layered silicates.[59] The potential use of PANI-based nanocomposites as electrorheologically sensitive fluids or the combination of dispersed layered silicates in a liquid crystal medium is also an attractive application. This could result in a stable electro-optical device that is capable of exhibiting a bistable and reversible electro-optical effect between an opaque and transparent state. In addition, nanocomposites have been in the improvement of ablative properties in aeronautics.[60]

15

1.8. Morphology Control through Clay-Polymer Interaction

Research over the last three decades on PCNs have been successful in synthesizing nanocomposites with improved physical properties or other material properties like biodegradability, flame retardation etc. when compared to the matrix polymer. Recent studies have shown that, control of organization of nanometer sized clay platelets at larger scale can be used to extend the range of available morphologies. Fine interaction with the nanoclay can influence the morphology of the matrix polymer and reports available in literature are summarized below.

Zeng et al.[61] synthesized polystyrene and poly (methyl methacrylate)- clay nanocomposite foams using super critical CO_2 as the foaming agent. They found that presence of small amount of clay particles greatly reduces foam cell size and increase the cell density. Cell morphology can be further manipulated by adjustment of polymer-clay-CO_2 interaction and foaming condition to achieve microcellular and submicrocellular foams. The high nucleation efficiency can produce microcellular nanocomposite foams at less stringent processing conditions, leading to cost-savings and processing flexibility.

Khakhar et al.[62] found that both unmodified clay and organoclays can act as efficient cell openers in both rigid and flexible polyurethane foams and a greater fraction of open cells was obtained with increasing clay concentration. The capacity of modified clays to open the cells was found to be much greater than that of unmodified clay. Both unmodified clay and organoclays were found to be superior to the conventional liquid chemical cell openers in opening the cells. A study of the foaming kinetics indicates that the addition of unmodified clay results in an increase in the rise

time but the cream time and gel time remain unchanged. The increase in rise time is attributed to hydrogen bonding of water with the hydroxyl groups on the clay. The bound water is released only when the temperature becomes high enough, resulting in a slower blowing reaction. In the case of modified clays the gel time is reduced but the cream time and rise time remain the same as that for the foam without clay. Hydrogen bonding of water with the clay is thus not significant, and the accelerated gelling reaction may be due to the catalytic activity of the surfactants used for modifying the clay. In this case cell opening may be due to rupture of foam lamellae by liquid matrix phobic clay particles.
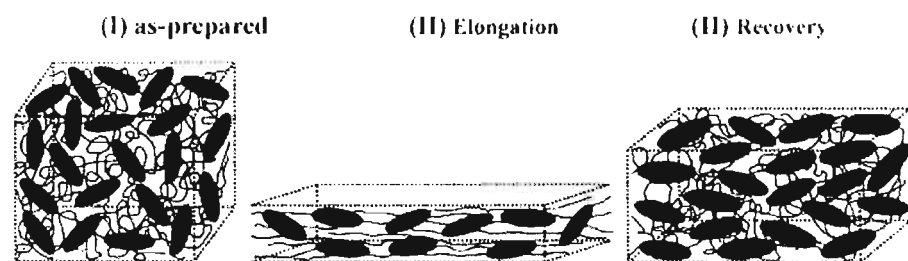
Figure 1.7. *Schematic representation of the structural model for nanocomposite gels in the course of elongation process.*[64]

Recently, Haraguchi et al.[63] developed a breakthrough method by making hydrogels of an organic-inorganic network using laponite clay. They used nanoclay instead of the chemical cross-linker. These nanocomposite gels are novel, and destroy the prevailing common sense on conventional gels. It was found that mechanical properties of the nanocomposite gels were improving with clay content. For gels with low clay content, the clay platelets may be aligned perpendicular to the stretch direction. However, in nanocomposite gels with high clay content, it was estimated from the changes in mechanical properties that the clay platelets may be orientated

parallel to the stretch direction. Because of the high concentration of clay and their cooperative alignment toward the stretch direction on elongation, the orientation as well as the strain is partially retained, even after long relaxation times, resulting in much-improved mechanical properties (Figure 1.7).[64]
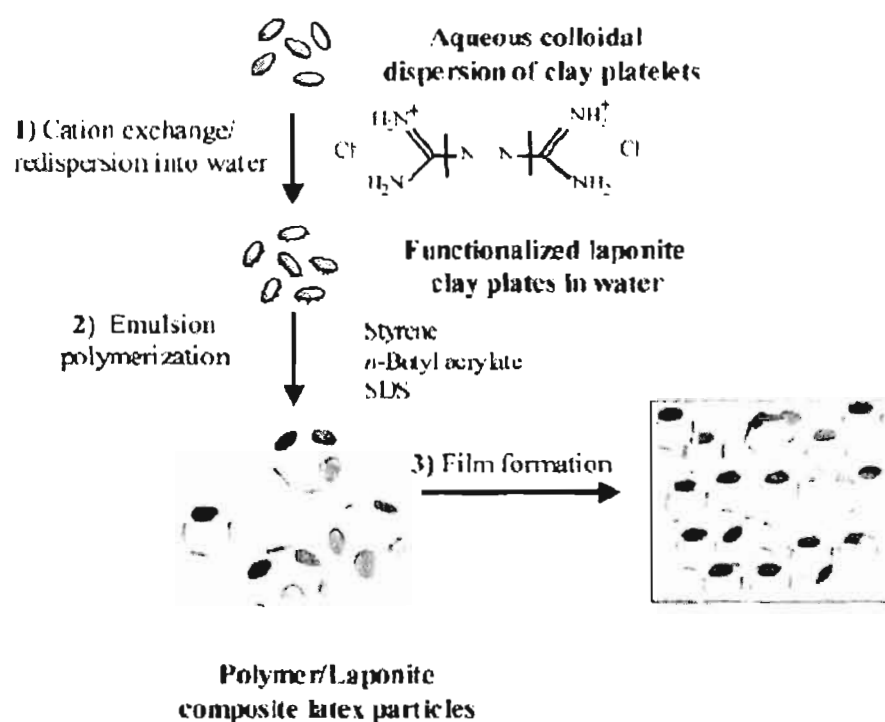
Figure 1.8. *Scheme illustrating the synthesis of poly (Sty-co-BuA) /Laponite nanocomposite latexes and film formation.*[65]

Lami et al.[65] reported the formation of transparent polymer-laponite nanocomposite films, which contained an unconventional honeycomb laponite network, whose microstructure resulted from the original armored morphology of the composite latex particles. The films were obtained by drying a suspension of latex particles synthesized through emulsion polymerization of styrene and butyl acrylate (BuA) in the presence of laponite clay particles intercalated with cationic initiator

18

molecules. The different reaction steps are illustrated in (Figure 1.8) and involve (i) initiator intercalation, (ii) in situ free radical emulsion polymerization in the presence of the functionalized clay plates, and (iii) film formation by water evaporation and composite particles coalescence.

Using a similar approach Caruso et al.[66] prepared laponite hollow spheres using composite particles comprising a PS core and well defined laponite nanoparticle/PE multilayers fabricated by using the layer-by-layer approach. The hybrid core-shell particles were subsequently calcined to create well-defined hollow spheres with predetermined diameters (Figure 1.9).
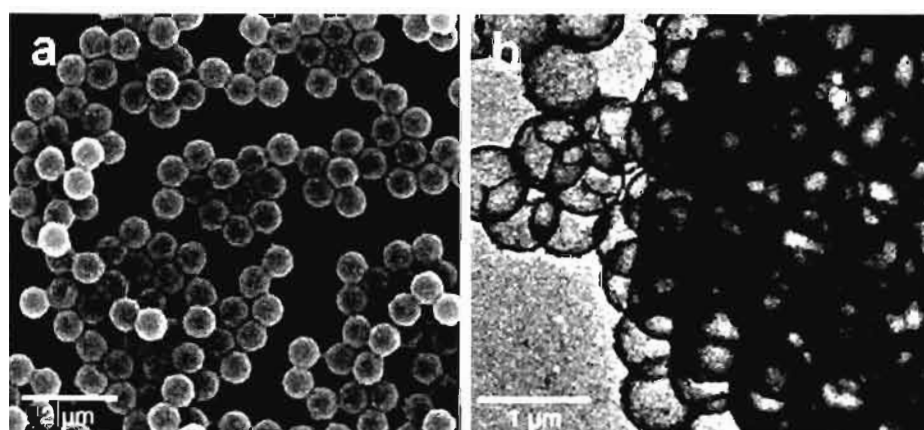
Figure 1.9. *SEM (a) and TEM (b) images of hollow laponite spheres obtained after calcination of PS spheres (640 nm).*[66]

More recently, Weisner et al.[67] observed hexagonally patterned lamellar morphology in ABC triblock copolymer poly (ethylene-*alt*-propylene-*block*-ethylene oxide-*block*-*n*-hexyl methacrylate)-clay nanocomposites. Level set modelling confirmed that this patterning of the PEO-aluminosilicate sheets is consistent with micellar PEP domains forming either pillars through the sheet (Figure 1.10). The

hybrid materials possess structure within the PHMA and PEO aluminosilicate domains at the 1-3 nm length-scale. These results establish that ABC triblock copolymers can be used to direct the assembly of inorganic precursors into hybrid materials with complex, hierarchical structures.
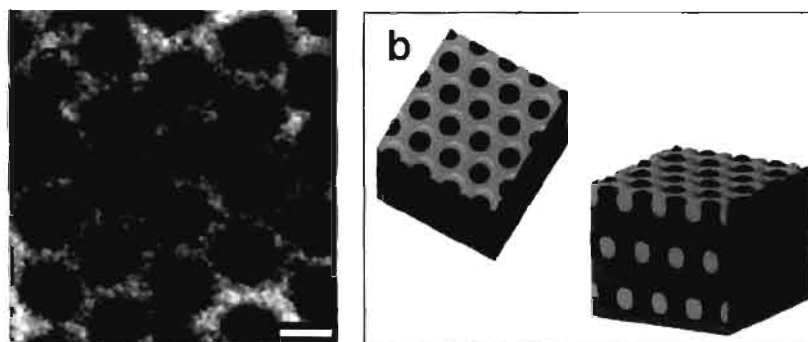
Figure 1.10. *(a) Hexagonal pattern. Scale bar represent 20 nm, and (b) structural model for PEP-b-PEO-b-PHMA block copolymer-clay lamellar morphologies with a small PEP block. The PEO (red) and PHMA (green) chains stretch into their respective domains while the aluminosilicate particles partition into the hydrophilic PEO domain and the small PEP block (blue) forms round micellar domains.* [67]

1.9. Limitation of Conventional Organoclays

Melt intercalation is the broadly applicable method for the synthesis of many commodity and engineering polymer nanocomposites. These polymers are produced on a large scale and it is desirable to use these materials as they are currently produced. Melt compounding is a flexible and commercial process capable of producing a variety of products on large volume scales. Since Giannellis and co-workers conducted the melt intercalation of PS with MMT, the melt intercalation method has become a mainstream technique for the fabrication of PCNs in extrusion or injection molding. Moreover, the high shear environment of the melt extruder can assist the delamination or exfoliation of clay platelets.[68] The disadvantage of melt intercalation is related to

low thermal stability of the organomodifiers. Although alkylammonim cations render the layered silicates more organophilic, the main limitation of the organoclays is derived from their low thermal stability during melt processing at high temperatures. This situation becomes more serious for melt-compounding of many high performance polymers such as polyetherimide with high melting point. Vanderhart et al.[69] studied the thermal stability of MMT modified with dimethyl, dehydrogenated-tallow ammonium during melt blending with Nylon 6 at 240 °C. They reported that most of the organic modifier on the clay surface decomposes, releasing a free amine with one methyl and two tallow substituents. This was caused by the combined effects of the temperature and shear stress during melt blending.

Gelfer et al.[70] studied the thermally induced phase transitions and morphological changes in organoclays. Figure 1.11 shows the proposed morphological model for organoclays in three temperature zones. In zone 1 temperature range (room temperature to about 40 °C), a bimodal organic layer thicknesses distribution exists in organoclays. The thinner organic layer contains a monolayer with surfactant molecules bound to the adjacent clay surfaces. The thicker layer contains two monolayers of surfactant with only about half of them being bound to the clay surface. This assembly was termed the double layer structure with a thickness of exactly twice that of the thin layer thickness. The double layer content was found to increase with the overall surfactant loading. In zone 2 temperature range (40-180 °C), the content of thicker layers drastically decreases. Organoclays undergo a melting-like order-disorder transition, resulting in the randomization of surfactant conformation. The thickness of the thinner organic layer is about the same as that of the thin layer in zone 1. In the zone 3 temperature range (180-260 °C), the layer thickness distribution becomes

bimodal again, organoclays containing disordered monolayers of bound surfactant and fused silicate layers. The drastic increase in the content of fused silicate layers above 200 °C can be attributed to thermal degradation and/or escape of bound surfactant molecules.
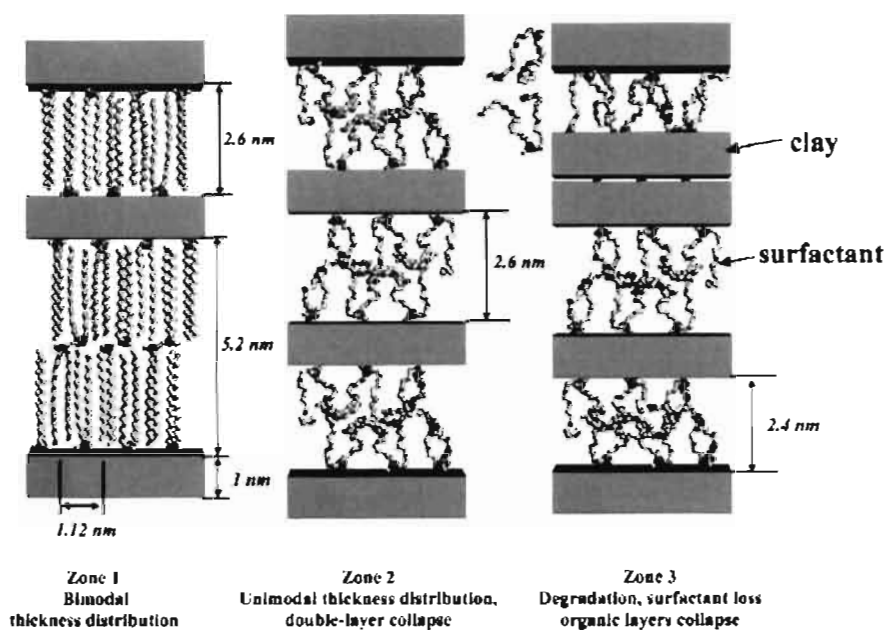
Figure 1.11. *The proposed morphological model for organoclays in three temperature zones.*[70]

Vaia et al. [71] also studied thermal degradation chemistry of alkyl quaternary ammonium montmorillonite including (1) the temperature regimes of thermal degradation reactions within alkyl quaternary ammonium montmorillonite and natural montmorillonite, (2) the onset temperatures, stages, and products of organic decomposition within organoclays (3) structural changes to the organoclay during the initial stages of organic decomposition, and (4) the mechanism and pathways of organic decomposition for organoclays. They found that onset temperature of decomposition of these organoclays was approximately 180 °C. Analysis of decomposition products

22

indicates that the initial degradation of the surfactant in the organoclays follows a Hoffmann elimination reaction and that the architecture (trimethyl or dimethyl), chain length, surfactant mixture, exchanged ratio, or preconditioning (washing) does not alter the initial onset temperatures. However, these factors do affect the initial mass loss. Relative to the parent alkyl quaternary ammonium salt, catalytic sites on the aluminosilicate layer reduce the thermal stability of a fraction of the surfactants by an average of 15-25 °C.

1.9.1. Alternatives for Conventional Organomodifier

Numerous concepts have been proposed that offer alternatives to conventional organoclays when thermal limitations are a concern. These include emulsion and suspension polymerization in which unmodified (alkalimetal-containing) montmorillonite is used,[72] sol/gel technology which consists of a direct crystallization of organically modified layered silicates by hydrothermal treatment with a gel containing organics and organometallics,[73] partially exchanged systems which decrease the volume fraction of surfactant needed,[74] montmorillonite, charge balanced by protons (so called proton clays),[75] alkyl imidazolium as the surfactant to increase the initial decomposition temperature (Figure 1.12),[76] phosphonium-based surfactants to improve the thermal stability[77,78] and Polyhedral oligomeric silsesequioxanes (POSS) cations.[79-81] Other cations, such as pyridinium, and iminium, have also been used to treat the layered silicate because of their greater thermal stabilities.[82] New thermally stable systems should enable the preparation of PCNs from thermoplastic engineering polymers with high melt-processing temperatures and from thermoset resins with high cure temperatures without loss of properties due to the presence of degradation products, loss of molecular mass, or network structural defects.

23

Dimethyl alkyl imidazolium salts
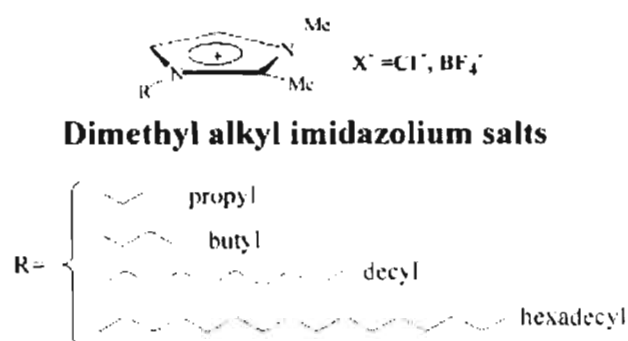
Figure 1.12. *Structures of various imidazolium salts used to treat sodium montmorillonite.*[76, 83]

Among the alternatives for conventional organomodifiers, octameric POSS have been of particular interest due to the synergic benefits that can expect for POSS-modified clay filled nanocomposites. POSS are an interesting class of thermally stable macromers derived from hydrolytic polycondensation of trifunctional organosilane monomers $RSiX_3$, where X being an easily hydrolyzable group, e.g. $-OCH_3$ or $-Cl$. A variety of stoichiometrically well-defined POSS frameworks with synthetically useful functional groups are available in literature and also the number of available frameworks are expanding rapidly with the improvement in analytical instrumentation. The term silsesquioxane is generally used to describe any substance that is derived from the condensation of $RSi(OH)_3$, where R is an organic group attached to Si via Si-C bond. Ideal empirical formula of $[RSiO_{3/2}]_n$ are used to represent fully condensed silsesquioxane frameworks and incompletely-condensed silsesquioxanes possess reactive Si-OH groups which can form additional Si-O-Si linkages. Heterosilsesquioxanes are derived by substitution of a main group, transition-metal atom for one or more Si atoms in a silsesquioxane.[84-85] The typical POSS octamers consist of cube-octameric siloxane core of size of about 0.5 nm with the organic groups attached to the corner Si atoms (Figure 1.13).

24
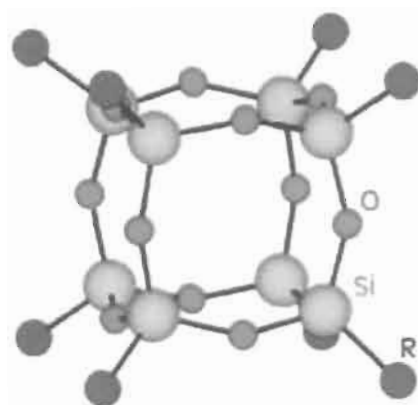
Figure 1.13. *Structure of POSS.*

POSS are widely used as precursors to hybrid inorganic/organic materials. Incompletely condensed POSS have been used as comonomers for silsesquioxane based polymers and for network solids. Fully condensed POSS frameworks are precursors to photocurable resins, liquid crystals, electroactive films, catalytically active organometallic gels etc. One of the most promising application of POSS is that fully-condensed POSS with polymerizable pendant group can be used as comonomers for excellent mechanical, thermal stability, flame retardation etc of the matrix polymer (Figure 1.14). [86-88]
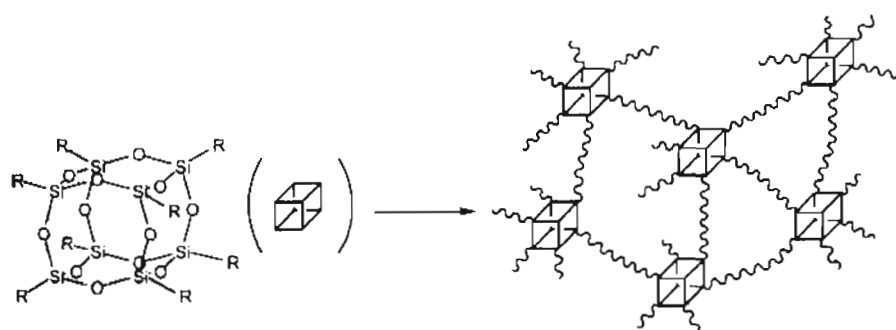
Figure 1.14. *Nanocomposite formation from POSS via cross-linking of functional groups with monomers.*

POSS having cationic functional groups have long been used as intercalating agent for layered materials through cation exchange reactions. Thus octa-aminopropyl

POSS has been known as ideal silica pillaring agent for clays because they can form homogenously distributed pillars and the cubic geometry of the POSS cages offers only one possible orientation in the interlayer zone of the clay to produce controlled pore-size and distribution. Petridis et al.[89] studied the intercalation of a cubic octamer derived from the controlled hydrolysis of 3-aminopropyltriethoxysilane with smectite clays. The main conclusion of work was the high tendency of smectite clays to insert into their surfaces three dimensional POSS in amounts exceeding the CEC of the mineral, the excess being in the form of physically adsorbed ion pairs.

POSS-modified clays have also been of particular interest in the preparation of polymer nanocomposites for various reasons. First, high thermal stability of POSS monomers, up to 300 °C or higher for typical amino-functionalized POSS, make them ideal clay-modifiers for processing of composites, especially at elevated temperatures at which the conventional low molecular weight organo-modifiers find limitations. Second, the relatively large d-spacings and large organic surface area of POSS-modified clay should facilitate their dispersion in a variety of polymers. Third, the resulting composites containing two types of nano-reinforcements would show synergic effects.

Epoxy and polystyrene clay nanocomposites, respectively using octa-aminopropyl POSS and (aminopropyl)iso-butyl POSS as clay-modifiers, were reported recently.[79,80] It was shown that intercalation of POSS in the clay facilitated the formation of exfoliated polymer-clay nanocomposites. The POSS-modified clay improved the thermal stability of polystyrene when conventional organo-modified clay did not show any improvement. Fox and coworkers reported the preparation of a new iso-butyl POSS-imidazolium surfactant and its use as clay modifier.[81] The modified-

clay showed interesting features such as large d-spacing (3.6 nm) due to formation of bilayer of the POSS bearing surfactant in the clay-gallery and high thermal stability, 200 °C higher than of a conventional organo-modifier, useful for nanocomposites by industry-preferred melt-process method (Figure 1.15).
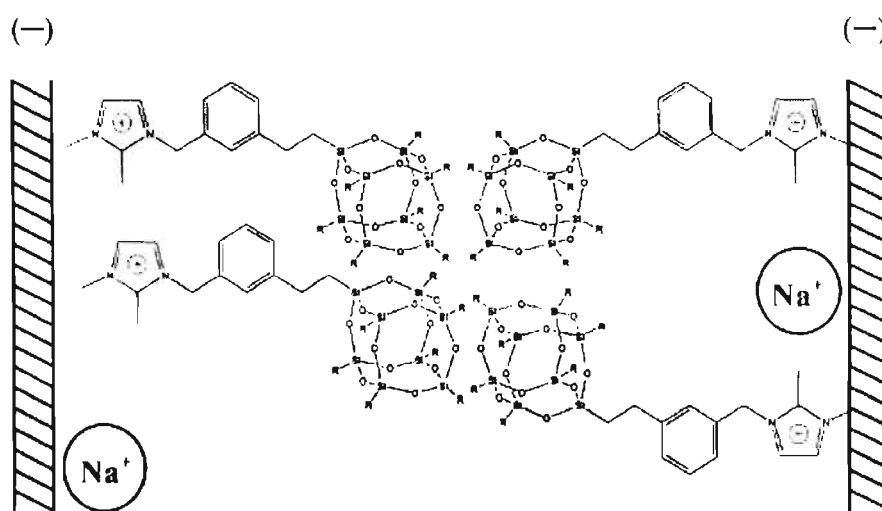
Figure 1.15. *Bilayer structure of POSS-imidazolium exchanged montmorillonite.*[81]

More recently Wan et al.[90] synthesized novel porous (3-aminopropyl)iso octyl (POSS) modified montmorillonite clay complexes with large interlayer distance and specific surface area via ion-exchange reaction, followed by freeze-drying procedure. The morphology of the POSS-modified clay is highly influenced by the POSS concentration, suspension acidity and drying procedure, but the interlayer distance of the POSS-modified clays does not change much when the POSS concentration is above 0.4 CEC. The partial surface coverage of POSS on the clay surface leaves high-energy surface uncovered, resulting in formation of card-house structure. The special texture and properties of the POSS-modified clay was used as catalyst supporter for cyclic butylene terephthalate oligomers (CBT) polymerization reaction. The POSS-modified clay supported Sn catalyst is fully delaminated by the melted CBT oligomers, but it

reorganizes into ordered structure after polymerization. However, it can be redelaminated after melt compounding with commercial PBT resin.

1.10. Scope and Objectives of the Present Investigation

The use of reactive organomodifiers with unsaturated bonds or other reactive functional groups for clay is a good strategy to improve the strength of the interface between the inorganic and the polymer matrix. These groups are expected to react with the growing polymer chains so that the polymer chains remain attached to the clay surface. POSS-modified organoclays with reactive functional groups will be particularly attractive in this regard. None of the POSS-modified clays reported in literature contain reactive functional groups like vinyl. Also vinyl POSS can undergo a wide range of useful reactions including free-radical addition reactions, catalytic hydrogenation, Diels-Alder reactions, cross-metathesis with olefins, hydroboration and epoxidation etc.

Thus the objectives of the present work are

1) To prepare POSS-modified clay having vinyl functional groups so that the POSS molecules intercalated in the clay can take part in polymerization reactions or be further modified through the reactive vinyl group.

2) To study the structure and dispersibility of the POSS-modified clays and hence its usefulness for the synthesis of polymer-clay nanocomposites.

3) To study the structure and properties of polymer-clay nanocomposites from POSS-modified clays.

1.11. References

1. Andrei. A. *Macromolecules* **2001**, *34*, 3081.

2. Xie. W.; Gao. Z.; Pan. W.P.; Hunter, D; Singh, A.; Vaia, R. *Chem. Mater.* **2001**. *13*, 2979.

3. *Plast. Add. Compd.* **2002**, *4*, 30.

4. Steward, R. *Plast. Eng.* **2004**, *60*, 23.

5. Manias, E.; Touny, A.; Wu, L.; Strauhecker, K.; Lu, B.; Chung, T.C. *Chem. Mater.* **2001**. *13*, 3516.

6. Wang, Z.; Pinnavaia. T. J.; *Chem. Mater.* **1998**, *10*, 3769.

7. Yu, M. F.; Lourie, O.; Dryer, M. J.; Molor, K.; Kelly, T. F.; Ruoff, R. S. *Science* **2000**. *287*, 637.

8. Iijima, S. *Nature*, **1991**, *354*, 56.

9. Chan. C. M.; Wu, J.; Li, J. X.; Cheung, Y. K. *Polymer* **2002**, *43*, 2981.

10. Musto, P.; Ragosta, G.; Scarinzi, S.; Mascia, L. *Polymer* **2004**, *45*, 4265.

11. Petrovic, Z. S.; Javni, I.; Waddon, A.; Banhegyi, G. *J. Appl. Polym. Sci.* **2000**, *76*, 133.

12. Okada, A.; Kawasumi, M.; Usuki, A.; Kojima, Y.; Kurauchi, T.; Kamigaito, O. *MRS Symposium Proceedings. Pittsburgh*, **1990**, *171*, 45.

13. Vaia. R. A.; Ishii, H.; Giannelis, E. P. *Chem. Mater.* **1993**, *5*, 1694.

14. Okada, A.; Usuki, A. *Macromol. Mater. Eng.* **2006**, *291*, 1449.

15. Tjong, S. C. *Mater. Sci. Eng. R.* **2006**, *53*, 73.

16. Ray, S. S.; Okamoto, M. *Prog. Polym. Sci.* **2003**, *28*, 1539.

17. Alexandre, M.; Dubois, P. *Mater. Sci. Eng. R.* **2000**, *28*, 1.

18. Carastan, D. J.; Demarquette, N. R. Int. Mat. Rev. **2007**, *52*, 345.

19. Kawasumi, M. *J. Polym. Sci., Part A: Polym. Chem.* **2004**, *42*, 819.

20. Zanetti, M.; Lomakina, S.; Camino, G. *Macromol. Mater. Eng.* **2000**, *279*, 1.

21. Bailey, S. W.: Structures of layer silicates, in: G.W. Brindley, G. Brown (Eds.), Crystal Structures of Clay Minerals and Their X-ray Identifications, Monograph No. 5, Mineralogical Society, London, **1980**, 1–123.

22. Moore, D. M.; Reynolds, R. C. X-ray Diffraction and the Identification and Analysis of Clay Analysis of Clay Minerals, Oxford University Press, Oxford, **1997**, 104–120.

23. Osman, M. A.; Ploetze, M.; Skrabal, P. *J. Phys. Chem. B* **2004**, *108*, 2580.

24. Fornes, T. D.; Yoon, P. J.; Hunter, D. L.; Keskula, H.; Paul, D. R. *Polymer* **2002**, *43*, 5915.

25. Fu, X. A.; Qutubuddin, S. *J. Colloid Interface Sci.* **2005**, *283*, 373.

26. Krishnamoorti, R.; Vaia R. A.; Giannelis, E. P.; *Chem. Mater.* **1996**, *8*, 1728.

27. Lagaly, G. *Solid State Ionics*, **1986**, *22*, 43.

28. Vaia, R. A.; Telokolsky, R. K.; Giannelis, E. P. *Chem. Mater*, **1994**, *6*, 1017.

29. Aranda, P.; Ruiz-Hitzky, E. *Chem. Mater.* **1992**, *4*, 1395.

30. Greenland, D. J. *J. Colloid Sci.* **1963**, *18*, 647.

31. Francis, C. W. *Soil Sci.* **1973**, *115*, 40.

32. Parfitt, R. L.; Greenland, D. J. *Clay Miner* **1970**, *8*, 305.

33. Jimenez, G.; Ogata, N.; Kawai, H.; Ogihara, T. *J. Appl. Polym. Sci.* **1997**, *64*, 2211.

34. Ogata, N.; Jimenez, G.; Kawai, H.; Ogihara, T. *J. Polym. Sci., Part. B: Polym. Phys.* **1997**, *35*, 389.

35. Jeon, H. G.; Jung, H, T.; Lee, S. W.; Hudson, S. D. *Polym. Bull.* **1998**, *41*, 107.

36. Vaia, R. A.; Giannelis, E. P. *Macromolecules* **1997**, *30*, 7990.

37. Chen, T. K.; Tien, Y. I.; Wei, K. H. *J. Polym. Sci., Part A: Polym. Chem.* **1999**, *37*, 2225.

38. Okamoto, M.; Morita, S.; Taguchi, H.; Kim, Y. H.; Kotaka, T.; Tateyama, H. *Polymer* **2000**, *41*, 3887.

39. Okamoto, M.; Morita, S.; Kotaka, T. *Polymer* **2001**, *42*, 2685.

40. Tudor, J.; Willington, L.; O'Hare, D.; Royan, B. *Chem. Commun.* **1996**, 2031.

41. Bergman, J. S.; Chen, H.; Giannelis, E. P.; Thomas, M. G.; Coates, G. W. *J. Chem. Soc. Chem. Commun.* **1999**, *21*, 2179.

42. Imai, Y.; Nishimura, S.; Abe, E.; Tateyama, H.; Abiko, A.; Yamaguchi, A.; Aoyama, T.; Taguchi, H. *Chem. Mater.* **2002**, *14*, 477.

43. Lee, J.; Yee, A. F. *Polymer* **2000**, *41*, 8363.

44. Vaia, R. A.; Jant, K. D.; Kramer, E. J.; Giannelis, E. P. *Chem. Mater.* **1996**, *8*, 2628.

45. Giannelis, E. P. *Adv. Mater.* **1996**, *8*, 29.

46. Giannelis, E. P.; Krishnamoorti, R.; Manias, E., *Adv. Polym. Sci.*, **1999**, *138*, 107.

47. Ray, S. S.; Yamada, K.; Okamoto, M.; Ueda, K. *Polymer* **2003**, *44*, 857.

48. Zilg, C.; Mulhaupt, R.; Finter, *J. Macromol. Chem. Phys.* **1999**, *200*, 661.

49. Wang, Z.; Lan, T.; Pinnavaia, T. J. *Chem. Mater.* **1996**, *8*, 2200.

50. Blumstein, A. *J. Polym. Sci. A* **1965**, 3, 2665.

51. Gilman, J. W.; Ksahiwagi, T.; Giannelis, E. P.; Manias, E.; Lomakin, S.; Lichtenhan, J. D.; Jones, P. Flammability properties of polymer-layered silicate nanocomposites. In: Al-Malaika, S.; Golovoy, A.; Wilkie C. A. editors. Chemistry and technology of polymer additives. Oxford: Blackwell Science; **1999**.

31

52. Gilman, J. W.; Kashiwagi, T.; Lichtenhan, J. D. *SAMPE J.* **1997**, *33*, 40.

53. Fujiwara, S.; Sakamoto, T. Kokai patent no. SHO511976-109998; **1976**.

54. Zhu, J.; Morgan, A. B.; Lamelas, F. J.; Wilkie, C. A. *Chem. Mater.* **2001**, *13*, 3774.

55. Yano, K.; Usuki, A.; Okada, A.; Kurauchi, T.; Kamigaito, O. *Polym. Prepr. (Jpn).* **1991**, *32*, 65.

56. Yano, K.; Usuki, A.; Okada, A. *J. Polym. Sci., Part A: Polym. Chem.* **1997**, *35*, 2289.

57. Tetto, J. A.; Steeves, D. M.; Welsh, E. A.; Powell, B. E. *ANTEC'99*, 1628.

58. Lee, S. R.; Park, H. M.; Lim, H. L.; Kang, T.; Li, X.; Cho, W. J.; Ha C. S. *Polymer* **2002**, *43*, 2495.

59. Nam, P. H.; Maiti, P.; Okamoto, M.; Kotaka, T. *Proceeding Nanocomposites*, June 25–27, 2001, Chicago,Illinois, USA; ECM Publication; **2001**.

60. Kim, J. W.; Kim, S. G.; Choi, H. J.; Jhon, M. S. *Macromol. Rapid. Commun.* **1999**, *20*, 450.

61. Zeng, C.; Han, X.; Lee, L. J.; Koelling, K. W.; David, L.; Tomasko, *Adv. Mater.* **2003**, *15*, 1743.

62. Harikrishnan, G.; Patro, T. U.; Khakhar, D. V.; *Ind. Eng. Chem. Res.* **2006**, *45*, 7126.

63. Haraguchi, K.; Matsuda, K. *Chem. Mater.* **2005,** *17*, 931.

64. Haraguchi, K.; Li, H. J. *Macromolecules* **2006**, *39*, 1898.

65. Herrera, N. N.; Putaux, J. L.; David, L.; Haas, F. D.; Lami, E. B. *Macromol. Rap. Commun.* **2007**, *28*, 1567.

66. Caruso, R. A.; Susha, A.; Caruso, F. *Chem. Mater.* **2001,** *13*, 400.

67. Toombes, G. E. S.; Mahajan, S.; Thomas, M.; Du, P.; Tate, M. W.; Gruner, S. M.; Wiesner, U. *Chem. Mater.* **2008**, *20*, 3278.

68. Lee, S. R.; Park, H. M.; Lim, H. L.; Kang, T.; Li, X.; Cho, W. J.; Ha, C. S.; *Polymer* **2002**, *43*, 2495.

69. Vanderhart, D. L.; Asano, A.; Gilman, J. W. *Chem. Mater.* **2001**, *13*, 3796.

70. Gelfer, M.; Burger, C.; Fadeev, A.; Sics, I.; Chu, B.; Hsiao, B.S.; Heintz, A.; Kojo, K.; Hsu, S. L.; Si, M.; Rafailovich, M. *Langmuir* **2004**, *20*, 3746.

71. Xie, W.; Gao, Z.; Pan, W-P.; Hunter, D.; Singh, A.; Vaia, R. *Chem. Mater.* **2001**, *13*, 2979.

72. Rossi, G. B.; Beaucage, G.; Dang, T. D.; Vaia, R. A. *Nano Lett.* **2002**, *2*, 319.

73. Carrado, K. A.; Xu, L. *Chem. Mater.* **1998**, *10*, 1440.

74. Ijdo, W. L.; Pinnavaia, T. J. *J. Solid State Chem.* **1998**, *139*, 281.

75. Lan, T.; Kaviratna, P. D.; Pinnavaia, T. J. *J. Phys. Chem. Solids* **1996**, *57*, 1005.

76. Gilman, J. W.; Morgan, A. B.; Harris, R. H.; Trulove, P. C.; DeLong, H. C.; Sutto, T. E. *Polym. Mater. Sci. Eng.* **2000**, *83*, 59.

77. Yeh, J. M.; Liou, S. J.; Lin, C. Y.; Cheng, C. Y.; Chang, Y. W.; Lee, K. R. *Chem. Mater.* **2002**, *14*, 154.

78. Zhu, J.; Morgan, A. B.; Lamelas, F. J.; Wilkie, C. A. *Chem. Mater.* **2001**, *13*, 3774.

79. Yei, D. R.; Kuo, S. W.; Su, Y. C.; Chang, F. C. *Polymer* **2004**, *45*, 2633.

80. Liu, H.; Zhang, W.; Zheng, S. *Polymer* **2005**, *46*, 157.

81. Fox, D. M.; Maupin, P. H.; Harris Jr. R. H.; Gilman, J. W.; Eldred, D. V.; Kastsoulis, D.; Trulove, P. C.; De Long, H. C. *Langmuir* **2007**, *23*, 7707.

82. Takekoshi, T.; Khouri, F. F.; Campbell, J. R.; Jordan, T. C.; Dai, K. H. *U.S. Patent* 5,707,439, **1998**.

83. Gilman, J. W.; Awad, W. H.; Davis, R. D.; Shields, J.; Harris Jr. R. H.; Davis, C.; Morgan, A. B.; Sutto, T. E.; Callahan, J.; Trulove, P. C.; DeLong, H. C. *Chem. Mater.* **2002**, *14*, 3776.

84. Voronkov, M. G.; Larent' yev, V. I. *Top. Curr. Chem.* **1982**, *102*, 199.

85. Feher. F. J.; Wyndham, K. D. *Chem. Commun.* **1998**, 323.

86. Zheng, L.; Farris. R. J.; Coughlin, E. B. *Macromolecules* **2001**, *34*, 8034.

87. Ni, Y.; Zheng, S. *Chem. Mater.* **2004**, *16*, 5141.

88. Madbouly, S. A.; Otaigbe, J. U.; Nanda, A. K.; Wicks, D. A. *Macromolecules*, **2005**, *38*, 4014.

89. Szabo, A.; Gournis, D.; Karakassides, M. A.; Petridis, D. *Chem. Mater.* **1998**, *10*, 639.

90. Wan, C.; Zhao, F.; Bao, X.; Kandasubramanian, B.; Duggan, M. *J. Phys. Chem. B* **2008**, *112*, 11915.

Chapter 2

Polyhedral Oligomeric Silsesquioxane (POSS)-Modified Organoclays using POSS Solution from Hydrolytic Co-condensation of 3-Aminopropyltriethoxysilane and Vinyltriethoxysilane

Chapter 2 presents synthesis of POSS-modified organoclays having reactive vinyl groups using POSS derived from hydrolytic co-condensation of 3-aminopropyl triethoxysilane (AS) and vinyltriethoxysilane (VS). Effect of AS:VS mole ratio on the structure and properties of POSS-modified organoclays is investigated.

2.1 Introduction

Hydrolytic condensation of trifunctional organosilanes $XSiY_3$ where X being a non-hydrolysable group and Y being an easily hydrolysable group, e.g. $-OCH_3$ or $-Cl$ is the widely accepted method for the synthesis of Polyhedral Oligomeric Silsesquioxane (POSS).[1] Under controlled reaction conditions, the method yields octameric POSS cubes in good quantity. Synthesis of heterosubstituted POSS through hydrolytic poly condensation from mixtures of silanes was described by Voronkov and Larent'ev.[2] When hydrolytic condensation of $XSiY_3$ yield homosubstituted POSS, having general formula of $(RSiO_{1.5})_8$, hydrolytic co-condensation of a mixture of $XSiY_3$ and $X'SiY_3$ monomers usually gives heterosubstituted POSS, having general formula of $X_nX'_{8-n}(SiO_{1.5})_8$ where n vary from 0 to 8 which depends mainly on the molar ratio and reactivity of the initial organosilane monomer. In the case of an equimolar ratio of both monomers and similar rates of hydrolysis, POSS with an equal number of X and X', $X_4X'_4(SiO_{1.5})_8$, is formed in highest yield. Variations in the molar ratio of the organosilane monomers give rise to different products and yields. Thus, the $XSiY_3$-$X'SiY_3$ co-hydrolysis in the molar ratio 1:7 leads to the formation of $XX'_7(SiO1.5)_8$ in maximum yield.

In the present study, attempt has been made to produce POSS having both amino and vinyl groups by hydrolytic co-condensation of a mixture of 3-aminopropyltriethoxysilane (AS) and vinyltriethoxysilane (VS) in ethanol/water mixture (14:1 v/v ratio). Aminopropyl groups on POSS ensure cationic centre essential for exchange reaction with clay and vinyl groups will provide reactive groups towards olefinic monomers. Effect of AS:VS mole ratio on the structure and properties of POSS-modified organoclays is presented in chapter 2.

2.2 Experimental

2.2.1. Materials

The clay used in this work was Cloisite-Na$^+$ (Cation exchange capacity (CEC) 92.6 mequiv/ 100g) from Southern Clay Products. 3-aminopropyltriethoxysilane (AS, 99%) and vinyltriethoxysilane (VS, 97%) were purchased from Aldrich Chemicals. Polyester resin (isophthalic, unsaturated), MEK-peroxide (initiator) and Cobalt naphthanate (accelerator) were purchased locally. Benzoyl peroxide and absolute ethanol was purchased from S.d Fine Chem Limited, India. Millipore grade water was used.

2.2.2. Preparation of POSS Solutions

POSS solutions from AS/VS compositions were prepared by following the procedure reported for the preparation of octa-aminopropyl POSS.[3] A premix of AS and VS of desired composition was diluted with ethanol-water mixture (v/v = 14/1) to a concentration of 0.45 M and the solutions were aged at ambient conditions for at least seven days. AS:VS mole ratio was varied between 1:0 and 1:7. The solutions from VS/AS mole ratio >3 produced gels upon aging and hence omitted from further analysis since it was not useful for intercalation reactions in aqueous medium. The POSS-organomodifiers were represented in general as Oxy where x represents number of aminopropyl group on the POSS and y, the number of vinyl groups with approximation that eight functional groups on the POSS is in the same ratio as in the organosilane mixture.[2] The silane compositions obtained from AS:VS mole ratio of 3:1, 1.5:1, 1:1, 1:1.5, 1:3 are respectively designated as O62, O53, O44, O35 and O26. For comparative purpose, octaaminopropyl POSS (O80) from AS was also prepared.

37

2.2.3. Synthesis of POSS-Modified Organoclay

POSS-modified organoclays were prepared by reacting aqueous clay suspension (0.5 wt %) with calculated amount of POSS solution (equivalent to 2*CEC of the clay with respect to amine content) at ambient conditions for 48 hrs, under stirring. The POSS solutions were acidified with dilute HCl, sufficient for protonating the amino groups. Modified clays were separated by centrifugation, washed with ethanol by re-dispersing, separated by centrifugation and finally dried in vacuum at 80 °C. The POSS-modified organoclays from the AS/VS compositions O80, O62, O53, O44, O35 and O26 are referred, respectively as OC80, OC62, OC53, OC44, OC35 and OC26 (in general OCs).

2.2.4. Characterization

POSS-modified clays were characterized using ^{29}Si and ^{13}C NMR, FT-IR, TGA, XRD and CHN elemental analysis. Solid state ^{29}Si and ^{13}C NMR spectra were recorded on a Bruker DRX-500 spectrometer operated at a frequency of 59 MHz and 75 MHz, respectively using broad-band CP/MAS probe. Samples were spun at 8 or 10 kHz using 4 mm zirconia rotors. The spectra were referenced externally to TEOS at -82.4 ppm for ^{29}Si and to methane carbon at 29.46 ppm of adamantine for ^{13}C NMR. FT-IR measurements were made on a Perkin-Elmer Spectrum one spectrophotometer in the range of 4000-400 cm^{-1} using KBr pellets containing ca. 2 wt % sample. X-ray powder diffraction (XRD) data were collected on a Philips X'pert Pro X-ray diffractometer equipped with graphite monochromator and X'celerator detector. The tests were carried out in reflection mode using nickel filtered CuKα_1 (λ= 0.15405 nm) radiation. The measurements were performed over a 2θ range of 2° to 14° using a step size of 0.033°. Thermogravimetric analysis was performed on a TGA-50 (Shimadzu)

38

thermogravimetric analyzer employing a heating rate of 10 °C/min from 40 to 800 °C under a nitrogen flow of 20 mL/min. Elemental analysis was performed on a Perkin Elmer Series II CHN analyzer and the vinyl/aminopropyl ratio was calculated from the C/N ratio. Dispersion characteristics of the POSS-modified clays were characterized by preparing composite films (generally referred as ONCs) with polyester resin. Generally composite films were prepared by soaking the modified clay (5 wt %) for overnight in commercial unsaturated isophthalic polyester laminating resin, dispersing by vigorous stirring and cured at room temperature after mixing with MEK- peroxide (initiator) and cobalt naphthanate (accelerator). The films were post-cured at 100 °C for 2 hrs.

2.3. Results and Discussion

2.3.1. Nature of POSS Solutions

AS/VS compositions in alcohol-water mixture can undergo hydrolytic condensation without an external catalyst, owing to the internal catalytic activity of the basic alkyl amino group of AS which upon reacting with water produces nucleophilic OH^-. Hydrolytic co-condensation of a mixture of $XSiY_3$ and $X'SiY_3$ monomers usually gives heterosubstituted POSS, having general formula of $X_nX'_{8-n}(SiO_{1.5})_8$ where n vary from 0 to 8 which depends mainly on the molar ratio and reactivity of the initial monomers.[2] Therefore POSS cages produced from AS:VS mole ratio between 3:1 and 1:3 contain vinyl and aminopropyl groups predominantly in the same mole ratio. The aged solutions of AS/VS compositions of AS:VS mole ratio up to 1:3 was stable when neutralized with dilute HCl for producing POSS ammonium for facilitating cation exchange reactions with the clay. The solutions of VS/AS ratio >3 produced gel upon aging and hence omitted from further analysis as it was not useful for intercalation reactions in aqueous media.

However, drying of POSS solution yielded solids insoluble in common organic solvents and showed IR spectral features of typical POSS containing siloxane polymer. It indicates that the POSS molecules become unstable when the solvent is removed under the given preparative method, as reported for base-catalyzed hydrolytic condensation mechanism. Base-catalyzed hydrolytic condensation reactions are 'thermodyanamically controlled' since the formation and hydrolytic cleavage of Si-O-Si linkages are facile. This prevented the separation and identification of the POSS molecules derived from the AS/VS compositions using common characterization

techniques like GPC and ^{29}Si NMR. However, octaaminopropyl POSS was stable when intercalated in the clay.[3] Therefore, evidences for the formation of POSS molecules from AS/VS compositions and the possible variations in their structure were derived from the characterization of the POSS-modified clays.

2.3.2. Nature of the POSS-Modified Clays

POSS solutions from AS:VS mole ratio between 3:1 and 1:3 were used for preparing POSS-modified clays. When the hydrolyzed siloxane solutions were added to aqueous clay suspension, the clay particles tended to flocculate in the medium. Upon drying, OC80 formed hard agglomerate because tethering of the adjacent clay layers by the amino groups around the POSS molecule prevented its dispersion in polymer. Whereas OC44, OC35 and OC26 yielded soft powder, dispersible in common organic solvents and monomers, OC62 and OC35 also resisted dispersion. Thus POSS-modified clays from VS/AS ratio <1 was not suitable for the preparation of nanocomposite and OC44, OC35 and OC26 were characterized for its structure and dispersibility. OC80 was analyzed as the standard for comparison.

2.3.2.1. ^{29}Si and ^{13}C NMR

Figure 2.1 and 2.2, respectively show the ^{29}Si and ^{13}C NMR spectra of OC26 as a representative of POSS modified clays containing vinyl groups and OC80. In ^{29}Si NMR spectra, OC80 showed two peaks, at -92.1 and -69 ppm, respectively from the clay silicate layer and aminopropyl functionalized triply condensed Si of POSS.[4,5] In OC26, an additional peak at -81 ppm corresponds to vinyl functionalized triply condensed Si.[6] A similar observation was made in the ^{13}C NMR spectra, wherein OC26 showed the peaks due to vinyl group at 131 and 135 ppm, in addition to the peaks due to the aminopropyl group at 10, 22 and 44 ppm for OC80.[6,7]
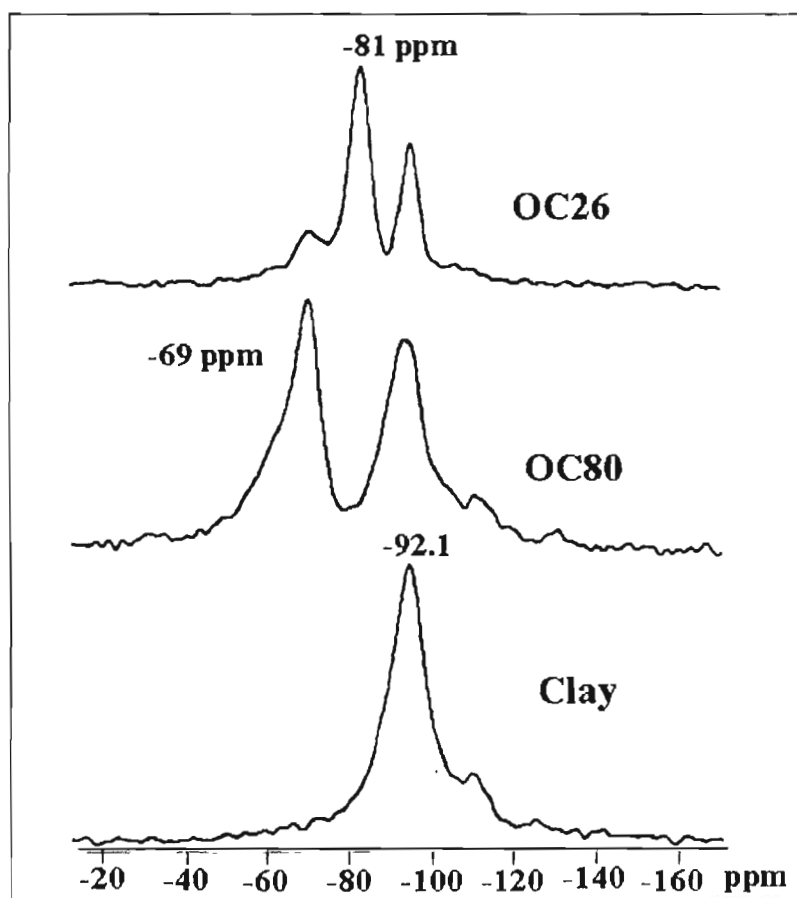
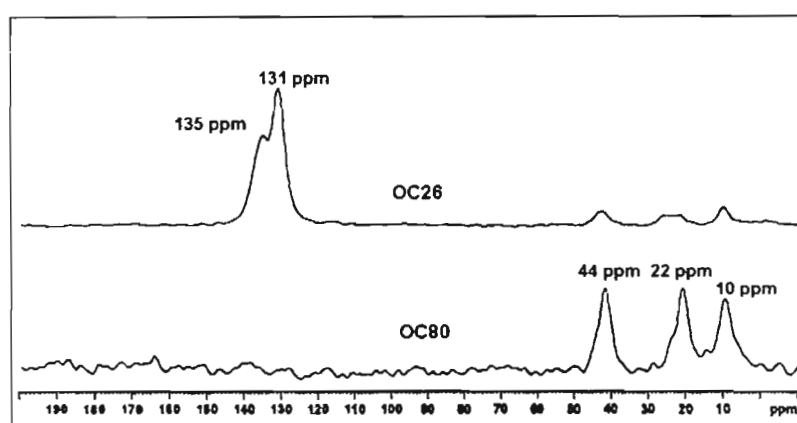**Figure 2.1.** *^{29}Si NMR spectra of Cloisite-Na$^+$, OC80 and OC26.*

Figure 2.2. *^{13}C NMR spectra of OC80 and OC26.*

42

2.3.2.2. FT-IR Spectroscopy

Figure 2.3 shows the FT-IR spectra of the pristine clay and the modified clays. The unmodified clay showed bands due to Si–O–Si asymmetric stretching of silicate layer (1030 cm^{-1}), structural hydroxyls and adsorbed water (3300-3600 cm^{-1} and 1650 cm^{-1}). For the modified clays, additional bands appeared due to the POSS cages (Si–O–Si asymmetric stretching at 1130 cm^{-1}) and the organic functional groups. For OC80, two bands appeared due to –NH$_3^+$ vibrations. These bands, at 1490 cm^{-1} and 1574 cm^{-1}, respectively were assigned to N–H bending vibrations of –NH$_3^+$ interacting with the clay surface and the anion, –NH$_3^+$Cl$^-$.[3] This phenomenon was observed when the amount of the intercalated O80 molecules exceeded the coverage imposed by the cation exchange capacity (CEC) of the clay and intercalation of O80 by more than 1.8 times of the CEC has been reported.[3] The free space, that was available after saturation of the exchange sites of the clay with O80, could host additional molecules as physically adsorbed ion-pairs. However, IR spectra of the vinyl POSS-modified clays showed a single band for –NH$_3^+$ at 1490 cm^{-1}, indicating the absence of such physically adsorbed ion-pairs. The spectra also showed the bands due to vinyl group (-CH=CH$_2$). With decreasing number of aminopropyl group, the intensity of the bands due to C–H stretching of alkyl (2931, 2873 and 1290-1370 cm^{-1}) and N–H bending of amino group (1490 cm^{-1}) diminished and the bands due to the vinyl group (3062 and 3025 cm^{-1} for C–H stretching, 1603 cm^{-1} for C=C stretching and 1410 cm^{-1} for C–H bending) became prominent. From the intensities of the corresponding peaks, amino/vinyl ratio was found as 1:1.2, 1:1.8 and 1:2.8, respectively for OC44, OC35 and OC26, which is in agreement with the experimental ratio of 1:1, 1:1.5 and 1:3.
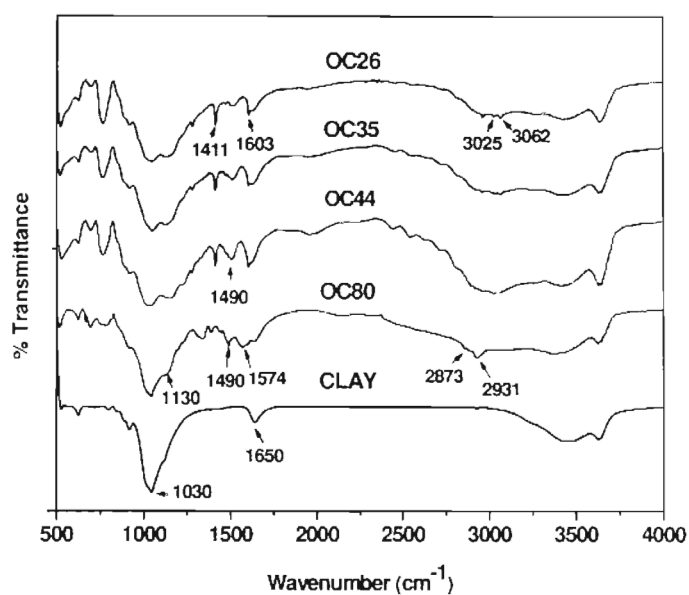
Figure 2.3. *FT-IR spectra of Clay, OC80, OC44, OC35 and OC26.*

2.3.2.3. CHN Elemental Analysis

Table 2.1. *CHN elemental analysis of OC44, OC35 and OC26.*

Modified clay	% (Experimental)		C/N mole ratio	Aminopropyl/Vinyl ratio (calculated)
	Carbon	Nitrogen		
OC44	4.72	1.1	5	1:1
OC35	5.7	1.05	6.3	1:1.5
OC26	11.9	1.51	9.9	1:3.3

Table 2.1 gives the CHN elemental analysis results of OC44, OC35 and OC26.
C/N mole ratio of 5, 6.3 and 9.9 was obtained respectively for OC44, OC35 and OC26.
The results also support that hydrolytic co-condensation of AS/VS mixtures at 1:1,
1:1.5 and 1:3 mole ratio yield predominantly POSS containing aminopropyl and vinyl
groups in the same molar ratio.

2.3.2.4. Thermogravimetry

Figure 2.4 shows the thermogram of the POSS-modified clays. All the samples were thermally stable up to about 270 °C. The decomposition path followed two-step weight loss, one at 270-420 °C and the other at 420-630 °C. The former is caused by the sublimation of the POSS molecules and the latter by the production of volatiles through C-C and Si-C bond cleavage.[9,10] It can be seen that OC44, though contained significantly lower amount of POSS as inferred from CHN analysis, showed distinctly higher weight loss due to POSS sublimation when compared to OC35 and OC26. Vinyl POSS aggregates were reported to resist sublimation due to thermal polymerization through the vinyl groups leading to POSS cross-linking. Therefore, lower POSS sublimation in OC35 and OC26 could be caused by enhanced POSS-POSS interactions due to high amount of POSS.
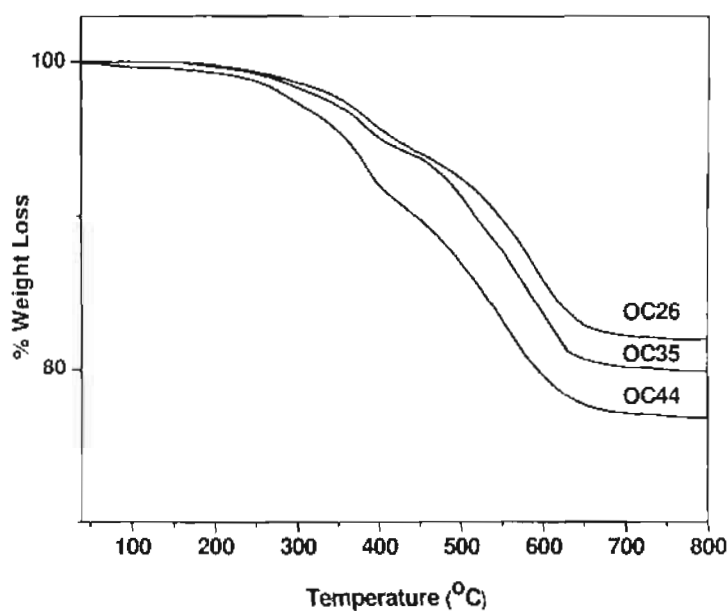

Figure 2.4. *TGA curves of OC44, OC35 and OC26.*

45

2.3.2.5. X-Ray Diffraction

Figure 2.5 shows the XRD patterns of the pristine clay and the modified clays. The pristine clay exhibited 001 reflection at 12.1 Å, whereas the modified clays showed a higher d-spacing due to intercalation of POSS. OC80 exhibited a d-spacing of 21.6 Å with additional reflections at 10.8 Å and 7.2 Å. OC44 exhibited a pattern similar to that observed for OC80, but with 001 reflection at a lower value of 20.59 Å and a corresponding 002 reflection at 10.24 Å. OC35 also showed 001 reflection at about 20.6 Å, but the reflection broadened towards lower angle apparently due to merging with an additional reflection at around 26.5 Å. In contrast, OC26 exhibited a peak at 26.35 Å.
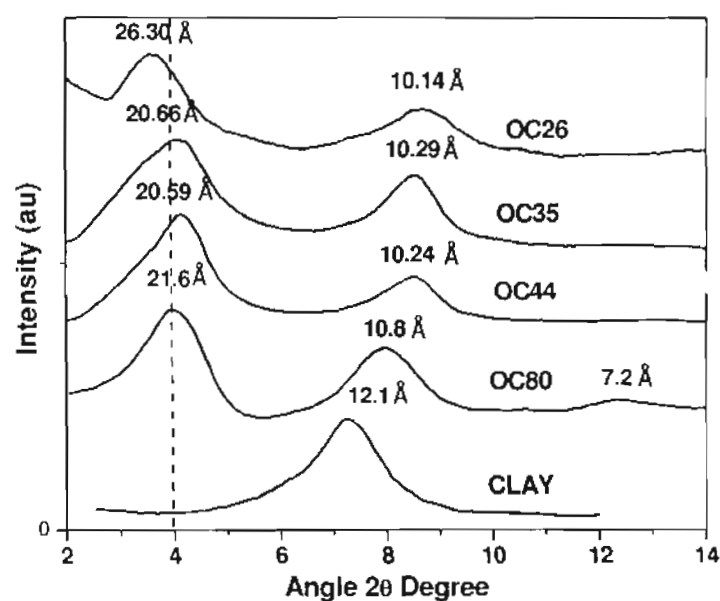

Figure 2.5. *Powder X-ray diffraction patterns of Cloisite- Na⁺, OC80, OC44, OC35 and OC26.*

Depending on the amount intercalated in the clay, POSS can take horizontal or vertical orientation, as shown in figure 2.6 for octaaminopropyl POSS.[3] For OC80, the

46

d-spacing of 21.6 Å is indicative of the clay galleries saturated with a monolayer of vertically oriented POSS molecules along with physically adsorbed ion pairs. The additional reflections observed at 10.8 Å and 7.2 Å are, respectively caused by 002 and 003 planes. Considering that the replacement of the aminopropyl groups with shorter vinyl groups would reduce the lateral dimension of oriented POSS, the observed d-spacing of 20.59 Å for OC44 can be attributed to closely packed monolayer of aminopropyl vinyl POSS. For OC26, the increase in d-spacing from 20.6 to 26.35 Å, which is by more than the size of the POSS cage (0.53 nm) is indicative of the formation of POSS-bilayer in the clay gallery. The formation of POSS-bilayer in OC26 was also evidenced from the reflection at 10.14 Å which was less than the value expected (13 Å) for 002 reflection.
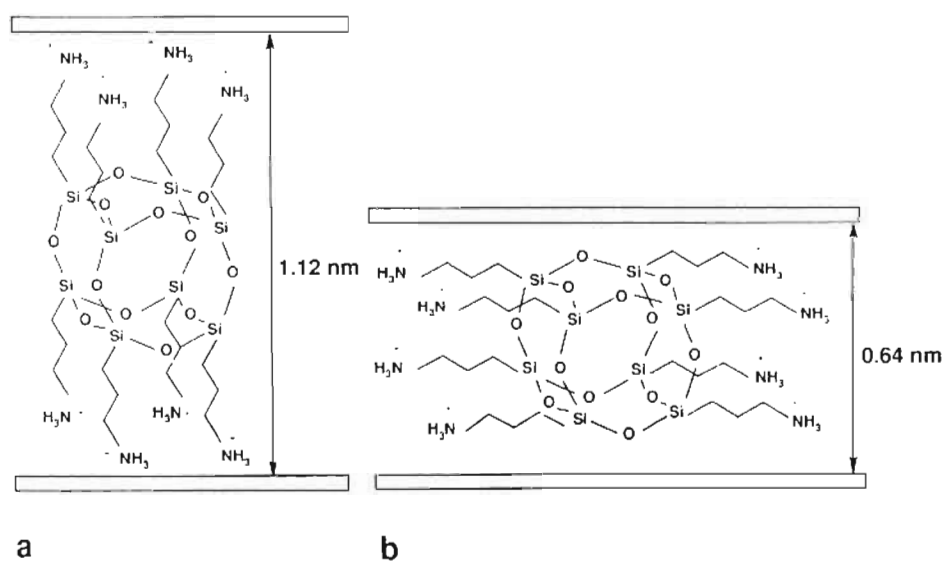

Figure 2.6. *(a) Vertical and (b) horizontal orientation of octaaminopropyl POSS molecules in the clay gallery.*[3]

POSS in its pure state will be highly crystalline and POSS cages can be treated as spheres which pack hexagonally in ABCA sequence in which spheres in one layer

lie above the interstitial spaces in adjacent layers. Corner units occupy space in the structure and prevent "close-packing" of the spheres (Figure 2.7).[11] POSS show four strong reflections at 2θ in the range of 8-20° where the reflection around 8° (d-spacing around 10 Å) is caused by size of the POSS and remaining peaks at higher 2θ's are produced by the hexagonal or rhombohedral crystalline structure of the POSS aggregates.[11]
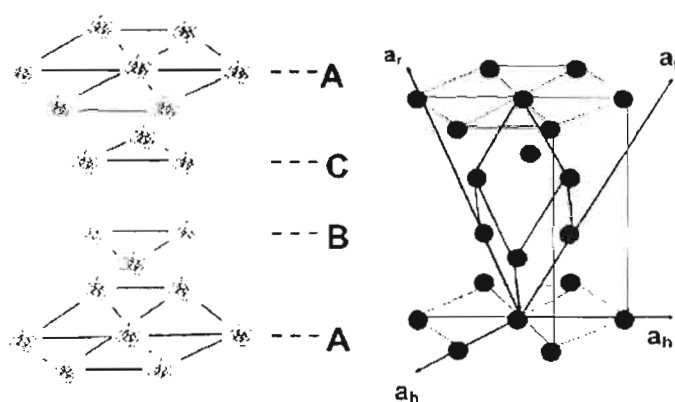
Figure 2.7. *Schematic of hexagonally packed POSS molecules. The sequence of packing in adjacent layers is ABCA.*[11]

These reflections, particularly the strongest peaks that observed around 8° and 19° were also seen in POSS-polymer nanocomposites where POSS formed two-dimensional/bilayer assembly within the polymer matrix. In isobutyl POSS-polymer nanocomposites bilayer assembly was detected by the XRD reflection at 10.8 Å and 4.66 Å.[12,13] The former was caused by the size of the POSS molecule and the latter by the two-dimensional crystal structure of the POSS aggregates.[11] Recently, the formation of POSS bilayer structure in iso-butyl POSS-imidazolium exchanged clay was also confirmed by the presence of XRD reflection at 10.8 Å.[14] Therefore, the reflection at 10.14 Å for OC26 can be assigned to the reflection caused by POSS

bilayer assembly. The reflection that was expected at about 19° for the POSS-bilayer assembly could not be detected for further confirmation due to the presence of strong hk reflections of the clay.[15]

It is evident from CHN elemental analysis that the clay absorbed increasing amounts of POSS with increase of vinyl concentration which promoted the formation of POSS-bilayer in the clay gallery. In order to confirm this, OC26 was also prepared at lower concentration of POSS solution (equivalent to CEC with respect to amine content). Figure 2.8 shows the XRD pattern obtained using POSS solution equivalent to CEC and 2xCEC. The increase in d-spacing at lower concentration of POSS (~ CEC) corresponds to the formation of POSS monolayer in the clay gallery, with a d_{001} spacing of 20.25 Å and d_{002} spacing of 10.34 Å. This again confirms that the peak at 10.14 Å for OC26 is due to POSS-bilayer arrangement. Beyond 2xCEC, no further increase in d-spacing was observed.
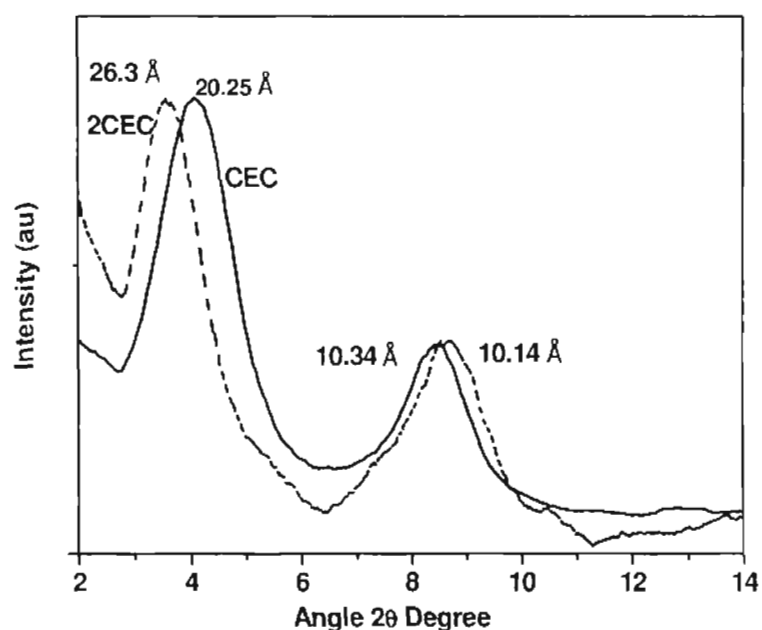
Figure 2.8. *XRD pattern of OC26 treated with POSS equivalent to CEC and 2CEC.*

2.3.2.6. Dispersion Characteristics in Polyester Resin
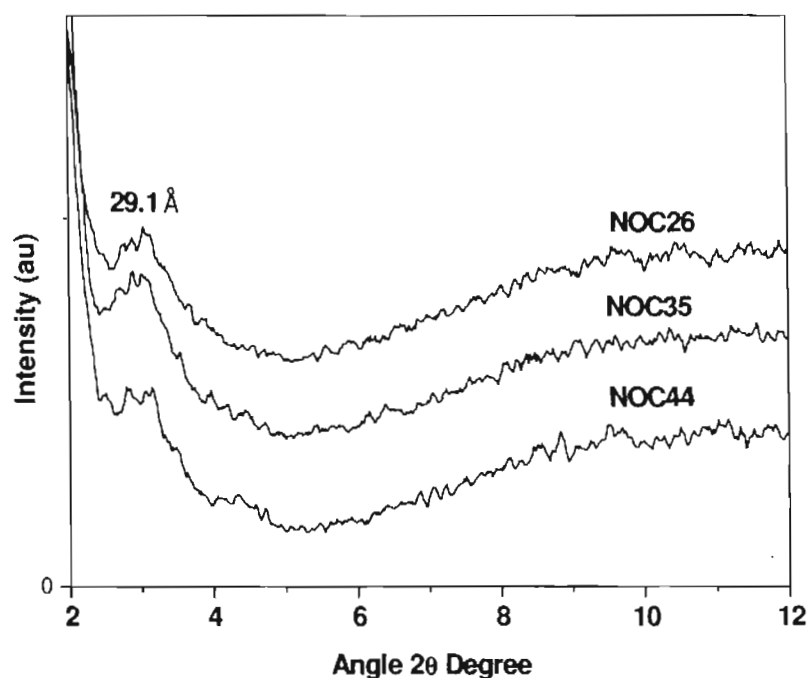
Figure 2.9. *XRD pattern of polyester composites NOC44, NOC35 and NOC26.*

Dispersibility of OCs were further assessed by making composite with a commercial polyester resin. OC80 was found not dispersible in polyester resin matrix whereas OC44, OC35 and OC26 formed intercalated nanocomposites. Figure 2.9 shows the XRD patterns of OC/polyester resin nanocomposites (NOCs) from OC44, OC35 and OC26. All the composites exhibited intercalated morphology with a d-spacing of about 29.1 Å. It indicated that both monolayer and bilayer POSS-modified clays were equally successful for the synthesis of intercalated nanocomposites. Intercalated or orderly exfoliated morphologies were generally obtained for thermoset polymer nanocomposites, which were cured under quiescent conditions, where no external force acted on the clay layers.[27] However, expansion to higher d-spacing than observed was expected because the POSS molecules provided large organic surface

(vinyl group) for high order of interaction with styrene and the unsaturated polyester. The equilibrium nature of polymer-clay nanocomposites is strongly related to the nature of the interactions occurring at the polymer-organoclay interface which depends on the nature of the polymer (polar or apolar), surface polarity of the silicate layer and structure of the surfactant molecules.[16,17] It was evident that under the given preparative technique, the geometrical constraints imparted by the rigid POSS molecules in clay gallery prevent effective polymer diffusion and complete exfoliation of the clay platelets.

2.3.2.7. Structure of POSS and POSS-Modified Clays
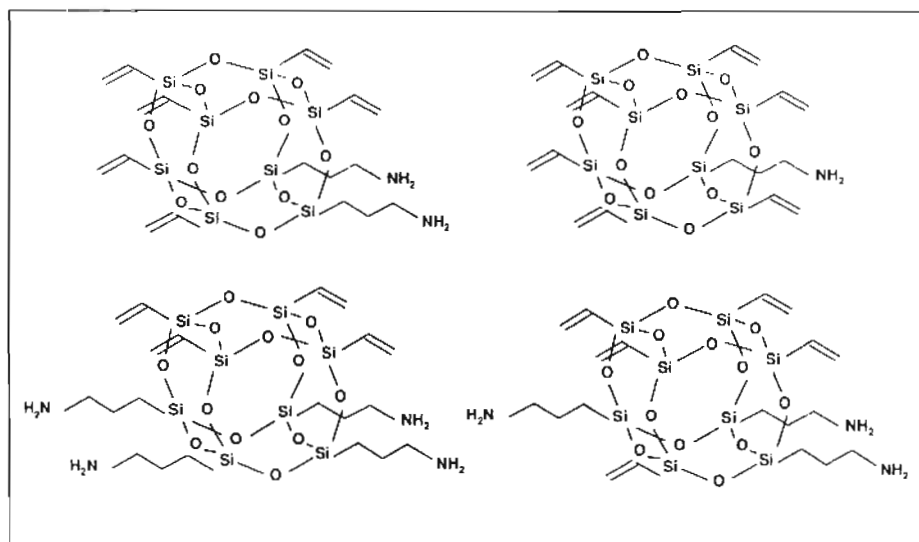
Figure 2.10. *Possible structures of POSS.*

OC44, OC35 and OC26 unlike OC80 were equally dispersible in organic solvents and polyester resin. This was possible when one face of the POSS cage was modified with the vinyl groups which could prevent the adjacent clay platelets from tethering together. Thus hydrolytic condensation reactions lead to the formation of POSS having vinyl groups in one face of the cube and the vinyl and aminopropyl

groups on the other face, however, do not prevent the formation of a mixture of tetra, tri, di and mono-aminopropyl derivatives of vinyl-POSS octamers. Figure 2.10 shows possible structures of POSS produced.
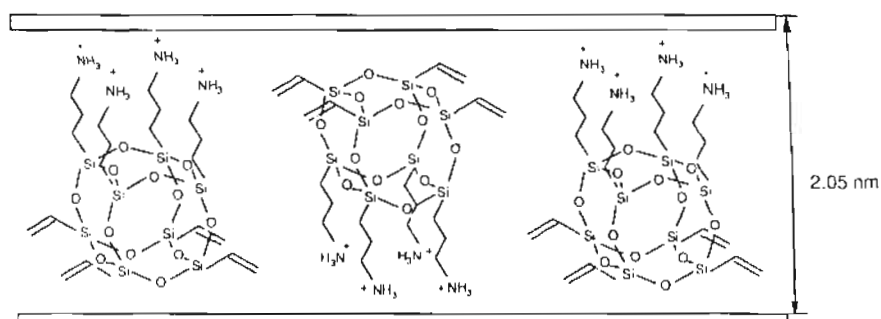
Figure 2.11. *Schematic representation of POSS monolayer in OC44.*
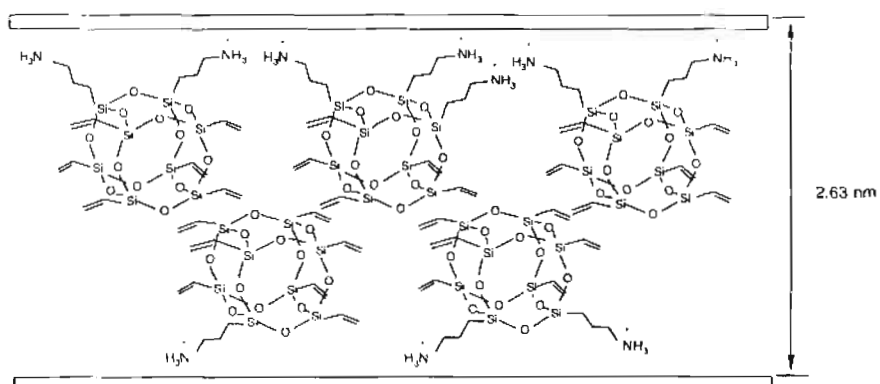
Figure 2.12. *Schematic representation of POSS bilayer in OC26.*

The cation exchange reaction is followed by progressive depletion of Na^+ from the clay. The tetra-aminopropyl POSS has exchange capacity four times higher than of the mono-aminopropyl POSS. As a result, the abosrption of POSS from the tetra-aminopropyl POSS enriched solution will be restricted to a lower amount than from the solution enriched with the mono-aminopropyl POSS. Thus in OC44, the amount of POSS absorbed might have been restricted to the formation of monolayer (Figure 2.11). Apparently, the formation of the bilayer structure (Figure 2.12) in OC26 was promoted

due to the absorption of POSS higher than the amount that could be accomodated as a monolayer. However, CEC of the clay would play a major role in the formation of POSS-bilayer structure by the above mechanism.

2.4. Conclusions

POSS-modified organoclays with reactive vinyl groups, useful for the preparation of polymer-clay nanocomposites were prepared using POSS solutions derived from hydrolytic co-condensation of mixtures of 3-aminopropyltriethoxysilane (AS) and vinyltriethoxysilane (VS). It is proposed that POSS synthesis from the AS/VS compositions occurred in a defined manner leading to the formation of mixture of tetra, tri, di and mono aminopropyl vinyl POSS. As a result, the clay absorbed increasing amounts of POSS with the increase of vinyl concentration which promoted the formation of POSS bilayer structure in the clay gallery. Both the monolayer (d-spacing 20.05 Å) and POSS-bilayer modified clays (d-spacing 26.35 Å) produced intercalated polyester resin-nanocomposites proving its non-tethered structure. The present study was aimed to provide insight into the structure of the POSS-modified organoclays and their general dispersion behaviour in polymer matrix.

2.5. References

1. Feher, F. J.; Newman, D. A. ; Walzer, J. F. *J. Am.Chem. Soc.*, **1989**, *111*, 1741.

2. Voronkov, M. G.; Larent' yev, V. I. *Top. Curr. Chem.* **1982**, *102*, 199.

3. Szabo, A.; Gournis, D.; Karakassides, M. A.; Petridis, D. *Chem. Mater.* **1998**, *10*, 639.

4. Fetter, G.; Tichit, D.; Massiami, P.; Durartre, R.; Figueras, F. Clays Clay Miner. **1994**, *42*, 161.

5. Xu, H.; Yang, B.; Wang, J.; Guang, S.; Li, C. *Macromolecules* **2005**, *38*, 10455.

6. Ek, S.; Iiskola, E. I.; Niinisto, L.; Vaittinen, J.; Pakkanen, T. T.; Keranen, J.; Auroux, A. *Langmuir* **2003**, *19*, 10601.

7. Wahab, M. A. ; Imae, I.; Kawakami, Y.; Ha, C. S. *Chem. Mater.* **2005**, *17*, 2165.

8. Farmer, V. C.; Mortland, M. M. *J. Phys. Chem.* **1965**, *69*, 683.

9. Mantz, R. A.; Jones, P. F.; Chaffee, K. P.; Lichtenhan, J. D.; Gilman, J. W.; *Chem. Mater.* **1996**, *8*, 1250.

10. Fina, A.; Tabuani, D.; Carniato, F.; Frache, A.; Boccaleri, E.; Camino, G. *Thermochimica Acta* **2006**, *440*, 36.

11. Waddon, A. J.; Coughlin, E. B. *Chem. Mater.* **2003**, *15*, 4555.

12. Zheng, L.; Waddon, A. J.; Farris, R. J.; Coghlin, E. B. *Macromolecules* **2002**, *35*, 2375.

13. Zheng, L.; Hong, S.; Cardoen, G.; Burgaz, E.; Gido, S. P.; Coughlin, E. B. *Macromolecules* **2004**, *37*, 8606.

14. Fox, D. M.; Maupin, P. H.; Harris Jr., R. H.; Gilman, J. W.; Eldred, D. V.; Kastsoulis, D.; Trulove, P. C.; De Long, H. C. *Langmuir* **2007**, *23*, 7707.

15. Alba, M. D.; Becerro, A. I.; Castro, M. A.; Perdigon, A. C. *American Mineralogist.* **2001**, *86*, 115.

16. Balazs, A. C.; Singh, C.; Zhulina, E. *Macromolecules* **1998**, *31*, 8370.

17. Vaia, R. A.; Giannellis, E. P. *Macromolecules* **1997**, *30*, 7990.

Chapter 3

Polystyrene-Clay Nanocomposite Exhibiting Solvent-assisted Self-assembling Properties

In situ intercalative polymerization of styrene with the POSS-modified clays yielded discrete nanocomposite particles which exhibited solvent-assisted self-assembling properties in solvents like THF. Chapter 3 presents a detailed investigation on the formation of nanocomposite particles, their self-assembling properties and the resultant morphologies.

3.1. Introduction

Dispersibility of POSS- monolayer and bilayer modified clays in polyester resin matrix gave insight into their structure as explained in chapter 2. The POSS-modified clays with high vinyl content can graft large amount of polymer chains through polymerization reactions involving olefinic monomers such as styrene. The use of POSS with reactive functional groups as cores to produce spherically symmetric dendrimers was reported in literature.[1-4] POSS-cored dendrimers have a relatively globular conformation and few entanglements of their branches with a high proportion of terminal functional groups positioned on the external surface of the dendrimers. Therefore the grafting of POSS-modified clays with polymer chains can produce nanocomposite particles. Chapter 3 deals with the synthesis of polystyrene-POSS-modified clay nanocomposite particles through *in situ* intercalative polymerization of styrene monomer. Interestingly the nanocomposite particles obtained after the removal of cross-linked fraction and free polymer exhibited self-assembling properties in solvents like THF to give different morphologies. A detailed investigation on the mechanism of observed concentration dependent morphological transitions is given in chapter 3.

3.2. Experimental

3.2.1. Materials

Styrene monomer was purchased from Aldrich Chemicals and benzoyl peroxide from S.d Fine Chem Ltd, India. Toluene and methanol were of extra pure grade and tetrahydrofuran of HPLC grade from Merck Specialties Pvt. Ltd, India. Styrene was washed with 5 % sodium hydroxide solution to remove the inhibitor, followed by repeated washing with distilled water to remove the alkali and finally distilled under reduced pressure. The inhibitor free monomer was stored under ice-cold conditions.

3.2.2. Synthesis of Polystyrene-Clay Nanocomposite

Polystyrene-clay nanocomposite was synthesized by in situ intercalative polymerization of styrene with the POSS modified organoclay. Nanocomposites using different loading of the modified-clay (1, 5, 10 and 15 wt % of the monomer) were synthesized by the following procedure. Desired amount of the modified-clay was dispersed in styrene by sonication, added benzoyl peroxide (2 wt % of the monomer) and, under nitrogen atmosphere and magnetic stirring (100 rpm), heated at 70 °C for 30-60 minutes to form a soft gel and then at 90 °C for 12 hours to obtain the nanocomposite. Any free polymer present was removed by soxhlet extraction of the nanocomposite using toluene. The residue was dispersed in toluene, centrifuged to remove insoluble/suspended particles and the soluble fraction was then precipitated by adding methanol, filtered and dried at 100 °C in vacuum.

3.2.3. Characterization

The nanocomposites were characterized using X-ray diffraction (XRD), thermogravimetry (TG), dynamic light scattering (DLS), optical transmission

57

microscopy (OTM), scanning electron microscopy (SEM), transmission electron microscopy (TEM) and atomic force microscopy (AFM). Samples for SEM and OTM were prepared by drop-casting dilute solutions of NC in THF with concentrations in the range of 0.001-50 mgmL^{-1}, on glass slides followed by evaporation of the solvent at ambient temperature. The samples were prepared on Formvar coated copper grid for TEM analysis and on mica sheet for AFM. All the samples were dried at ambient conditions for overnight. OTM photographs were taken using Leica DMRX Microscope. SEM images were taken in JEOL JSM-5600 LV scanning electron microscope using samples provided with a thin gold coating using JEOL JFC-1200 fine coater. TEM analysis was performed in FEI, TECNAI 30G^2 S-TWIN microscope at an accelerating voltage of 100 kV. DLS measurements were done in Nano ZS Malvern instrument employing a 4 mW He-Ne laser (λ = 632.8 nm) and equipped with a thermostated sample chamber. AFM images were recorded under ambient conditions using a Digital Instrument Ntegra operating in the tapping mode regime using microfabricated silicon cantilever tops (MPP-11100-10) with a resonance frequency of 299 kHz and a spring constant of 20-80 Nm^{-1}. TGA was performed on a TGA-50 (Shimadzu) thermogravimetric analyzer employing a heating rate of 10 °C/min. XRD data were collected on a Philips X'pert Pro X-ray diffractometer equipped with graphite monochromator and X'celerator detector. Differential scanning calorimetry was performed using Perkin Elmer Pyris 6 DSC calibrated using indium as standard and glass transition temperature was measured on second heating. Dye-encapsulated vesicles were characterized using Leica DM LB2 fluorescence microscope.

3.3. Results and Discussion

As experimentally observed, the nanocomposite by the *in situ* intercalative polymerization, after removing the free polymer, contained soluble and insoluble fractions in toluene. The nanocomposites using the POSS-bilayer modified clay when compared to those from POSS-monolayer modified clay, showed relatively higher yield of the soluble fraction, hereafter referred as NC, which exhibited solvent-assisted self-assembling properties. This can be due to high vinyl content of POSS-bilayer modified clay. Hence, NC from the POSS-bilayer modified clay (OC26) was used for further studies. Table 3.1 shows the variation in the yield of NC with the amount of POSS-bilayer modified clay. The yield of NC increased with the modified-clay loading, to a maximum of 73.3 % at 10 wt % loading, and then decreased at higher loading. It was observed that the amount of free polymer decreased and the insoluble fraction increased with the modified-clay loading. The low yield for 1 wt % loading was due to free polymer whereas the loss above 5 wt % loading was due to the insoluble fraction.

Table 3.1. Variation of yield and inorganic content of NC with modified-clay loading

Loading w.r.t weight of styrene monomer (wt %)	Yield of Nanocomposite (%)	Inorganic content (wt %) (TGA residue at 700 °C)
1	43.2	~ 2.5
5	50.1	~ 2.69
10	73.3	~ 3.2
15	56.3	~ 3.3

Table 3.1 also shows the inorganic content of NCs, as measured from TGA residue at 700 °C. A typical thermogram of NC is shown in Figure 3.1. The NC was thermally stable up to 270 °C. Interestingly, the NCs prepared from different modified-

clay loading showed inorganic content in a close range of 2.5 to 3.3 wt %. NC showed a glass transition temperature of 86.2 °C as measured from differential scanning calorigram (Figure 3.2).
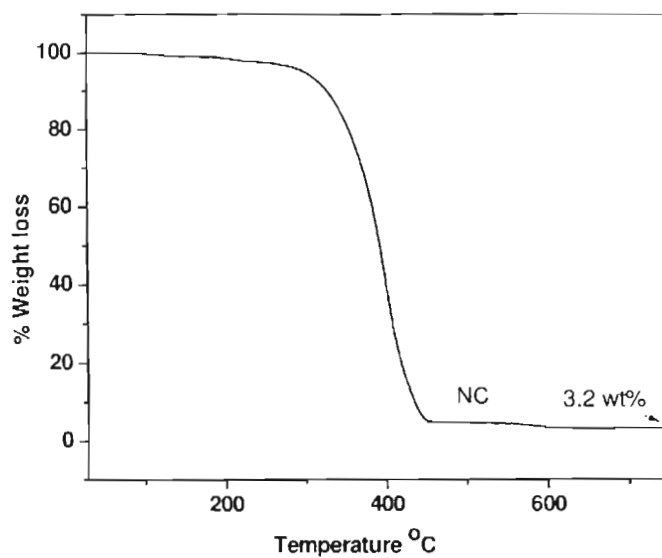

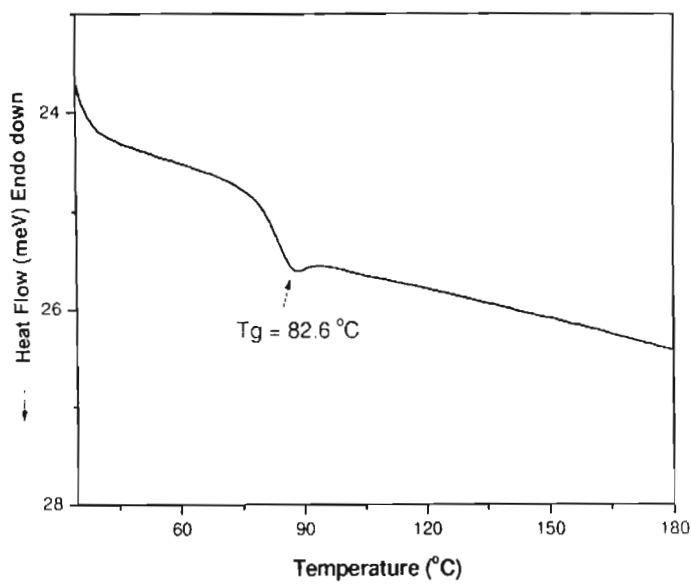**Figure 3.1.** *A typical thermogram of NC.*

Figure 3.2. *Differential scanning calorigram of NC.*

Figure 3.3 shows the XRD pattern of NC. The NC exhibited intercalated morphology, as observed earlier for polyester based nanocomposite, with a d-spacing of 29.35 Å, disrupting the crystalline nature of the POSS-bilayer assembly.
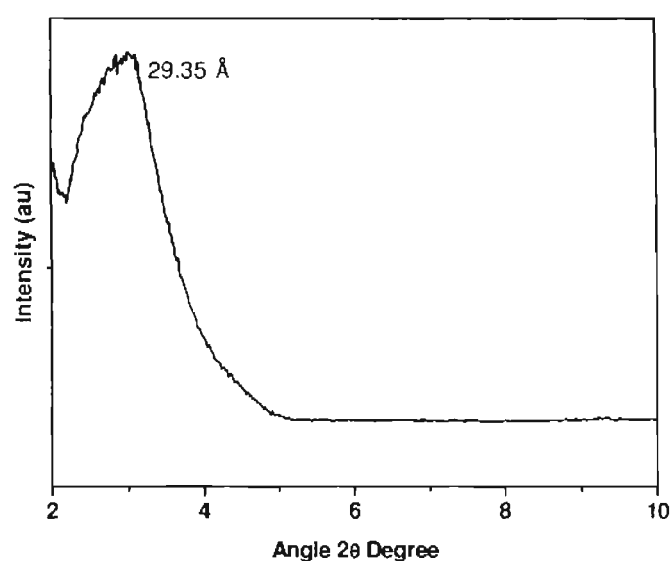

Figure 3.3. *XRD pattern of NC.*

3.3.1. Particulate Nature of NC

NC exhibited particulate nature as characterized by SEM, TEM and AFM. Figure 3.4a and b respectively show the SEM and TEM of samples prepared by drop-casting and drying of a dilute solution of NC (0.001 mgmL^{-1}) in tetrahydrofuran (THF). The particle size varied in the range of 190-810 nm, as measured from the images. The particles that appeared as spherical in nature in SEM appeared flat in TEM, possibly due to the effect of substrate surface used for the preparation of the samples. This prompted us to examine the particle morphology by AFM. Figure 3.5 shows the AFM image of NC particles. Cross-sectional analysis revealed anisotropic nature of the particles with thickness significantly lower than the lateral dimension. A typical particle having lateral dimension of 600 nm showed a thickness of 120 nm. Also, the

61

particle on the mica surface showed surface contour resembling that of a deformed spherical particle.
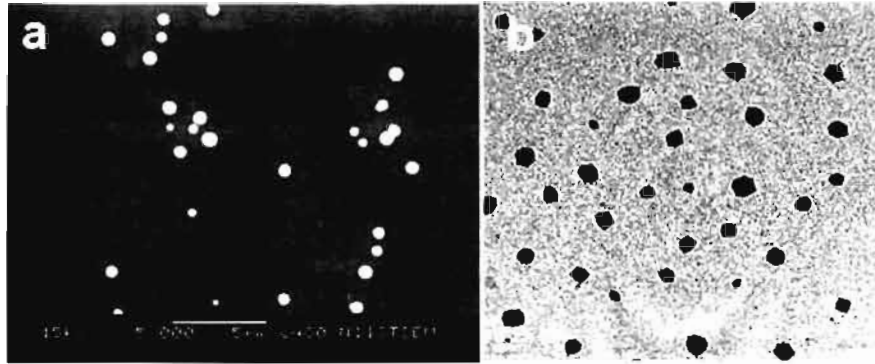
Figure 3.4. *(a) SEM and (b) TEM images of NC particles drop-cast from THF of solution concentration of 0.001 mgmL^{-1}.*
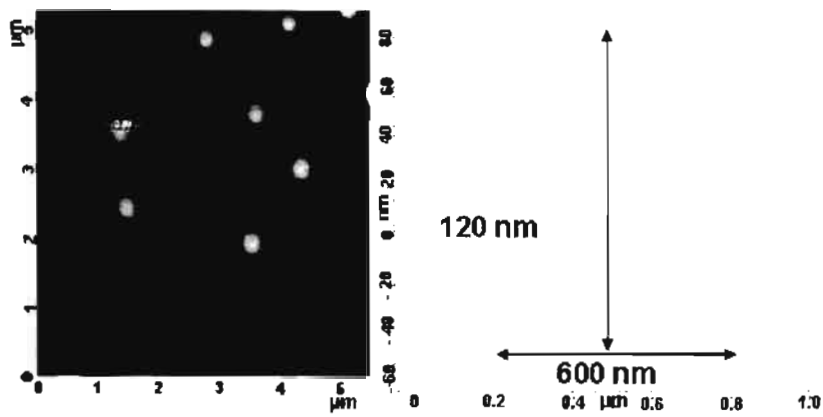
Figure 3.5. *Tapping mode AFM image and cross-sectional analysis of NC particles.*

3.3.2. Concentration Dependent Self-assembling Properties of NC Particles

The residue that was prepared by drop-casting solutions of NC in THF at different concentrations showed different dimensions and morphological features, indicating the possibility of self-assembly of the particles in the solution or during drying. Dynamic light scattering (DLS) provides a method for analyzing the association of particles in solution. Figure 3.6 shows DLS histogram of NC solutions in THF at two

different concentrations. From the figure, it can be seen that the particles at solution concentration of 0.001 mgmL⁻¹ showed an average hydrodynamic diameter of 550 nm. On the other hand, the particles at higher solution concentration of 1 mgmL⁻¹ showed additional bands due to particle size of 2-3.5 μm, indicating its self-aggregation properties in THF solution.
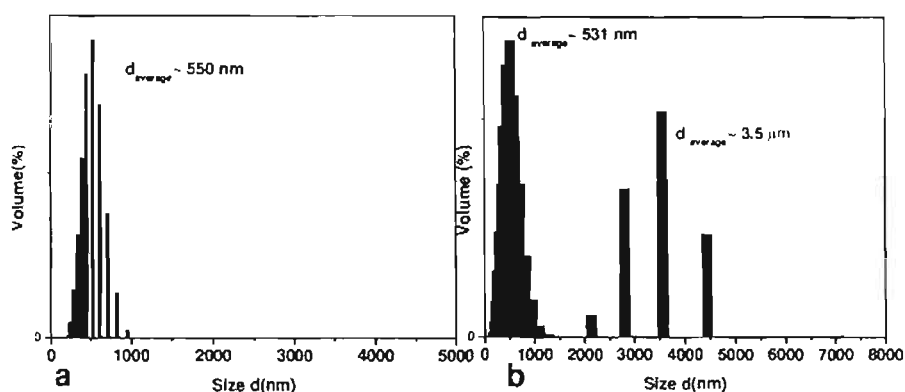
Figure 3.6. *DLS histograms of NC samples in THF at solution concentration of (a) 0.001 mgmL⁻¹ and (b) 1 mgmL⁻¹.*

DLS measurements showed erratic results as the particle concentration increased. Also, the aggregation property was solvent specific that the property was observed in solvents such as tetrahydrofuran, but not in solvent like toluene. Therefore, concentration dependent aggregation and morphological transitions were studied in detail by observing the change in the microscopic features of drop-cast residues with increasing concentrations of NC solutions in THF. The changes in features were initially examined by Optical Transmission Microscopy (OTM). Figure 3.7 shows the optical micrographs of drop-cast residues from solutions of different concentrations. Whereas the residue from solution concentration of 1 mgmL⁻¹ showed the presence of sub-micrometer particles of different dimensions (Figure 3.7a), the residue from

concentrations between 5 mgmL^{-1} and 20 mgmL^{-1} showed distinctly different aggregation patterns (Figures 3.7b-d) and finally a featureless film at high concentration of 50 mgmL^{-1} (Figure 3.7e) was observed.

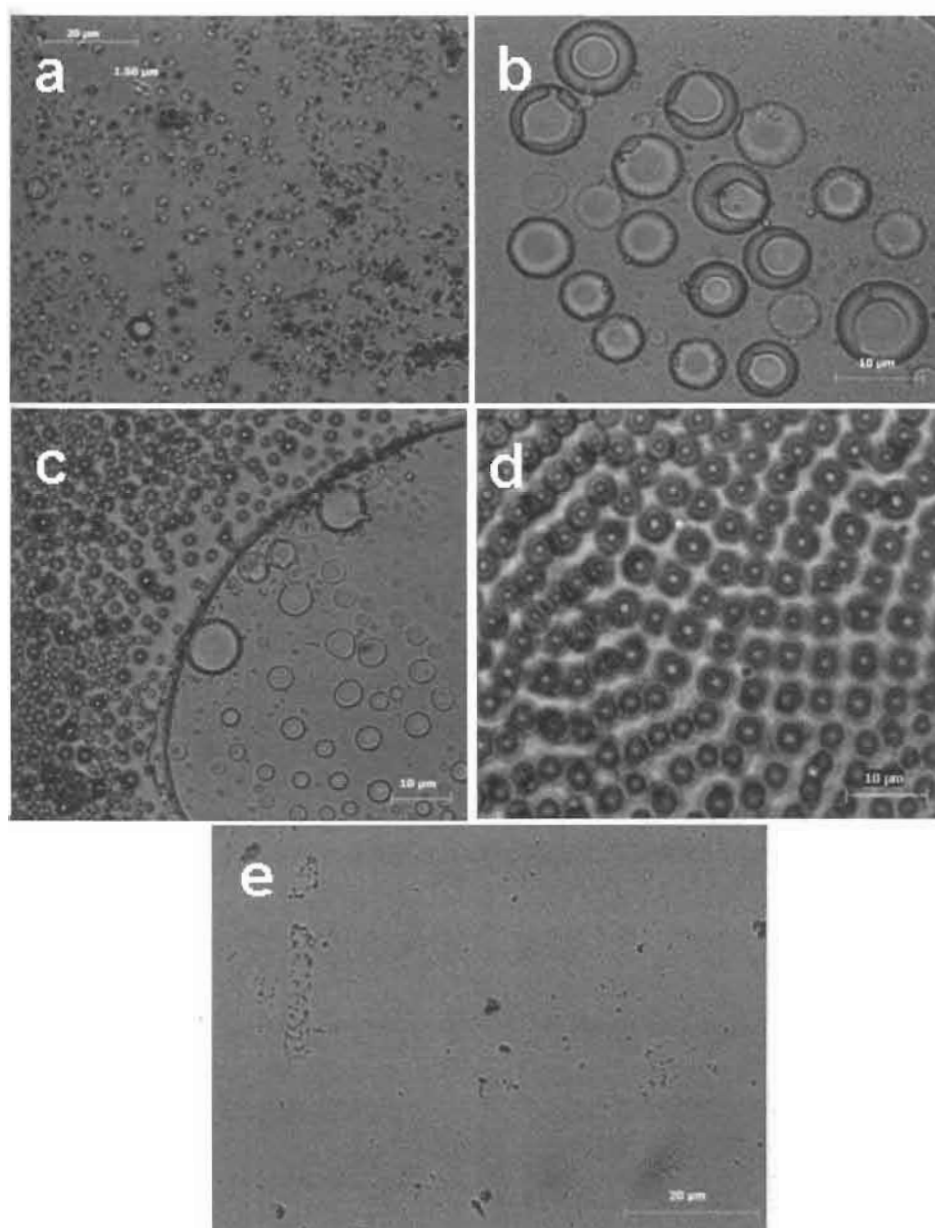**Figure 3.7.** *Optical transmission micrographs of NC in THF of solution concentration of (a) 1 mgmL^{-1}. (b) 5 mgmL^{-1} (c) 10 mgmL^{-1} (d) 20 mgmL^{-1} and (e) 50 mgmL^{-1} in THF. Scale bar represents (a & e) 20 μm, (b, c & d) 10 μm.*
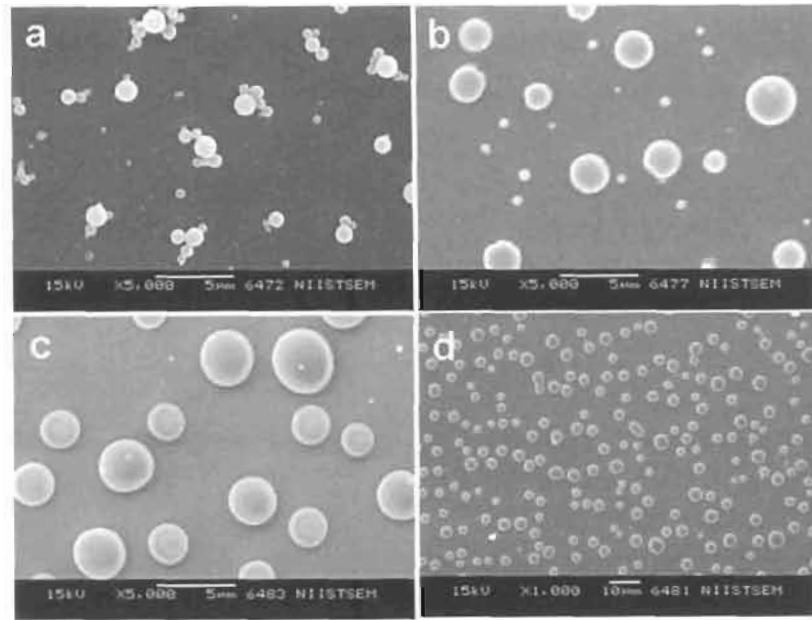
Figure 3.8. *SEM images of NC drop cast from THF solution of concentration (a) 0.1 mgmL⁻¹ (b) 1 mgmL⁻¹ (c & d) 2.5 mgmL⁻¹.*

A clear picture of the aggregation patterns and morphological transition was obtained by SEM and TEM. Figures 3.8 and 3.9 show the SEM images of drop-cast residues from solutions of different concentrations. As mentioned earlier, the residue from concentration of 0.001 mgmL⁻¹ showed particles of size 190-810 nm (Figure 3.4). The particle size dramatically increased with increase in concentration at the expense of primary particles and microspheres were found to form at concentrations between 1 mgmL⁻¹ and 2.5 mgmL⁻¹, as shown in figure 3.8. At concentration of 2.5 mgmL⁻¹, the residue was consistent with essentially microspheres of size in the range of 2.5-3.5 µm consuming all the primary particles (Figure 3.8c & d). The spheres were found hollow in nature as observed under TEM (discussed later). Mixed morphological features were observed at concentrations between >5 mgmL⁻¹ and <20 mgmL⁻¹ (Figures 3.9), a mixture of near-to-circular platelets and giant spheres of size >10 µm at 5 mgmL⁻¹ (Figures 3.9a, b & c) and porous film and spherical particles at 10 mgmL⁻¹ (Figure 3.9d). However evolution of more or less uniform microporous structure was observed

in the concentration range of 20-40 mgmL^{-1} (Figure 3.10) in which open pores formed

a two-dimensional array over a solid film.
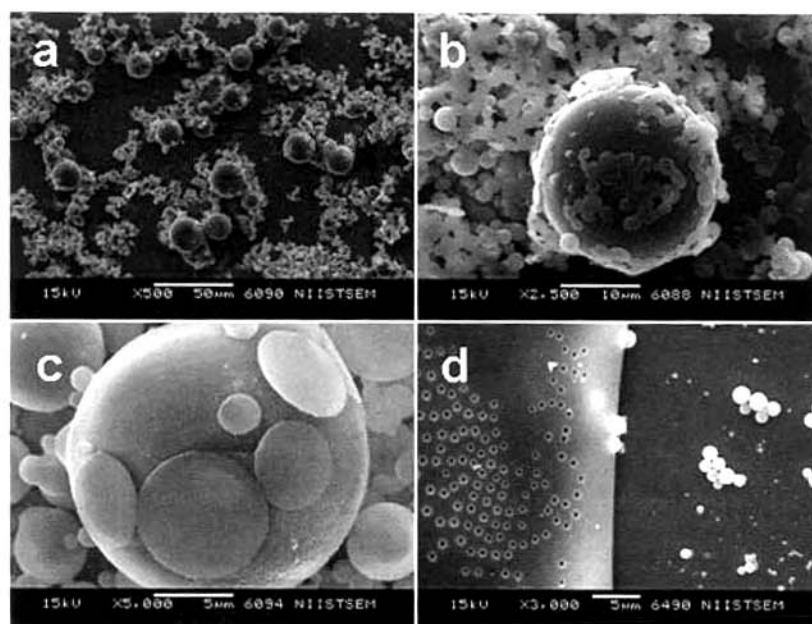
Figure 3.9. *SEM images of NC from solution concentration of (a & b) 5 mgmL^{-1} (c) 10 mgmL^{-1}. (d, e & b)20 mgmL^{-1}.*
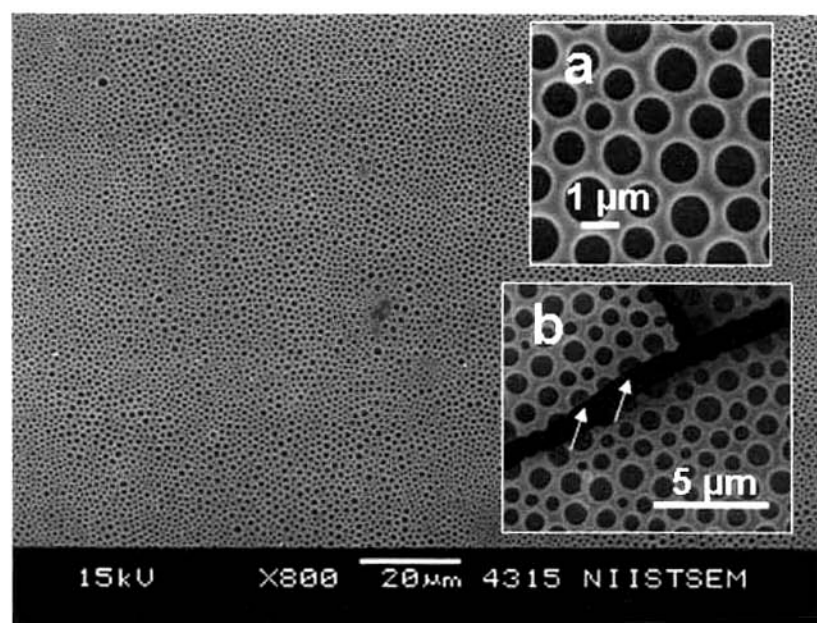
Figure 3.10. *SEM images of NC microporous film with long range order from THF of solution concentration of 20 mgmL^{-1}.* Inset shows (a) high magnification image and (b) broken edge of the film showing the solid film beneath the pores.

The micro-spheres (2.5-3.5 μm) as shown in figure 3.8 were vesicles (hollow spheres) as proved by TEM analysis (Figure 3.11). The vesicles showed an average membrane thickness of about 85 nm as measured from the TEM image. The giant spheres (Figure 3.9a-c) were also proved as vesicles by observing them in fluorescent microscope (FM). Figure 3.12 shows the FM image of the giant vesicle. The sample was prepared by drop-casting and drying of NC solution containing a fluorescent dye, 8-anilinonapthalene sulfonic acid. The giant-vesicle was appeared having large membrane thickness possibly due to multilamellar assembly of the NC particles.
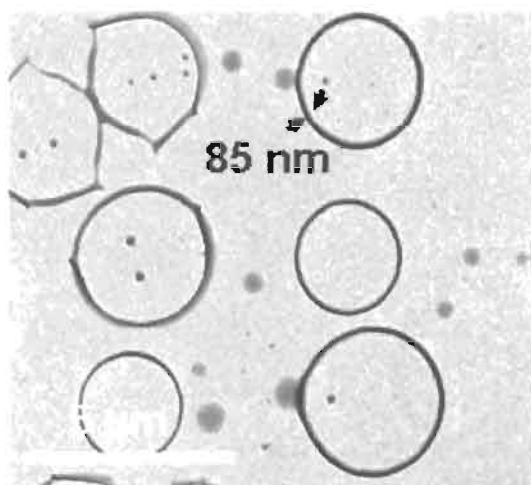
Figure 3.11. *TEM image of microspheres showing hollow structure with membrane thickness of ~85nm.*
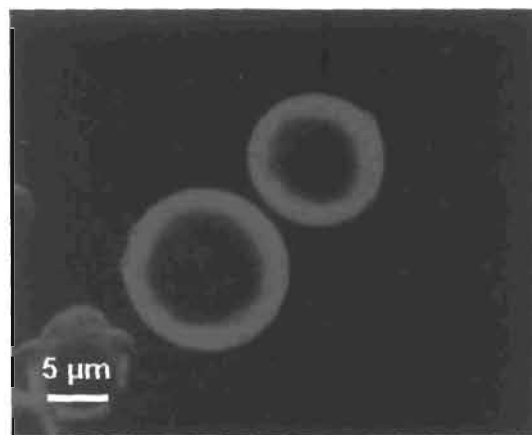
Figure 3.12. *Fluorescent micrograph of giant hollow spheres encapsulated with 8-anilinonaphthalene sulfonic acid.*

3.3.3. Structure of NC Particle and Mechanism of Morphological Transitions

As mentioned earlier, NC showed intercalated structure with a d_{001}-spacing of 29.3 Å due to polystyrene (PS) associated with POSS-intercalated parallel stack of silicate layers. Thickness (D) of the stack of the silicate layers was calculated from 001 reflection using Scherrer equation[5]

$$D = \frac{k\lambda}{\beta Cos\theta}$$

where k is a constant (the value generally = 0.9), λ is the X-ray wavelength (0.154 nm), β is the width of the XRD peak (in radian unit) and is measured by the full width at half-maximum, and θ is the WAXD peak position. D showed a value of 12.6 nm (126 Å). For a d-spacing of 29.3 Å, this value arises from stack of 4-5 individual clay layers separated by a repeat distance of 19.3 Å. Intercalated nanocomposites containing stacks of 4-5 clay layers as fine dispersions in the matrix have been reported in literature.[6,12] NC particle showed lateral dimension minimum of 190 nm (Figure 3.4) which was found matching with the lateral dimension of silicate layers of the clay (Cloisite-Na$^+$) that was used in the present study.[13] The sizes of larger particles were close to multiples of the size minimum. On the other hand, average membrane thickness of the vesicle was 85 nm, which was far less than the lateral dimension of particles, but close to the particle thickness. The above results suggested the following: (i) NC particles were formed from parallel stack of silicate layers and its aggregates through edge to edge association and (ii) vesicle was also formed by edge to edge association of the particles so that silicate layers lie flat along the vesicle membrane.

Formation of NC particle and vesicle can be explained by the following plausible mechanism. In styrene monomer, POSS-modified clay disperses to produce

68

domains (tactoids) containing individual stack of 4-5 clay layers. During intercalative polymerization, the silicate layers are tethered together by cross-linking reactions involving styrene and vinyl groups on the POSS within the clay galleries. On the other hand, PS chains originating and growing from the un-intercalated monomer are grafted to the tactoid surfaces through vinyl groups of POSS adsorbed on the tactoid surfaces. This mechanism favours the formation of NC particles having sandwich structure consisting of stacked silicate layers at the core and PS layers on either side, exposing the hydroxylated edges of the silicate layers desired for inter-particle interaction through H-bonding. The hydrophobic PS layers staying away from the hydrophilic edges of the silicate layers may explain the particle thickness (120 nm) higher than of vesicle membrane thickness (85 nm). Scheme of formation of NC particle is shown in figure 3.13.
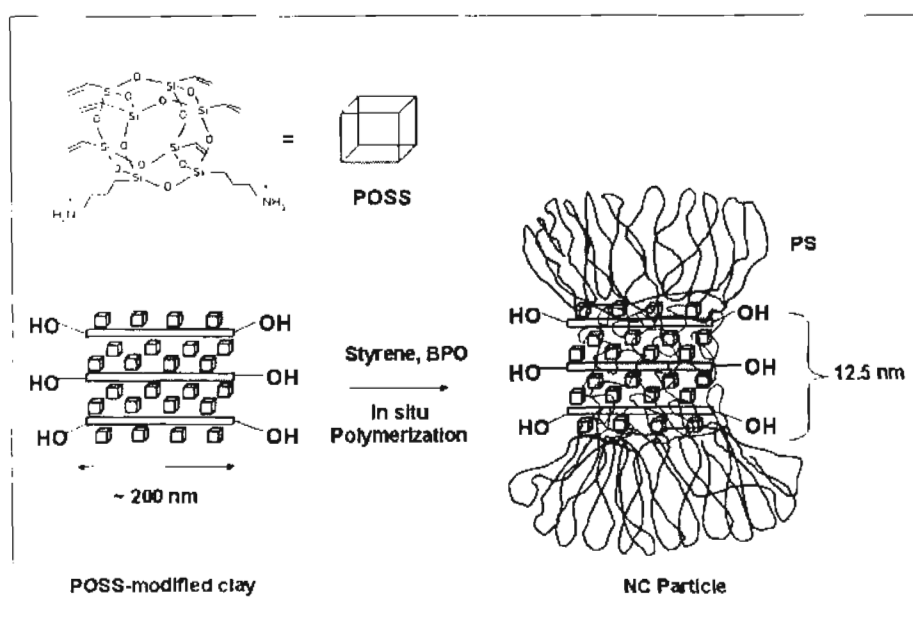
Figure 3.13. *Scheme of formation of NC particle.*

Block-copolymers when dissolved in solvents for one of the blocks spontaneously self-assemble into bilayer due to aggregation of the insoluble blocks through coulombic interactions, π-π interactions, H-bonds, dipolar interactions etc.[14-20] As the bilayer grows in size, its closure to vesicle becomes the predominant aggregation motif due to high surface tension. NC particle assumes the characteristic features of bilayer from amphiphilic block copolymer due to core-shell structure from stacked silicate layers bearing edge-hydroxyls sandwiched between hydrophobic PS layers. THF acts as a good solvent for the PS surface layers, but a poor solvent for the cross-linked silicate layers. Inter-particle interaction through the solvated PS layer is prevented due to steric repulsion. Instead, H-bonding interactions between the particles through hydroxylated edges of the silicate layers favour formation of extended bilayer, which closes to form microvesicle. The particles failed to produce vesicle when

Figure 3.14. *SEM image of NC from THF containing vinyltriethoxysilane (1 wt % of THF) for a solution concentration of 2.5 mgmL^{-1}.*

molecules such as long-chain carboxylic acids and alkyltriethoxysilane which can react with the free edge hydroxyls and inhibit edge-edge interaction of NC particle was

introduced in the solution (Figure 3.14) confirming the association of NC particles through H-bonding. Figure 3.15 shows schematic of microvesicle by self-assembly of NC particles. No vesicle formation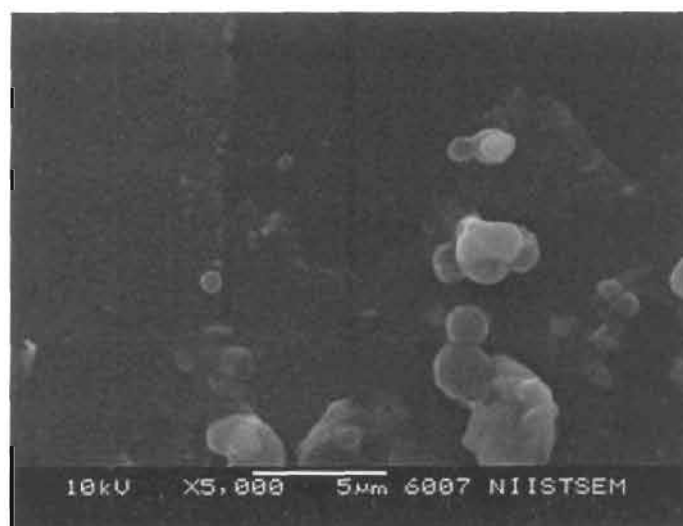 was observed in toluene, possibly due to swelling of the PS-POSS-intercalated stack of the silicate layers so that the PS chains extending outward from the galleries inhibit association of the particles through their edges.
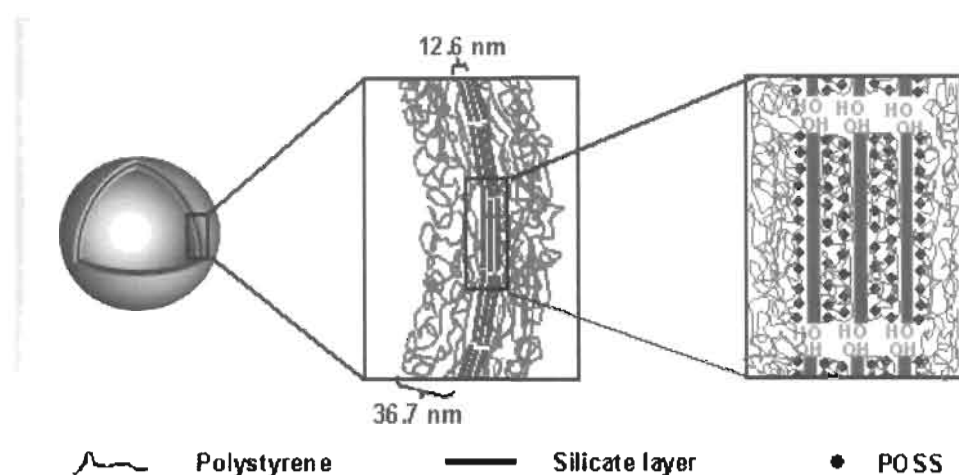
Figure 3.15. *Schematic representation of vesicle membrane cross-section showing PS-POSS intercalated clay tactoids at the core and PS layers on either side of the tactoid.*

The observed mixed morphologies for the residues from solution of concentrations in the range between 5-20 mgmL^{-1} can be explained as following. As described earlier, vesicle formation occurs by closure of the extended bilayer from lateral association of NC particles. It becomes clear that as the concentration increases beyond a critical value, closure of the extended bilayer becomes difficult due to volume constraint. As a result, partially closed vesicles may collapse during drying to form circular discs. The formation of giant vesicle having large membrane thickness, could be due to association of the extended bilayers and closure of resulting multi-lamellar assembly during the drying process. Generally, size of the vesicle increases as the bending modulus of the bilayer increases.[14] Multi-lamellar assembly should show

71

higher bending modulus than of uni-lamellar assembly. When the solution concentration is increased further, volume constraint becomes too high that the two dimensional assembly of the particles in the solution assumes close-packed lamellar arrangement of long-range order. Bending of the individual lamella being restricted, coalescence of the layers during drying of the solution leads to the formation of film, and as observed, microporous or neat film depending on the concentration.

The occurrence of two/three-dimensional microporous film can be explained by breath-figure (BF) mechanism as described below.[21,22] Due to evaporative cooling, water droplets nucleate on the surface of a polymer solution and grow subsequently. After sometime, rafts of non-coalescing droplets form and organize on the surface into hexagonally ordered and highly mobile array. These arrays do not coalesce, but start to sink into the solution. Now a second layer of droplets can be deposited on top of the first one. Arrays of pores are formed when drying of the remaining solvent leaves the imprint of the water droplets in the film. Pore-size greatly depends on the concentration of the solution, evaporation rate of the solvent and the relative humidity. However, BF does not form in an atmosphere that has less than 45-50 % relative humidity. In the present case, microporous films were obtained at ambient humidity of over 80 %. BF mechanism was further confirmed by the fact that porous film was not formed when casting and drying of the solution was carried out under non-humid condition in a glove box. Generally, the pore-size and strut-thickness does not vary significantly and the pores form uniform hexagonally close-packed structure. However, in the present case, the size of pores varied from 800 nm-1.3 µm and the thickness of strut varied from 210-750 nm. The strut thickness was of the order of the lateral dimension of the NC particles. This implies that the water droplets were channeled through the hydrophilic

72

interface between the NC particle as schematically shown in figure 3.16. Array of open

pores are formed during drying or coalescence of the remaining solvent or precipitation

of the particles around the water droplets. At very high concentration of 50 mgmL^{-1}, the

formation of pore could be restricted due to high viscosity of the solution or formation

a solid film over the surface of the solution which prevents sinking of the water

droplets.
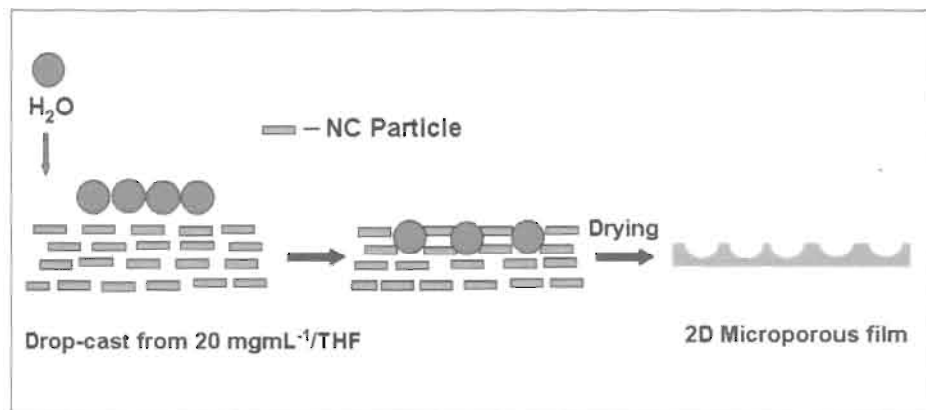
Figure 3.16. *Scheme of formation of NC microporous film through breath figure method.*

3.4. Conclusions

In situ intercalative polymerization of styrene with POSS-modified clay having

reactive vinyl groups produced nanocomposite particles exhibiting solvent-assisted

self-assembling properties when dissolved in a highly volatile solvent followed by

drop-casting and drying of the solutions on a substrate. The particles having lateral

dimensions of 190-810 nm consisted of sandwich structure having polystyrene-POSS-

intercalated clay tactoid of thickness of 12.6 nm at the core and polystyrene layers of

thickness of 31.6 nm on either side of the core, exposing the hydroxylated edges of the

silicate layers. As a result, the particles resembled a bilayer assembly consisting of

hydrophobic layers on either side of a hydrophilic rigid core from amphiphilic block copolymers. The drop-cast residues of solutions of the nanocomposite particles in THF showed concentration dependent well defined morphologies such as microvesicles of the size of 2.5-3.5 μm at solution concentration of 2.5 mgmL^{-1} and two-dimensional microporous film of long range order at solution concentration of 20-40 mgmL^{-1}. Microvesicles were formed by closure of the extended bilayer from lateral association of the nanocomposite particles by H-bonding interactions between edge-hydroxyls of the silicate layers. The breath figure mechanism has been proposed for the formation of the two-dimensional microporous film from solutions in which the extended bilayers formed closely packed lamellar arrangement.

3.5. References

1. Feher, F. J.; Wyndham, K. D. *Chem. Commun.* **1998**, 323.

2. Feher, F. J.; Wyndham, K. D. Soulivong, D.; Nguyen, F. *J. Chem. Soc. Dalton Trans.* **1999**, 1491.

3. Jaffrés, P.-A.; Morris, R. E. *J. Chem. Soc., Dalton Trans.* **1998**, 2767.

4. Zhang, X.; Haxton, K. J.; Ropartz, L.; Cole-Hamilton, D. J.; Morris, R. E. *J. Chem. Soc., Dalton Trans.* **2001**, 3261.

5. Ray, S. S.; Okamoto, K.; Okamoto, M. *Macromolecules* **2003**, *36*, 2355.

6. Okamoto, M.; Morita, S.; Kim, Y. H.; Kotaka, T.; Tateyama, H. *Polymer* **2001**, *42*, 1201.

7. Okada, A.; Usuki, A. *Macromol. Mater. Eng.* **2006**, *291*, 1449.

8. Tjong, S. C. *Mater. Sci. Eng R.* **2006**, *53*, 73.

9. Ray, S. S.; Okamoto, M. *Prog. Polym. Sci.* **2003**, *28*, 1539.

10. Alexandre, M.; Dubois, P. *Mater. Sci. Eng R.* **2000**, *28*, 1.

11. Triantafillidis, C. S.; LeBaron, P. C.; Pinnavaia, T. J. *Chem. Mater.* **2002**, *14*, 4088.

12. Ren, J.; Krishnamoorti, R. *Macromolecules* **2003**, *36*, 4443.

13. Ploehn, H. J.; Liu, C. *Ind. Eng. Chem. Res.* **2006**, *45*, 7025.

14. Antonietti, M.; Forster, S. *Adv. Mater.* **2003**, *15*, 1323.

15. Forster, S. Polymer   Vesicles. In Encyclopedia of Polymer Science and Technology; John Wiley & Sons; New York, **2005**.

16. Discher, D. E.; Eisenberg, A. *Science* **2002**, *297*, 967.

17. Tokarczyk, K. K.; Grumelard, J.; Haefele, T.; Meier, W. *Polymer* **2005**, *46*, 3540.

18. Discher, B. M. ; Hammera, D. A. ; Batesb, F. S. ; Discher D. E. *Curr. Opin. Colloid Interface Sci.* **2000**, *5*, 125.

19. Zhang, L.F.; Yu, K.; Eisenberg, A. *Science* **1996**, *272*, 1777.

20. Discher, M.; Won, Y. Y.; Ege, D. S.; Lee, J. C. M.; Bates, F. S.; Discher, D. E.; Hammer, D. A. *Science* **1999**, *284*, 1143.

21. Stenzel, M. H.; Barner-Kowollik, C.; Davis, T. P. *J. Polym. Sci., Part A: Polym. Chem.* **2005**, *44*, 2363.

22. Bunz, B. H. F. *Adv. Mater.* **2006**, *18*, 973.

Chapter 4

*Investigations on Guest-encapsulation and Release
Properties of Microvesicles*

*Chapter 4 presents preliminary studies on the guest-encapsulation and release
properties of polystyrene-clay nanocomposite microvesicles. Vesicles were
encapsulated with fluorescent dyes and oil. They were found stable in aqueous
medium and unstable in solvents for PS which resulted in total release of the dye
molecules. Slow release of the encapsulated dye molecules were observed in alcoholic
solvents.*

4.1. Introduction

In recent years vesicles have been receiving intense research attention because of their potential for applications in encapsulation/delivery of drugs, cosmetically active molecules, dyes and inks, catalysis, as micro-containers or reactors and sensors.[1-5] Various strategies have been adopted to synthesize polymer, inorganic and organic-inorganic hybrid vesicles. Amphiphilc polymers,[6-7] rod-coil diblock polymers,[8-9] dendrimers,[10-11] and foldamers[12] were shown to form vesicles through self-assembly in selective solvents. Alternatively, polymer vesicles can be synthesized through sacrificial template method.[13] Inorganic[14-15] and organic-inorganic hybrid[16-17] vesicles show superior stability and resistance to many external stimuli when compared to polymer vesicles, but they often need tedious synthetic strategy involving sacrificial template and layer-by-layer self-assembly. Hybrid vesicles through the facile solvent-assisted self-assembly is scant in literature.[18-20]

Polymeric and hybrid vesicles could be models for biological membranes and can have many practical applications. Their high mechanical stability, resistance to many external stimuli and ability to encapsulate both hydrophilic and hydrophobic compounds make them excellent candidates for use in medical, pharmaceutical and environmental fields.[21] They have the capability to further release the encapsulated molecules due to membrane diffusion, vesicle breaking, or after the application of a stimulus to the system. A continuous release of encapsulated substance can occur via permeation through the vesicle bilayer which depends on the bilayer thickness and vesicle radius, block lengths and vesicle preparation method. The vesicle can be intelligent responding to changes in pH, temperature, or ionic strength to encapsulate, transport and release of drugs, or genes for use in chemo and gene therapy. It was

78

necessary to analyze the usefulness of polystyrene-clay nanocomposite (NC) microvesicles for encapsulation and release applications. Preliminary investigation on the use of NC microvesicles for encapsulation and release applications were carried out and chapter 4 presents the results obtained.

4.2. Experimental

4.2.1. Materials

Rhodamine 6G (R6G) and 8-anilinonaphthalene sulphonic acid (ANS) were purchased from Aldrich Chemicals. Toluene and methanol were of extra pure grade and tetrahydrofuran of HPLC grade from Merck Specialties Pvt. Ltd. India.

4.2.2. Preparation of Guest-encapsulated Vesicles

In general guest-encapsulated vesicles were prepared by casting solutions of polystyrene-clay nanocomposite (NC) in THF (2.5 mgmL^{-1}) containing guest molecules (ANS, R6G or oil) on a glass plate followed by evaporation of the solvent at ambient temperature. R6G and ANS were taken 0.4 wt % and oil 1 wt % of NC. For encapsulating the ANS and R6G simultaneously, the dyes were dissolved in THF so that the total amount of dyes is 0.4 wt % to NC. Unencapsulated molecules were removed by repeated washing using methanol. Dye-encapsulated vesicles were characterized using Leica DM LB2 fluorescence microscope. ANS epifluorescence was obtained by using exciting light of wavelength 360 nm. For R6G, light of wavelength 480 nm was used for irradiating the sample.

4.2.3. Release Properties of Encapsulated R6G in Selected Solvents

NC was dissolved in THF (2.5 mgmL^{-1}) containing R6G (0.4 wt % to NC). Known volume of NC solution was drop-cast on different glass plates and then whole of the dye-encapsulated vesicles without removing the unencapsulated dye were suspended in a known volume of ethanol (5 mL), at regular time intervals. The vesicles were not washed with methanol since the leaching away of a few vesicles along with unencapsulated dye molecules can affect the quantitative analysis. The ethanol

solutions were filtered to remove the suspended vesicles and release characteristics were studied by measuring the fluorescence intensity using SPEX-Fluorolog F112X spectroflourimeter using an excitation wavel. The fluorescence intensity measured corresponds to released and unencapsulated dye molecules. Fluorescence intensity obtained immediately after suspending the dye-encapsulated vesicles in ethanol was considered to be that from unencapsulated dye molecules alone and was used to find the fluorescence intensity from the dye molecules released alone. A standard plot of concentration vs fluorescence intensity was also plotted to find the concentration of dye released with time, using which release plot was drawn. Adopting a similar procedure, release properties of the encapsulated dye molecules in water and toluene were also investigated.

4.3. Results and Discussion

4.3.1. Encapsulation of Gest-Molecules

Fluorescence microscopy is a very powerful to tool to characterize vesicles and the guest-encapsulation ability of the polystyrene-clay nanocomposite (NC) vesicle was proved by encapsulation with fluorescent probes 8-Anilinonaphthalene sulphonic acid (ANS) and Rhodamine 6G (R6G). Figure 4.1a & b, respectively shows the fluorescent micrograph (FM) of vesicles encapsulated with dyes ANS and Rhodamine 6G R6G. The dried vesicles appeared fluorescent due to dye molecules adhering to the inner walls since unencapsulated dye molecules were washed off using methanol. This further confirmed the uni-lamellar nature of the vesicle wall.
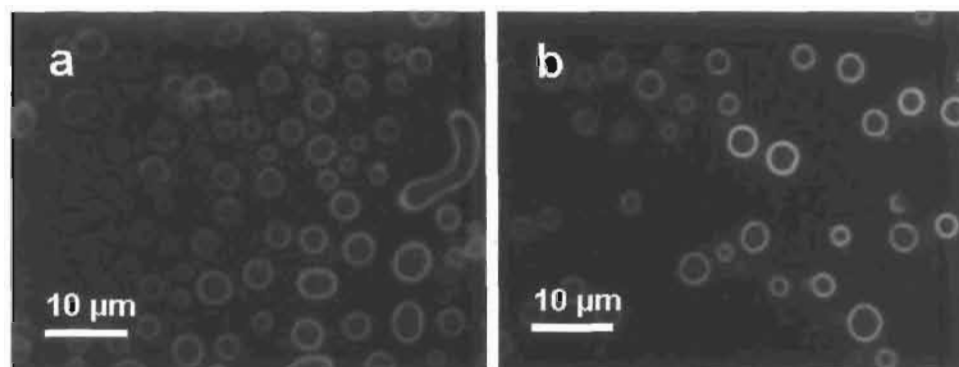
Figure 4.1. *Fluorescence micrographs of NC vesicles containing fluorescent probe (a) 8-Anilinonapthalene sulfonic acid and (b) Rhodamine 6G. Fluorescence was due to dye adhering to the inner wall of the dried vesicles.*

Vesicles were also encapsulated simultaneously with R6G and ANS by forming them in THF containing both the dyes. Figure 4.2 shows the fluorescence micrograph of the vesicles containing both the dyes and it was found that vesicles have no particular affinity towards either R6G or ANS. The result indicated that NC vesicles are useful for encapsulating two active molecules at the same time. The vesicles

encapsulated with dye molecules appeared as ring due to the fast drying nature of THF which causes the deposition of dye molecules on the inner walls of vesicles. Therefore we have used a triglyceride oil in which ANS was dispersed as the guest-molecule to observe the vesicles filled. Figure 4.3 shows fluorescent micrograph of the vesicles containing triglyceride oil in which ANS was dispersed. Vesicle encapsulated with oil appeared fully fluorescent due to slow drying nature of the solvent containing oil in which ANS was dispersed.
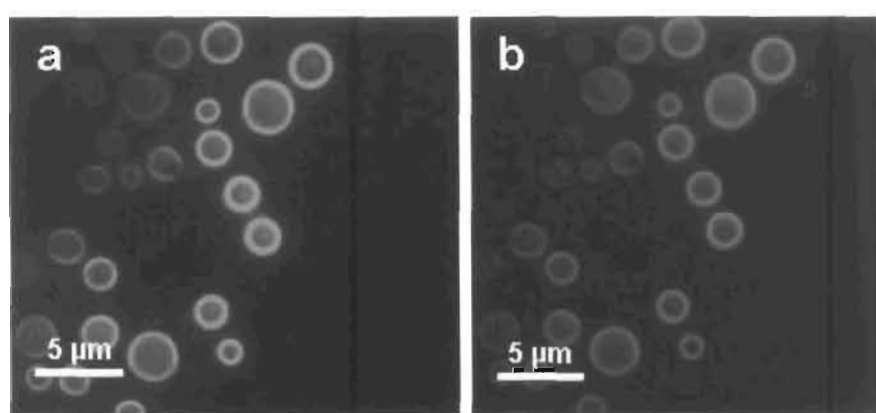

Figure 4.2. *Fluorescence micrograph of vesicles encapsulated simultaneously with dyes Rhodamine 6G (a) and ANS (b). The sample was irradiated at 480 nm*
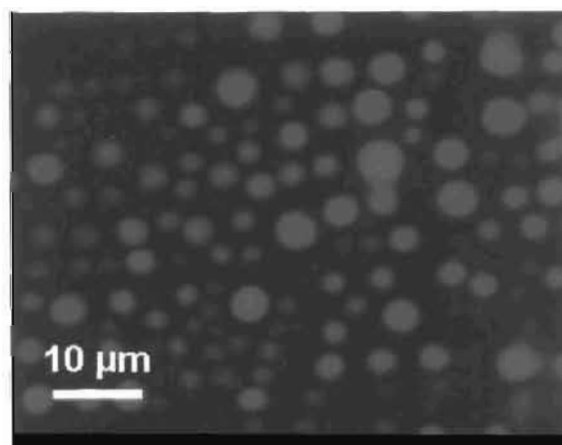
for R6G and 360 nm for ANS.

Figure 4.3. *Fluorescence micrograph of vesicles encapsulated with a triglyceride oil containing ANS.*

4.3.2. Release Properties of the Encapsulated R6G in Selected Solvents
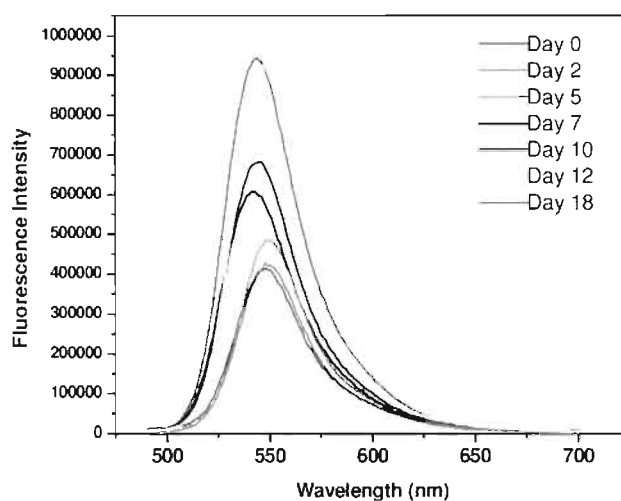

Figure 4.4. *Fluorescence spectra of R6G at various time intervals and fluorescence intensity corresponds to released and unencapsulated dye.*

The release properties of the encapsulated R6G from NC vesicles into ethanol, water and toluene were investigated. Figure 4.4 and 4.5, respectively shows the fluorescence spectra of the dye released at various time intervals and the release plot of the dye into ethanol with time. In figure 4.4, fluorescence intensity corresponds to the dye released and unencapsulated. The fluorescence intensity obtained immediately after suspending the vesicles in ethanol (D0 in figure 4.4) was subtracted from that obtained at regular intervals to obtain the fluorescence intensity from the dye released. Dye molecules showed gradual release into ethanol with time, which then stabilized after period of 15 days. Though polystyrene has limited swelling in ethanol, the hydrophilic dye molecules within the vesicle wall might have opened the path for diffusion of ethanol and the release of dye molecules. In order to confirm this, vesicles without dyes were put into ethanolic solution of R6G. Even after prolonged keeping for one month, no diffusion of ethanol/dye molecules inward to the vesicle was observed. In other

words, diffusion of ethanol was not taking place due to the highly hydrophobic polystyrene chains. The dye molecules present in the wall of dye encapsulated vesicle was necessary to facilitate the diffusion of ethanol inward to the vesicle.
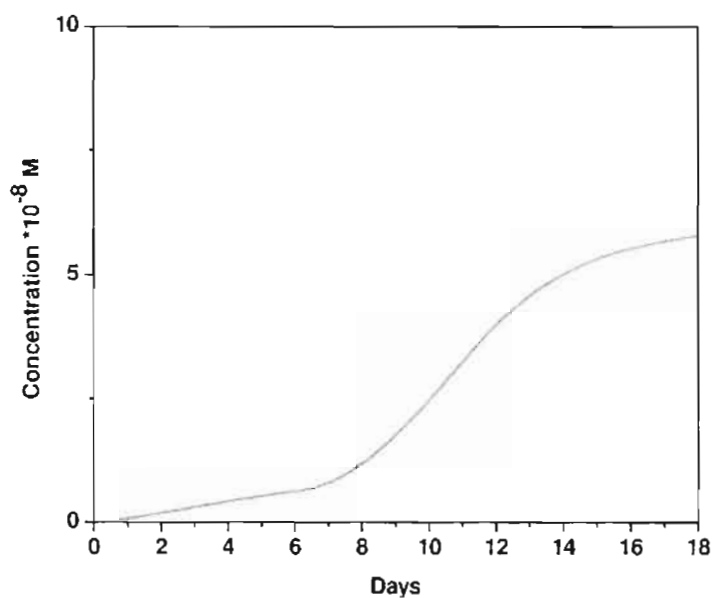

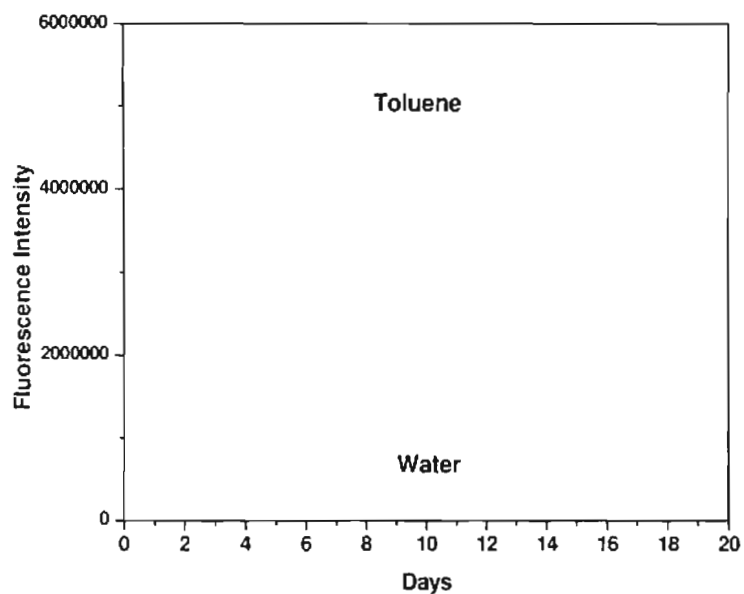**Figure 4.5.** *Release plot of R6G from vesicles into ethanol with time.*

Figure 4.6. *Release plot of R6G from vesicles into water and toluene with time.*

85

Adopting a similar method used for ethanol, release property of encapsulated dye molecules in water and toluene were also studied. It was found that in water no release of dye molecules was observed with time (Figure 4.6) and the fluorescence intensity obtained was from unencapsulated dye molecules. This could be due to the high stability of vesicles with hydrophobic polystyrene chains in aqueous medium. Whereas in toluene, complete dissolution of the vesicles with spontaneous release of the dye molecules was observed (Figure 4.6). Interestingly, it was observed that the vesicles can be broken to obtain the NC particles by sonication after suspending them in ethanol. ANS-encapsulated vesicles were put in ethanol and sonicated to obtain the NC particles and washed repeatedly with methanol. Figure 4.7 shows the fluorescence micrograph of NC particles obtained by breaking of dye encapsulated vesicles. The fluorescence was due to dye molecules intercalated in PS-POSS-clay tactoids since the dye molecules encapsulated were removed by breaking the vesicles.
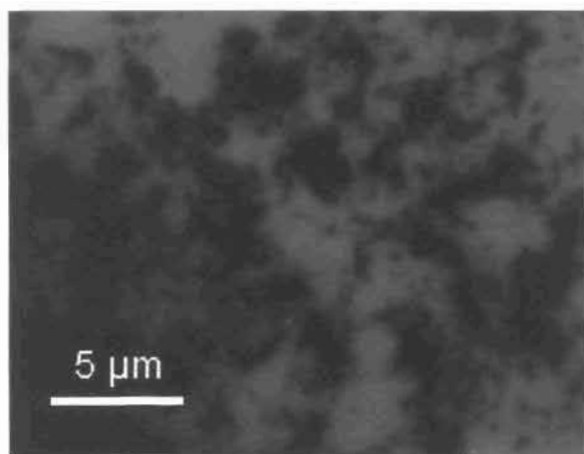

Figure 4.7. *Fluorescent micrograph of NC particles obtained by breaking the vesicles by sonication in methanol.*

NC vesicle was thermally stable up to 270 °C in nitrogen atmosphere with a glass transition temperature of 86.2 °C as described in chapter 3. Slow release of the

encapsulated dye molecule was observed in ethanol which makes the vesicles useful for alcohol assisted release applications. The vesicles were found stable in aqueous medium and therefore excellent as storage system under humid conditions. When the spontaneous release of the encapsulated molecules is required, solvent such as toluene can be employed.

4.4. Conclusions

Preliminary studies on the guest-encapsulation and release properties of polymer-clay nanocomposite vesicles were carried out. Encapsulation with dye molecules revealed uni-lamellar nature of vesicle wall. Vesicles were also encapsulated with triglyceride oil. They were found stable in aqueous medium and unstable in toluene which resulted in total dissolution and release of the dye molecules. Slow release of the encapsulated dye molecules was observed in ethanol. The high thermal stability along with barrier properties of polymer-clay nanocomposites may make the vesicle excellent micro-storage and reactor system and can also be useful for solvent-assisted release applications.

4.5. References

1. M. Antonietti, M.; Forster, S. *Adv. Mater.* **2003**, *15*, 1323.

2. Forster, S. Polymer Vesicles. In Encyclopedia of Polymer Science and Technology; John Wiley & Sons; New York, **2005**.

3. Discher, D. E.; Eisenberg, A. *Science* **2002**, *297*, 967.

4. Tokarczyk, K. K.; Grumelard, J.; Haefele, T.; Meier, W. *Polymer* **2005**, *46*, 3540.

5. Discher, B. M. ; Hammera, D. A. ; Batesb, F. S. ; Discher D. E. *Curr. Opin. Colloid Interface Sci.* **2000**, *5*, 125.

6. Zhang, L.F.; Yu, K.; Eisenberg, A. *Science* **1996**, *272*, 1777.

7. Discher, M.; Won, Y. Y.; Ege, D. S.; Lee, J. C. M.; Bates, F. S.; Discher, D. E.; Hammer, D. A. *Science* **1999**, *284*, 1143.

8. Jenekhe, S. A.; Chen, X. L. *Science* **1998**, 283, 372.

9. Vriezema, D. M.; Hoogboom, J.; Velonia, K.; Takazawa, K.; Christianen, P. C. M., Mann, J. C.; Rowan, A. E.; Nolte, R. J. M. *Angew. Chem.* **2003**, 115.

10. Vanhest, J. C. M.; Delnoye, D. A. P.; Baars, M.; Vangenderen, M. H. P.; Meijer, E. W. *Science* **1995**, *268*, 1592.

11. Yang, M.; Wang, W.; Yuan, F.; Zhang, X.; Li, J.; Liang, F.; He, B.; Minch, B.; Wegner, G. *J. Am. Chem. Soc.* **2005**, *127*,15107.

12. Cai, W.; Wang, G. T.; Xu, Y. X.; Jiang, X. K.; Li, Z. T. *J. Am. Chem. Soc.* **2008**, *130*, 6936.

13. Khopade, A. J.; Mohwald, H. *Adv. Funct. Mater.* **2005**, *15*, 1088.

14. Caruso, R. A.; Susha, A.; Caruso, F. *Chem. Mater.* **2001**, *13*, 400.

15. Buchold, D. H. M.; Feldmann, C. *Nan. Lett.* **2007**, 7, 3489.

16. Katagiri, K.; Ariga, K.; Kikuchi, J. I. *Chem. Lett.* **1999**, *28*, 661.

17. Katagiri, K.; Hamasaki, R.; Ariga, A.; Kikuchi, J. I. *J. Am. Chem. Soc.* **2002**, *124*, 7892.

18. Zhou, S. Q.; Burrger, C.; Chu, B.; Sawamura, M.; Nagahama, N.; Toganoh, M.; Hackler, U.E.; Isobe, H.; Nakamura, E. *Science* **2001**, *291*, 1944.

19. Du, J.; Chen, Y. *Angew. Chem. Int. Ed.* **2004**, *43*, 5084.

20. Du, J.; Chen, Y.; Zhang, Y.; Han, C. C.; Fischer, K.; Schmidt. M. *J. Am. Chem. Soc.* **2003**, *125*, 14710.

21. Lee, J. C. M.; Bermudez, H.; Discher, B. M.; Sheehan, M. A.; Won, Y. Y.; Bates, F. S. *Biotech. Bioeng.* **2001**, *73*, 135.

22. Hamley, I. W. *Nanotechnology* **2003**, *14*, 39.

Chapter 5

Bifunctionalized Hybrid Silica Spheres by Hydrolytic Co-condensation of 3-Aminopropyltriethoxysilane and Vinyltriethoxysilane

Bifunctionalized hybrid silica spheres were prepared by casting and drying of stable siloxane solution from hydrolytic co-condensation of 3-aminopropyltriethoxysilane (AS) and vinyltriethoxysilane (VS) with AS:VS mole ratio of 1:3 in ethanol/water mixture. HS was formed from co-precipitation of fully condensed polyhedral oligomeric silsesquioxane (POSS)-bilayer and incompletely condensed siloxanes (SIL) produced during drying.

5.1. Introduction

In recent years, design and synthesis of organic-inorganic hybrid materials have attracted considerable attention because of their potential applications in the area of catalysis,[1] drug delivery,[2] sensors,[3] separation[4] etc. Among these, hybrid silica have attracted much interest due to ease of formation in a wide range of sizes and morphologies, possibility of functionalization with a variety of organic groups and high stability to find different applications.[5]

Different routes to synthesize hybrid silica have been reported. The widely accepted method is by surface functionalization. In this procedure, pure silica particles synthesized by hydrolysis of tetraethyl orthosilicate (TEOS) or tetramethyl orthosilicate (TMOS), for example by Stöber method,[6] are organo-modified by reacting surface silanol groups with organo-silane.[7] However, the approach does not allow high surface coverage of organic groups and rarely spheres have been internally modified. In a different approach, hybrid silica have been prepared by co-condensation of TEOS/TMOS and functionalized trialkoxysilanes, although the reaction systems were too complex in alcohol-water mixture with the use of surfactants.[8] Alternatively, hybrid silica with organic moieties throughout the silica network have been possible by hydrolysis of corresponding trialkoxy organosilane precursor.[9-11] However, hybrid silica available in literature are limited with a few functional groups.[12, 13]

During attempt to synthesize POSS with reactive vinyl and amino groups as an organomodifier for clay by hydrolytic co-condensation of vinyl- and 3-aminopropyltriethoxysilanes, it was found that the same POSS solution can be useful for the synthesis of bifunctionalized hybrid silica spheres. Thus chapter 5 is a cognate

work to the main research topic and explains the synthesis of bifunctionalized hybrid silica spheres with vinyl and aminopropyl groups. The advantages of the method are as follows; (1) nonsurfactant route though high concentration of organosilanes is used (2) no external catalyst is required due to the self-catalytic activity of aminopropyl groups (3) use of organosilanes without other precursors such as TMOS or TEOS[11] (4) hybrid silica spheres will be having very high surface and internal organic content which can be useful as precursors for mesostructured silica and for the preparation of hybrid silica particles with complex structures[14].

5.2. Experimental

5.2.1. Materials

3-aminopropyltriethoxysilane (99%, AS) and vinyltriethoxysilane (97%, VS) were purchased from Aldrich Chemicals and absolute ethanol (spectroscopic grade) from s. d. Fine Chem Limited, India. Millipore-grade water was used.

5.2.2. Synthesis of Siloxane Solution and Hybrid Silica Spheres (HS)

Siloxane solution from AS/VS composition was prepared by following procedure for the preparation of octaaminopropyl polyhedral oligomeric silsesquioxane (POSS) solution from trialkoxyaminoproylsilane without using an external catalyst.[15] Typically, siloxane solution was prepared by diluting a mix of AS and VS with AS:VS mole ratio of 1:3 using ethanol-water mixture (v/v = 14/1) to a silane concentration of 0.45 M and aging the solution in a closed container at ambient temperature for a period over 7 days. HS was prepared by casting the solution on glass plate followed by evaporation of the solvent at ambient temperature and then drying at 80 °C for 6 hrs.

5.2.3. Synthesis of Polystyrene-HS Composite

Polystyrene- hybrid silica sphere (PS-HS) composites were prepared through solution-blending technique. Required amount of HS was dispersed in toluene, then mixed with solution of polystyrene in toluene and mixed thoroughly. Solvent was evaporated off at 90 °C under vacuum.

5.2.4. Characterization

Hybrid silica spheres (HS) were characterized using Fourier transform-Infrared Spectroscopy (FT-IR), differential scanning calorimetry (DSC), thermogravimetric

analysis (TGA), X-ray powder diffraction (XRD), scanning electron microscopy (SEM) and high resolution transmission electron microscopy (HRTEM). FT-IR measurements were made on Perkin-Elmer Spectrum one spectrophotometer in the range of 4000-400 cm^{-1} using KBr pellets containing ca. 2 wt % sample. TGA was performed on a TGA-50 (Shimadzu) Thermogravimetric Analyzer employing a heating rate of 10 °C/min from 30 to 800 °C under a nitrogen flow of 20 mL/min. DSC analysis was performed using Perkin Elmer Pyris 6 Differential Scanning Calorimeter calibrated using Indium as standard. X-ray powder diffraction (XRD) data at 2θ between 2° and 20° were collected on a Philips X'pert Pro X-ray diffractometer equipped with graphite monochromator and X'celerator detector. SEM images were taken in JEOL JSM-5600 LV scanning electron microscope using samples provided with a thin gold coating using JEOL JFC-1200 fine coater. TEM analysis was performed in FEI, TEC NAI 30G2 S-TWIN microscope with an accelerating voltage of 100 or 300 kV. For dielectric measurements, polystyrene composite was hot pressed in to pellets at 170 °C for 1 hour. Cylindrical pellets were electroded using silver-paste and dielectric measurements were carried out using LCR meter (HIOKI 3532-50 Japan). SEM fractograph of the composites were obtained by breaking the pellets after dipping in liquid nitrogen for 5 minutes.
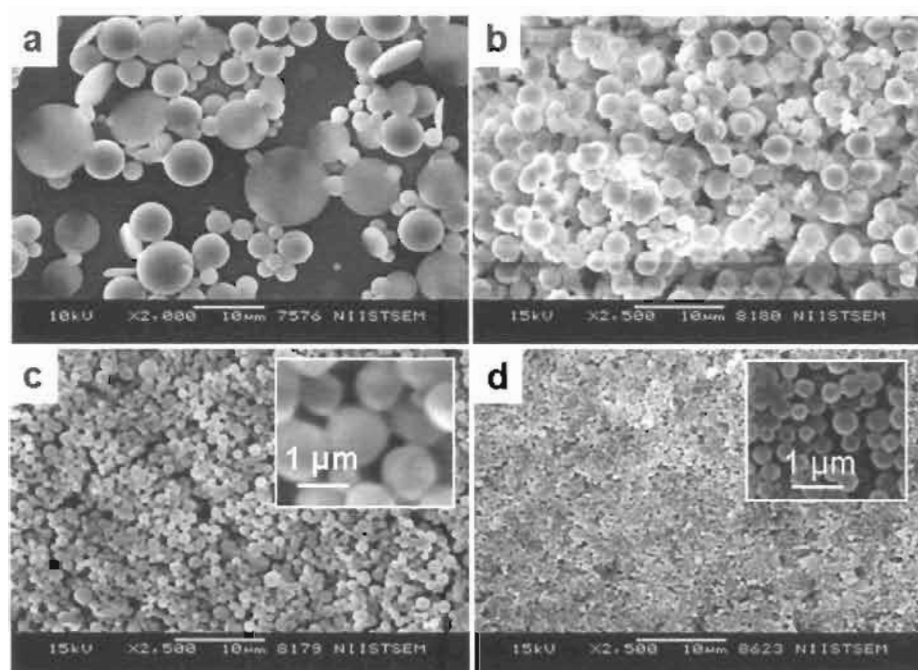
5.3. Results and Discussion

Figure 5.1. *SEM images of HS obtained at siloxane:ethanol v/v ratio (ratio of reacted siloxane to additional ethanol) of (a) 1:0 (b) 1: 1 (c) 1:5 and (d) 1:10, inset shows the SEM images at higher magnification, scale bar represents 10 μm.*
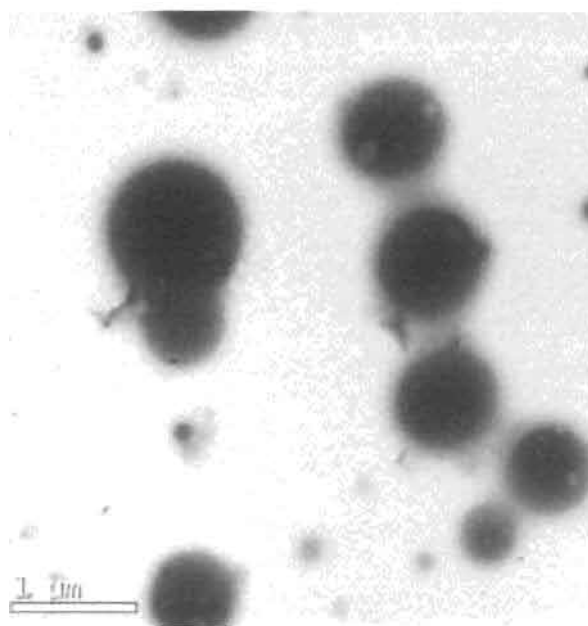

Figure 5.2. *TEM image of HS proving dense nature. Scale bar represents 1 μm.*

The siloxane solution from the AS/VS composition was clear and stable even after a period of 60 days. And, as generally observed, a T-gel was obtained on concentrating bulk of the solution by slow evaporation of the solvent.[16] On the other hand, the solution when cast on a glass plate and allowed to dry at ambient temperature yielded white powder composed of hybrid silica spheres (HS) having diameter ranging from 1-10 µm, as observed in SEM (Figure 5.1a). The aged siloxane solution upon diluting with ethanol produced essentially spherical particles, the size of which showed a decreasing trend with increasing amount of ethanol. While, the solution diluted with equal volume of ethanol produced predominantly spheres having average diameter of 2.5 µm (Figure 5.1b), dilution by five times yielded spheres of size in the range of 0.8-1.1 µm (Figure 5.1c) and dilution by ten times yielded spheres of size in the range of 250-370 nm (Figure 5.1d). Dense nature of the HS was evident from TEM image (Figure 5.2).

5.3.1. FT-IR Spectra

AS/VS composition in alcohol-water mixture undergoes hydrolytic co-condensation without an external catalyst, owing to the internal catalytic activity of the basic alkyl amino group of AS which upon reacting with water produces nucleophilic OH⁻. According to Voronkov,[15] hydrolytic co-condensation of a mixture of trifunctional silane monomers having similar reactivity usually gives hetero-substituted fully condensed polyhedral oligomeric silsesquioxane (POSS) as the major product. Thus, under the given experimental conditions, AS/VS composition was expected to yield POSS having aminopropyl and vinyl groups. However, under basic conditions, formation of POSS frameworks typically occurs with thermodynamic control because both formation and hydrolytic cleavage of Si-O-Si linkages are facile and precipitation
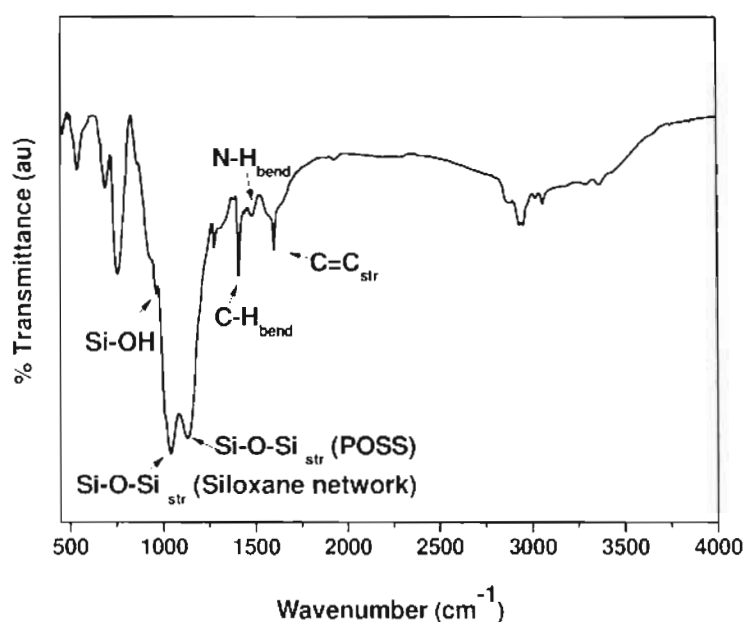
Figure 5.3. *FTIR spectra of HS showing peaks due to cage-structured polyhedral oligomeric silsesquioxane (POSS) and branching/network siloxanes.*

of POSS is normally the driving force for separating them in quantitative yields. Where precipitation of POSS does not occur, the siloxane solution at equilibrium will contain predominantly fully condensed POSS together with incompletely condensed POSS.[16] Slow drying of such solutions generally gives T-gels due to increase of solution concentration which promotes formation of incompletely condensed siloxanes (SIL) followed by shifting of the equilibrium in a progressive manner to produce siloxane network in the solution. However, in the present study, since the solvent was allowed to evaporate off fast, spontaneous precipitation of fully condensed POSS along with SIL formed during drying can occur. FT-IR spectral features of HS support this (Figure 5.3). The spectrum showed bands due to vinyl groups 1600 cm^{-1} (C=C$_{str}$), 1409 cm^{-1} (C-H$_{bend}$), 3062 and 3025 cm^{-1} (C-H$_{str}$), and aminopropyl groups 1500 cm^{-1} (N-H$_{bend}$), 3400 cm^{-1} (N-H$_{str}$), 2866 cm^{-1} and 2932 cm^{-1} (C-H$_{str}$). The peaks at 1130 cm^{-1} and 1030

cm^{-1} can be assigned due to Si-O-Si$_{str}$, respectively from cage-structured POSS and incompletely condensed linear/network SIL. The characteristic Si-O-Si band at 1130 cm^{-1} for a cage would be due to its highly symmetric structure.[17-19] The peak at 965 cm^{-1} confirmed the presence of Si-OH from incompletely condensed POSS/SIL. However, peak at 3360 cm^{-1} and 1650 cm^{-1} suggest the presence of adsorbed water/ethanol.[20]
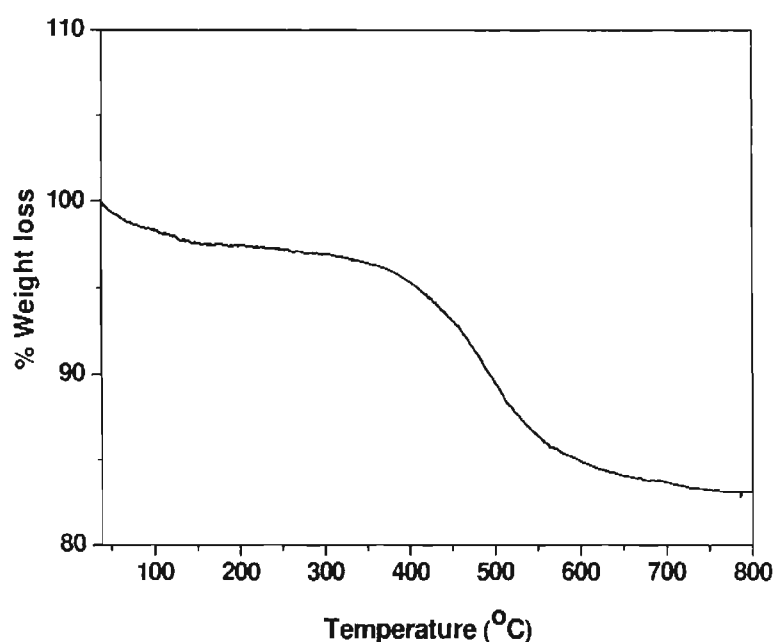
5.3.2. Thermal Analysis

Figure 5.4. *Thermogram of HS. Gradual loss below 150 °C is due to elimination of adsorbed water/ethanol and weight loss above 400 °C is associated with partial cleavage of organic functional group with production of volatiles.*

Figure 5.4 & 5.5, respectively shows the results of thermogravimetric (TGA) and differential scanning calorimetry (DSC) analyses of HS. Thermogram showed gradual loss of 3.4 wt % up to 150 °C and a more significant loss, starting above 400 °C leading to a final 83 wt % thermally stable residue at 800 °C. The gradual loss below 150 °C can be due to evaporation of adsorbed water/ethanol. The main weight loss at

temperature above 400 °C is associated with partial cleavage of organic functional group with production of volatiles. DSC (Figure 5.5) showed endothermic process below 150 °C and an exothermic process starting around 200 °C. HS showed softening behavior at temperature above 120 °C and, under pressure, they tended to form platelet structure as confirmed from SEM (Figure 5.8a). POSS, in general, show melting point above 200 °C and vinyl-substituted POSS decomposes without melting and exhibits exothermic peak starting around 200 °C due thermal polymerization through vinyl groups.[21,22] On the other hand, SIL can show low temperature melting characteristics. Therefore, the endothermic peak at 120-150 °C can be originated from evaporation of adsorbed water/ethanol and melting of SIL.

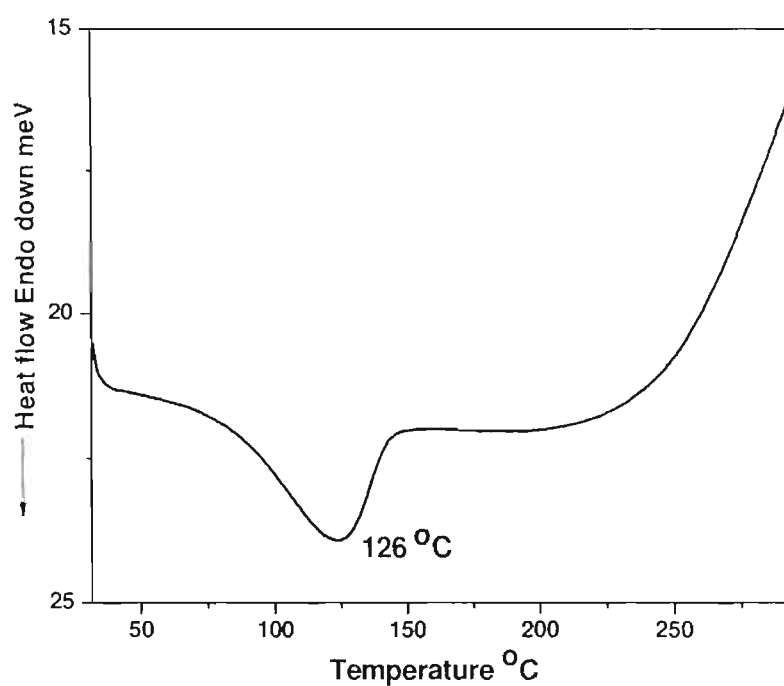

Figure 5.5. Differential Scanning Calorigram of HS. Endothermic peak at 120-150 °C is due to evaporation of adsorbed water and ethanol and melting of SIL. Exothermic peak starting around 200 °C due to thermal polymerization through vinyl groups.
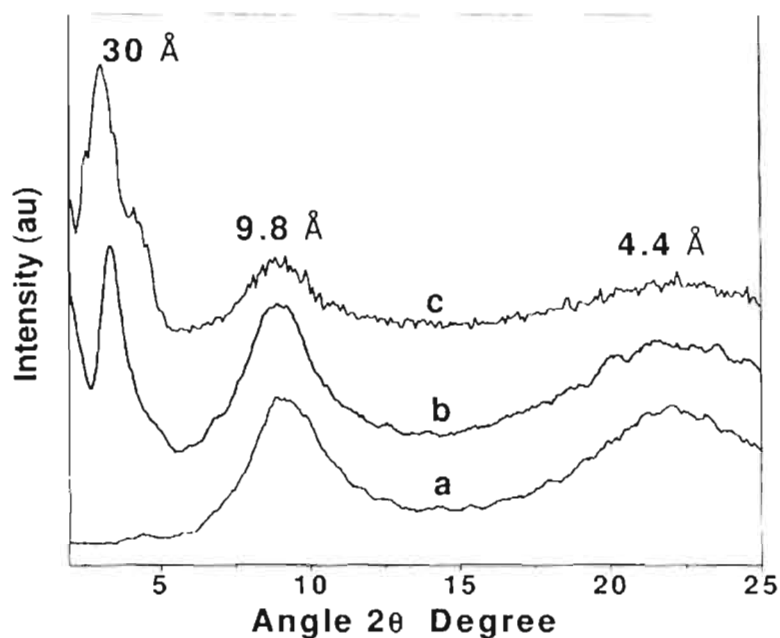
5.3.3. XRD of HS and Hot-pressed HS

Figure 5.6. *XRD of HS (a) as prepared (b) heated at 170 °C and (c) hot pressed at 170 °C.*

The XRD of HS dried at 80 °C (Figure 5.6a) exhibited broad reflections at around 2θ of 8° and 22° which respectively correspond to d-values of 9.8 Å and 4.4 Å. An additional reflection at 30 Å (Figure 5.6b) appeared for HS heated at 170 °C. The reflection became stronger (Figure 5.6c) when the powder was hot-pressed to form a pellet and XRD measurements were made on the pellet. POSS crystals generally show four strong reflections at 2θ in the range of 8-20° where the reflection around 8° (d-spacing around 10 Å) is caused by size of the POSS and remaining peaks at higher 2θ's are produced by the hexagonal or rhombohedral crystalline structure of the POSS aggregates.[23] These reflections, particularly the strongest peaks that observed around 8° and 19° were also seen in POSS-polymer nanocomposites where POSS formed

bilayer assembly within the polymer matrix.[24-26] The peak at 8° will appear only when POSS-assembly exhibit as a minimum two-dimensional ordering, indicating the presence of POSS-bilayer assembly in HS. The broad peak centered at 22° for HS can be due to merging of characteristic peak of POSS-bilayer arrangement with the amorphous halo from SIL. The XRD reflection at 30 Å for the heated HS indicates POSS-bilayer and SIL form ordered layered structure during melting and densification of SIL. FTIR spectra (Figure 5.7) of HS hot pressed at 170 °C showed intact vinyl groups and increase in SIL/POSS Si-O-Si$_{str}$ intensity ratio when compared to HS, further supporting melting and densification of incompletely condensed POSS and SIL during heating.[27] Hot-pressing promotes formation of two-dimensional lamellar structure by transforming spheres into plate-like structures (Figure 5.8a), causing the reflection to become more intense. Lamellar structure was further confirmed by HRTEM (Figure 5.8b-d) using sample which was prepared from hot-pressed pellets. The pellet was ground well using agate mortar and pestle. The fine powder thus obtained was ultrasonically dispersed in methanol and allowed the coarse particles to settle. The supernatant suspension was drop-cast on carbon-coated Cu grid and dried at 100 °C for viewing in HRTEM. The specimen appeared as produced by breaking and cleaving of particle having layered structure and exhibited features of two-dimensional lamellar structure. Also, disordered porous nature of the layers was confirmed from HRTEM image. The above results and observations suggest a randomly ordered structure for HS with POSS bilayers alternating with layers of SIL which rearrange on heating to form layered structure.
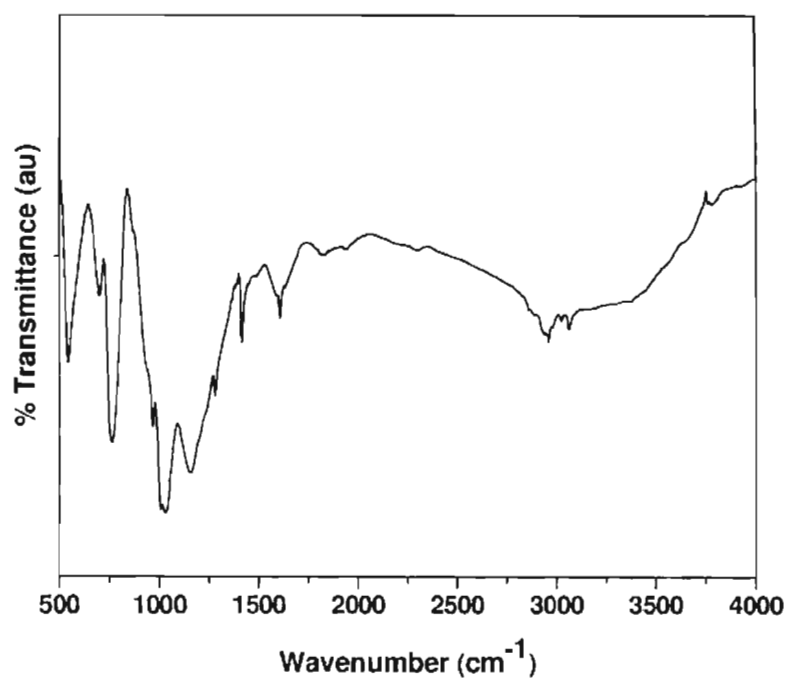
Figure 5.7. *FTIR spectra of hybrid silica spheres hot pressed at 170 °C showing intact vinyl groups and increase in siloxane network/POSS Si-O-Si $_{str}$ intensity ratio when compared to HS.*
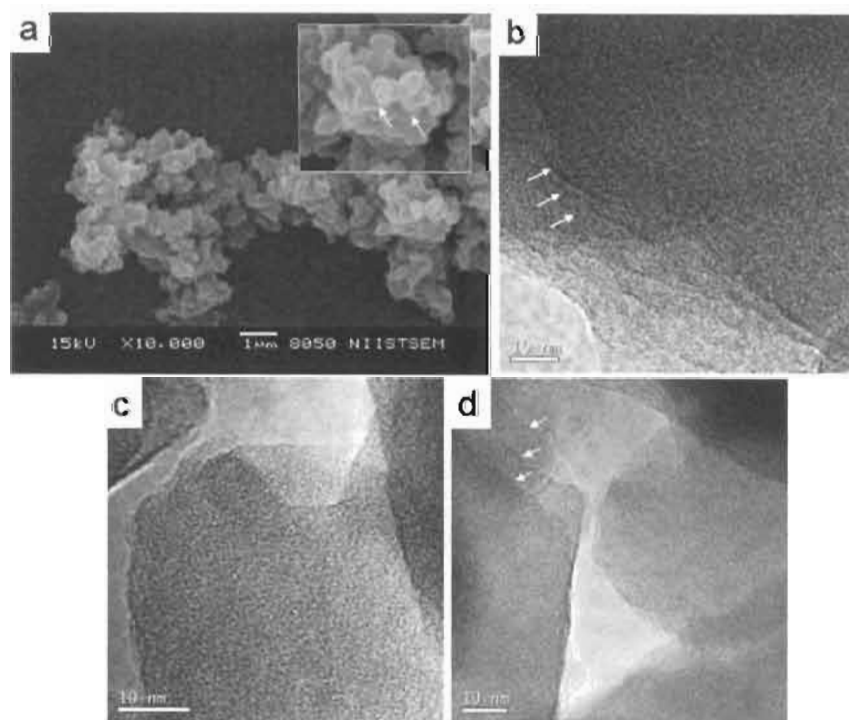

Figure 5.8. *(a) SEM (scale bar 1 μm) and (b-d) TEM (scale bar 10 nm) images of lamellar structures from HS hot pressed at 170 °C.*

5.3.4. Mechanism of formation of HS

As explained in Chapter 2, POSS-amine derived through hydrolytic condensation in ethanol/water mixture can be intercalated in layered materials through cation exchange mechanism.[28-30] Probable structure of POSS from AS/VS composition was derived by intercalating and stabilizing them in clay and analyzing the structure and behavior of the POSS-intercalated clay (For ^{29}Si and ^{13}C NMR spectra, FT-IR spectra, TGA, XRD, CHN elemental analysis and structure of POSS-bilayer modified clay see chapter 2). Modified clay showed approximately two aminopropyl group and six vinyl per POSS as was expected from co-condensation of AS and VS at 1:3 mole ratio. The POSS-bilayer in clay gallery has aminopropyl groups interacting and facing towards the clay surface with vinyl groups facing inward to the bilayer.

The effect of vinyl/amino ratio on the formation of HS was investigated by preparing silica from stable siloxane solution with AS:VS mole ratio of 3:1 and 1:1 under identical conditions. Interestingly, siloxane solution with 1:1 AS:VS mole ratio produced platelet morphology and with 3:1 mole ratio produced rod like morphology (Figure 5.9). It was evident that the aminopropyl:vinyl ratio and hence structure of POSS influence the aggregation pattern and also the formation of spheres. Based on the above observations, plausible mechanism for the formation of HS from the siloxane solution is proposed. During fast drying of the siloxane solution, self-assembly of POSS into bilayers takes place through hydrophobic interaction between the vinyl groups, preferentially with aminopropyl groups exposed outward to the bilayer and SIL will simultaneously self-assemble along with the POSS bilayers forming domains of POSS-SIL aggregates with hydroxyl groups of SIL interacting with aminopropyl groups. At lower concentration, number of adjacent domains will be less preventing

further aggregation and smaller particles were formed. At higher siloxane solution concentration these POSS-SIL domains will be in close proximity for further aggregation and spheres of larger size were formed. Scheme of POSS bilayer-SIL aggregate is shown in figure 5.10.
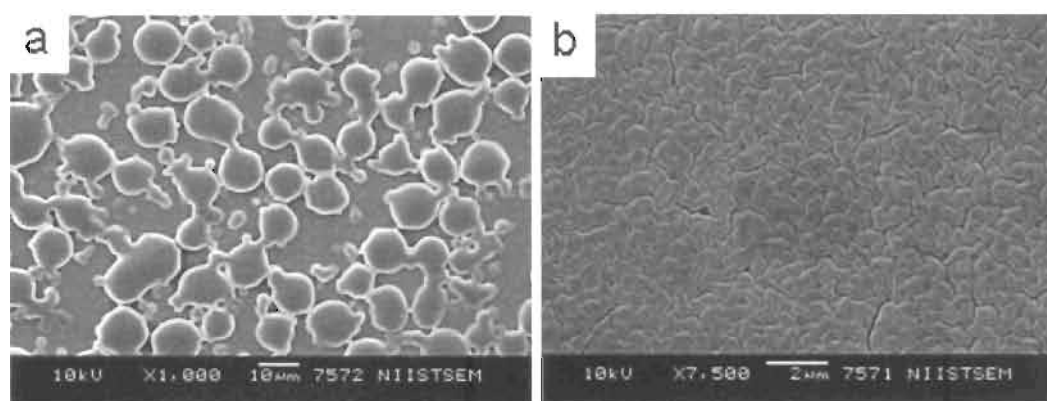

Figure 5.9. *Hybrid silica obtained from siloxane solution with AS:VS mole ratio (a) 1:1 (b) 3:1.*
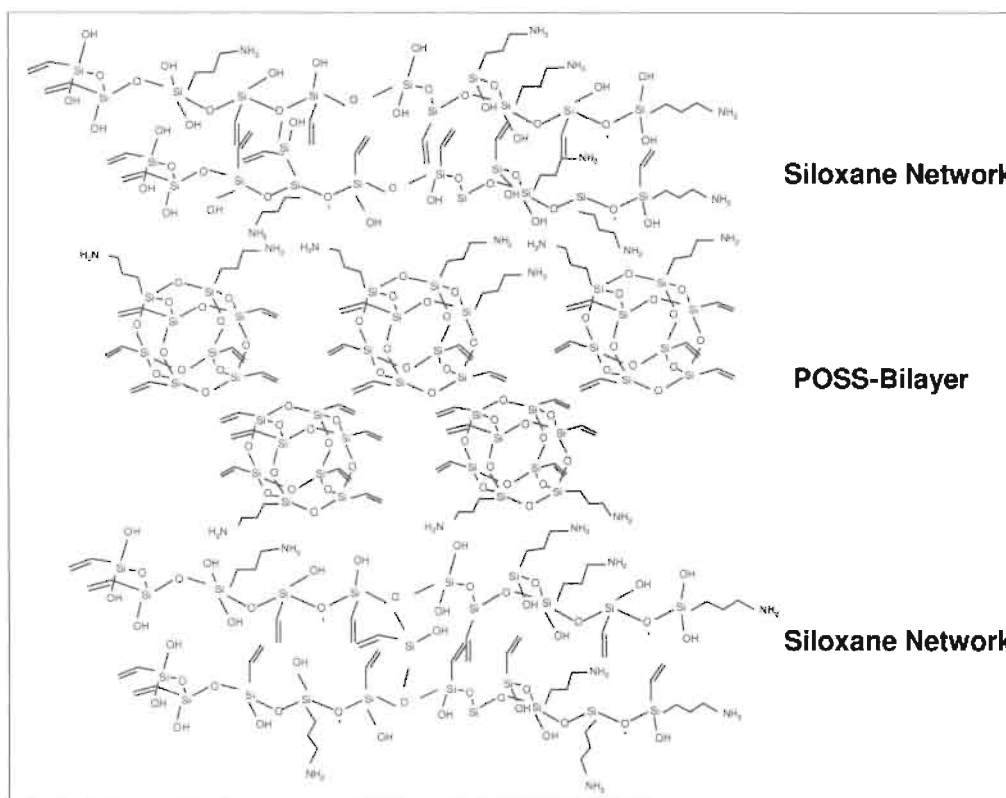

Figure 5.10. *Scheme of POSS bilayer-siloxane aggregate.*

POSS has been used for preparing polymer-composites with low dielectric constant, which can find application as packaging materials for microelectronic industry.[32,33] The decrease in dielectric constant for POSS-polymer composite was due to the structural porosity obtained through cross-linking of polymer segments with the reactive functional groups on the POSS and the internal porosity of the POSS cubes. Since HS contains POSS, we measured its dielectric constant and obtained a value of 3.5 when measurements were made on hot pressed pellets, compared to a value of 4 for pure silica. In order to check the usefulness of HS for the synthesis of polymer composite with low-dielectric constant, polystyrene-HS composite with different HS loading was prepared. It was found that the composite with 10 wt % HS exhibited a dielectric constant of 2.6 when compared to 3.1 for neat polystyrene. Figure 5.11 shows the SEM fractograph of polystyrene composite containing 10 wt % HS. Figure 5.12 shows the variation of dielectric constant with HS loading. A detailed investigation on the observed dielectric properties is in progress.
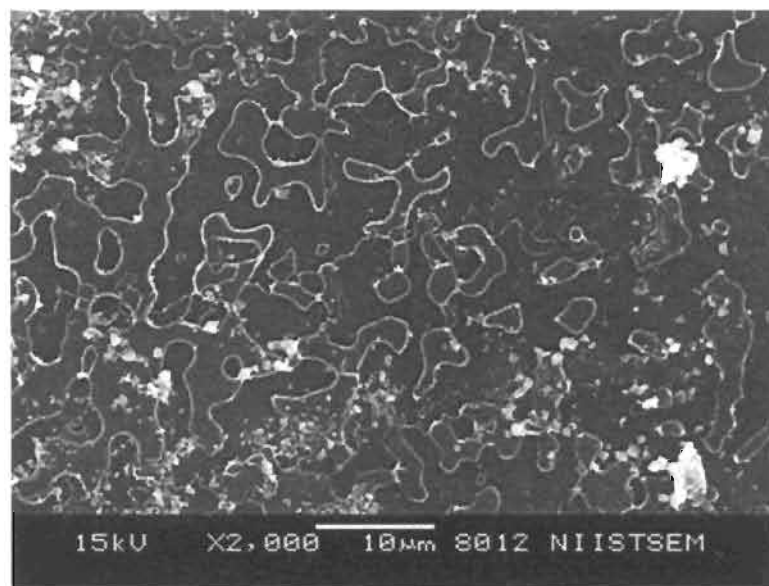
Figure 5.11. *SEM fractograph of polystyrene composite with 10 wt% HS.*
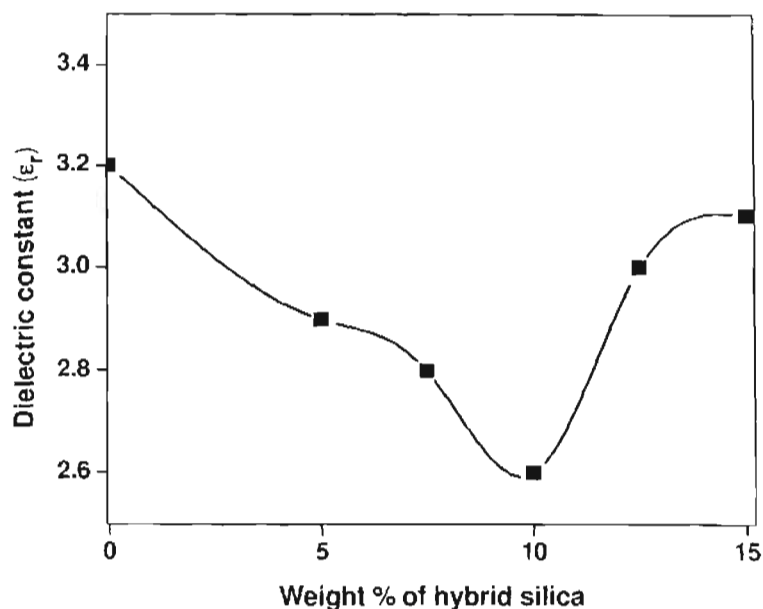
Figure 5.12. *Variation of dielectric constant with HS loading for polystyrene composite.*

5.4. Conclusions

In conclusion, synthesis of bifunctionalized hybrid silica spheres through surfactant-free method, using only organosilanes is illustrated. Casting and drying of siloxane solution from hydrolytic co-condensation of 3-aminopropyltriethoxysilane and vinyltriethoxysilane in ethanol/water mixture with 1:3 mole ratio produced hybrid silica spheres by spontaneous precipitation of POSS and incompletely condensed siloxanes. Control in the size of the spheres was achieved by dilution of the aged siloxane solution with ethanol. The hybrid silica was found useful for the synthesis of polymer-composites with low dielectric constant and a detailed investigation has been undertaken to explain the observed dielectric properties.

5.5. References

1.   Price, P. M.; Clark, J. H.; Macquarrie, D. J. *Dalton* **2000**, 101.

2.   Lai, C.-Y.; Trewyn, B. G.; Jeftinija, D. M.; Jeftinija, K.; Xu, S.; Jeftinija, S.; Lin, V. S. Y. *J. Am. Chem. Soc.* **2003**, *125*, 4451.

3.   Burleigh, M. C.; Dai, S.; Hagaman, E. W.; Lin, J. S. *Chem. Mater.* **2001**, *13*, 2537.

4.   Dai, S.; Burleigh, M. C.; Shin, Y.; Morrow, C. C.; Barnes, C.E.; Xue, Z. *Angew. Chem., Int. Ed.* **1999**, *38*, 1235.

5.   Radin, S.; El-Bassyouni, G.; Vresilovic, E. J.; Schepers, E.; Ducheyne, P. *Biomaterials* **2005**, *26*, 1043.

6.   Stober, W.; Fink, A. *J. Col. Interface Sci.* **1968**, *26*, 62.

7.   Wu, Z. J.; Han, H.; Han, W.; Kim, B.; Ahn, K.H.; Lee, K. *Langmuir* **2007**, *23*, 7799.

8.   Huh, S.; Wiench, J. W.; Yoo, J. C.; Pruski, M.; Lin, S. Y. *Chem. Mater.* **2003**, *15*, 4247.

9.   Kaneko, Y.; Iyi, N.; Kurashima,K.; Matsumoto,T.; Fujita,T.; Kitamura, K. *Chem. Mater.* **2004**, *16*, 3417.

10. Deng, T. S.; Zhang, Q. F.; Zhang, J. Y.; Shen, X.; Zhu, K.T.; Wu. J. L. *J. Col. Int. Sci.* **2009**, *329*, 292.

11. Lee, Y. G.; Park, J. H.; Oh, C.; Oh, S. G.; Kim, Y. C. *Langmuir* **2007**, *23*.10875.

12. Huh, S.; Wiench, J. W.; Trewyn, B. G.; Song, S.; Pruski, M.; Lin, V. S. Y. *Chem. Commun.* **2003**, 2364.

13. Huh, S.; Chen, H-T.; Wiench, J. W.; Pruski, M.; Lin, V. S. Y. *J. Am. Chem. Soc.* **2004**, *126*, 1010.

14. Brozek, E. M.; Zharov, I. *Chem. Mater.* **2009**, *21*, 1451.

15. Voronkov, M. G.; Larent' yev, V. I. *Top. Curr. Chem.* **1982**, *102*, 199.

16. Feher, F. J.; Wyndham, K. D.; *Chem. Commun.* **1998**, 323.

17. Lee, L. H.; Chen, W. C.; Liu, W. C. *J Polym Sci Part A: Polym Chem* **2002**, *40*, 1560.

18. Marcolli, C.; Calzaferri, G. *Appl. Organometal. Chem.* **1999**, *13*, 213.

19. Baney, R. H.; Itoh, M.; Sakakibara, A.; Suzukit, T. *Chem. Rev.* **1995**, *95*, 1409.

20. Jitianu, A.; Britchi, A.; Deleanu, C.; Badescu, V.; Zaharescu, M. *J Non-Cryst Solids* **2003**, *319*, 263.

21. Mantz, R. A.; Jones, P. F.; Chaffee, K. P.; Lichtenhan, J. D.; Gilman, J. W.; *Chem. Mater.* **1996**, *8*, 1250.

22. Fina, A.; Tabuani, D.; Carniato, F.; Frache, A.; Boccaleri, E.; Camino, G. *Thermochimica Acta* **2006**, *440*, 36.

23. Waddon, A. J.; Coughlin, E. B. *Chem. Mater.* **2003**, *15*, 4555.

24. Leu, C.M.; Chang, Y. T.; Wei, K. H. *Macromolecules* **2003**, *36*, 9122.

25. Zheng, L.; Waddon, A. J.; Farris, R. J.; Coughlin, E. B. *Macromolecules* **2002**, *35*, 2375.

26. Zheng, L.; Hong, S.; Cardoen, G.; Burgaz, E.; Gido, S. P.; Coughlin, E. B. *Macromolecules* **2004**, *37*, 8606.

27. Chen, W. C.; Lin, A. C.; Dai, B. T.; Tsai, M. S. *J Electrochem. Soc.* **1999**, *146*, 3004.

28. Cassagneau, T.; Jones, D. J.; Rozihe, J. *J. Phys. Chem.* **1993**, *97*, 8678.

29. Szabo, A.; Gournis, D.; Karakassides, M. A.; Petridis, D. *Chem. Mater.* **1998**, *10*, 639.

30. Liu, H.; Zhang, W.; Zheng, S. *Polymer* **2005**, *46*, 157.

31. Fox, D. M.; Maupin, P. H.; Harris Jr., R. H.; Gilman, J. W.; Eldred, D. V.; Kastsoulis, D.; Trulove, P. C.; De Long, H. C. *Langmuir* **2007**, *23*, 7707.

32. Leu, C. M.; Chang, Y. T.; Wei, K. H.; *Chem. Mater.* **2003**, *15*, 3721.

33. Su, R. Q.; Muller, T. E.; Prochazka, J.; Lercher, J.A. *Adv. Mater.* **2002**, *14*, 1369.

Chapter 6

Summary and Conclusions

Chapter 6 gives a brief summary of the thesis and future directions of the work.

Among the alternatives tried for conventional oraganomodifiers for clays when thermal limitations are a concern, Polyhedral Oligomeric Silsesquioxanes (POSS) have been of particular interest due to its high thermal stability and synergic benefits from dual nano-reinforcements. POSS-modified organoclays with reactive functional groups such as vinyl can be useful for the synthesis of novel polymer-clay nanocomposite, but were not available in the literature. The main objective of the research was to prepare POSS-modified organoclay having vinyl functional groups so that the POSS molecules intercalated in the clay can take part in polymerization reactions or be further modified through the reactive vinyl group. The other objective was to study the structure and dispersibility of the POSS-modified clays and hence its usefulness for the synthesis of polymer-clay nanocomposites.

POSS-modified oraganoclays with reactive vinyl groups were synthesized by using POSS solution from hydrolytic co-condensation of a mixture of 3-aminopropyltriethoxysilane (AS) and vinyltriethoxysilane (VS). The POSS solutions from VS/AS mole ratio >3 produced gels upon aging and was not useful for intercalation reactions in aqueous medium. Effect of AS:VS mole ratio on the structure of POSS-modified clay was also investigated. POSS-modified clays from VS/AS ratio <1 resisted dispersion in common organic solvents and was not suitable for the preparation of nanocomposite. Modified clays from VS/AS mole ratio between 1:1 and 3:1 were characterized using ^{29}Si and ^{13}C NMR spectroscopy, FT-IR spectroscopy, TGA, XRD and CHN elemental analysis. It was found that with increasing concentration of vinyl group, clay adsorbed increasing amount of POSS, producing POSS-monolayer (d_{001} spacing of 20.5 Å) and POSS-bilayer modified organoclays (d_{001} spacing of 26.35 Å). Dispersion characteristics of the modified clays in polyester

resin matrix indicated equal dispersibility for both monolayer and bilayer modified clay and produced intercalated nanocomposites proving its non-tethered structure.

In situ intercalative polymerization of styrene with POSS-modified clay produced polystyrene-clay nanocomposite particles exhibiting solvent-assisted self-assembling properties when dissolved in highly volatile solvent like THF. The particles having lateral dimensions of 190-810 nm consisted of sandwich structure having polystyrene-POSS-intercalated clay tactoid with thickness of 12.6 nm at the core and polystyrene layers of thickness of 31.6 nm on either side of the core, exposing the hydroxylated edges of the silicate layers. The particles resembled a bilayer assembly consisting of hydrophobic layers on either side of a hydrophilic rigid core from amphiphilic block copolymers. The drop-cast residues of solutions of the nanocomposite particles in THF showed concentration dependent well defined morphologies such as microvesicles of the size of 2.5-3.5 µm at solution concentration of 2.5 mgmL^{-1} and two-dimensional microporous film of long range order at solution concentration of 20-40 mgmL^{-1}. Microvesicles were formed by closure of the extended bilayer from lateral association of the nanocomposite particles by H-bonding interactions between edge-hydroxyls of the silicate layers. The breath figure mechanism has been proposed for the formation of the two-dimensional microporous film from solutions in which the extended bilayers formed closely packed lamellar arrangement.

Preliminary studies on the guest-encapsulation and release properties of polymer-clay nanocomposite vesicles were carried out. Encapsulation with dye molecules revealed uni-lamellar nature of vesicle wall. Vesicles were also encapsulated with triglyceride oil. They were found stable in aqueous medium and unstable in toluene

which resulted in total dissolution and release of the dye molecules. Slow release of the encapsulated dye molecules was observed in ethanol. The high thermal stability along with barrier properties of polymer-clay nanocomposites may make the vesicle excellent micro-storage and reactor system and can also be useful for solvent-assisted release applications.

The POSS solution from AS:VS mole ratio of 1:3 was found useful for the synthesis of bifunctionalized hybrid silica spheres (HS). HS with vinyl and aminopropyl groups was synthesized by casting and drying of stable siloxane solution from hydrolytic co-condensation of AS and VS with AS:VS mole ratio of 1:3 in ethanol/water mixture. No sphere formation was observed from siloxane solutions of AS:VS mole ratio <1:3. Hybrid silica was formed from co-precipitation of fully condensed polyhedral oligomeric silsesquioxane (POSS)-bilayer and incompletely condensed siloxanes produced during drying. Control in the size of the spheres was achieved by dilution of the aged siloxane solution with ethanol. The hybrid silica was found useful for the synthesis of polymer-composites with low dielectric constant.

Scope for future work include

- ⮞ Synthesis of polymer-clay nanocomposite from vinyl-POSS modified clays using olefinic monomers such as methyl methacrylate.

- ⮞ Synthesis of POSS-modified organoclays and hence vesicles of smaller size using clays having very low aspect ratio like laponite.

- ⮞ Preliminary studies on the use of vesicles for encapsulation and release application were carried out using fluorescent dyes. Future work includes

encapsulation of the vesicles with active molecules such as drug or cosmetics and to study its release properties in solvents.

➤ Vesicles can act as recoverable templates for producing hollow/spherical morphologies of polymer or silica after leaching out the vesicle shell. Studies in this respect have been in progress.

➤ Preliminary studies indicated the use of bifunctionalized hybrid silica for the synthesis of low-dielectric constant polymer composite. Systematic analysis of the observed reduction in dielectric constant is underway.

List of Publications

International Patent

1. **Bindu Prasannakumaran Nair** and Chorappan Pavithran "Nanocomposite forming micro-capsules for guest encapsulation and process thereof" (Applied for International Patent, Filed provisionally in India, Application Number **0969DEL2009**, Filing Date **12-05-2009**)

Research Articles

1. **Bindu Prasannakumaran Nair** and Chorappan Pavithran "Bifunctionalized Hybrid Silica Spheres by Hydrolytic Cocondensation of 3-Aminopropyltriethoxysilane and Vinyltriethoxysilane" (*Langmuir*, 2009, Accepted, Published on web, DOI: 10.1021/la902432r)

2. **Bindu P. Nair**, Chorappan Pavithran, Jannardhanannair D. Sudha and Vadakkethonippurathu S. Prasad "Microvesicles through Self-assembly of Polystyrene-clay Nanocomposite" (Resubmitted after Minor Revision, *Langmuir*, 2009, Manuscript ID: la-2009-03360e)

3. **Bindu P. Nair**, T. S. Sasikala, M. T. Sebastian and C. Pavithran "Polystyrene-Hybrid Silica Sphere Composite with Low Dielectric Constant" (Communicated to *Materials Letters*)

4. **Bindu P. Nair** and C. Pavithran "2D Microporous Film from Polystyrene-Clay Nanocomposite Particles" (To be communicated)

5. **Bindu P. Nair** and C. Pavithran "Rod-shaped Hybrid Silica from Auto-catalyzed Hydrolytic Condensation of 3-Aminopropyltriethoxysilane without using Surfactants" (To be communicated)

Conference Proceedings

1. **Bindu P. Nair** and C. Pavithran "In-situ generated silica-nanoparticle mediated exfoliation of smectite for polymer-clay nanocomposites". MACRO-2006, Pune, *2006*.

2. **Bindu P. Nair** and C. Pavithran "Clay Compositions with (3-Aminopropyl) vinyl Polyhedral Oligomeric Silsesquioxane (POSS) for Polymer Nanocomposites". ICAMC-2007, Trivandrum, *2007*.

114